Crosstalk between neutral lipid and sphingolipid metabolism regulates cellular lipid homeostasis

Inaugural-Dissertation

zur Erlangung des Doktorgrades
der Mathematisch-Naturwissenschaftlichen Fakultät
der Heinrich-Heine-Universität Düsseldorf

vorgelegt von

Manuel Hertel
aus Lutherstadt-Wittenberg

Düsseldorf, März 2023

aus dem Institut für Klinische Diabetologie (Deutsches Diabetes-Zentrum)
der Heinrich-Heine-Universität Düsseldorf

Gedruckt mit der Genehmigung der
Mathematisch-Naturwissenschaftlichen Fakultät der
Heinrich-Heine-Universität Düsseldorf

Berichterstatter:

1. Jun. Prof. Dr. Mathias Beller

2. Prof. Dr. Michael Roden

Tag der mündlichen Prüfung: 28.08.2023

List of abbreviations

µ	Micro
3HA	Triple hemagglutinin
3KDS	3-keto-dihydrosphingosine
AA	Antibiotic-antimycotic
ACAT	Mammalian acyl-coenzyme A:cholesterolacyltransferas
AID	Auxin-inducible degron
AKT	Protein kinase B
APS	Ammonium persulfate
Are1/2	Yeast acyl-coenzyme A:sterol acyltransferases
ASAT	Yeast acyl-coenzyme A:sterol acyltransferase
Aur1	Yeast phosphatidylinositol:ceramide phosphoinositol transferase
bp	Base pairs
Cer	Ceramide
CerS 1-6	Ceramide synthases 1-6
ChREBP	Carbohydrate response element-binding protein
Cys	Cysteine
DAG	Diacylglycerol
Dga1	Diacylglycerol acyltransferase 1
Dgk1	Diacylglycerol kinase
DHC	Dihydroceramide
DHS	Dihydrosphingosine
DMEM	Dulbecco's Modified Eagle Medium
DMSO	Dimethyl sulfoxide
DNA	Deoxyribonucleic acid
DNL	De novo lipogenesis

dNTP	Deoxyribose nucleoside triphosphate
dsDNA	Double strand DNA
E. coli	*Escherichia coli*
EDTA	Ethylenediaminetetraacetic
EGTA	Ethylenediaminetetraacetic acid
FBS	Fetal bovine serum
g	Gram
G3P	Glycerol-3-phosphate
G6Pase	Glucose 6-phosphatase
GFP	Green fluorescence protein
GK	Glucokinase
GP	Glycogen phosphorylase
GPAT	Glycerol-3-phosphate-acyltransferase
GS	Glycogen synthase
h	Hour
HDEL	Target peptide sequence of ER proteins (Histidine-aspartic acid-glutamic acid-leucine)
HeLa	Human cervical cancer cells (Henrietta Lacks)
HEPES	2-(4-(2-Hydroxyethyl)piperazin-1-yl)ethanesulfonic acid
HepG2	Human hepatoblastoma cell line
HRP	Horseradish peroxidase
INSR	Insulin receptor
IPC	Inositol-phosphoryl-ceramide
IRK	Insulin receptor kinase
IRS1	Insulin receptor substrate 1
kDa	Kilo Dalton
l	Liter

Lcb1	Long-chain base 1
Lcb2	Long-chain base 2
LC-MS/MS	Liquid chromatography–tandem mass spectrometry
LD	Lipid droplet
LPA	Lysophosphatidic acid
M	Molar
M(IP)2C	Mannosyl-diinositolphosphorylceramide
min	Minute
MIPC	Mannosyl-inositolphosphorylceramide
m	Milli
NAFLD	Nonalcoholic fatty liver disease
NEFA	Nonesterified fatty acids
OD_{600}	Optical density at 600 nm wavelength
OsTIR1	TIR1 from *Oryza sativa*
PA	Phosphatidic acid
Pah1	Phosphatidic acid phosphohydrolase
PC	Phosphatidylcholine
PCR	Polymerase chain reaction
PE	Phosphatidylethanolamine
PH	Pleckstrin homology
PHC	Phytoceramide
PHS	Phytosphingosine
PHS1P	Phytosphingosine-1-phosphate
PI	Phosphatidylinositol
PI3K	Phosphatidylinositol 3-kinase
PKC	Protein kinase C

PLP	Pyridoxal phosphate
p	Pico
ppb	Parts per billion
PS	Phosphatidylserine
PtdIns(4)P	Phosphatidylinositol 4-phosphate
PVDF	Polyvinylidene fluoride
RFP	Red fluorescence protein
RPM	Rounds per minute
RT	Room temperature
RT-qPCR	Reverse transcriptase quantitative PCR
S1P	Sphingosine-1-phosphate
Sac1	Phosphatidylinositol 4-phosphate phosphatase
SD	Standard deviation
SDS	Sodium dodecyl sulfate
SDS-PAGE	Sodium dodecyl sulfate polyacrylamide gel electrophoresis
sec	Second
SEM	Standard error of the mean
Ser	Serine
siRNA	small interfering RNA
SM	Sphingomyelin
SPT	Serine palmitoyltransferase
SPTLC1-3 (hLCB)	Mammalian Long-chain base 1-3 (human Long-chain base)
ssDNA	Single-strand DNA
ssSPT	small subunit of SPT
T2D	Type 2 diabetes
TAE	TRIS-acetate-EDTA

TAG	Triacylglycerol
TBST	TRIS-buffered saline with Tween20
TCA	Trichloroacetic acid
TEMED	N-Tetramethylethylendiamine
Tgl	Triacylglycerol lipase
Thr	Threonine
TIR1	F-box transport inhibitor response 1 domain
TMD1	Transmembrane domain 1
TRIS	TRIS(hydroxymethyl)-aminomethane
Tsc3	Temperature-sensitive Suppressors of Calcium Sensitive Growth mutants 3
Tyr	Tyrosine
v	Volume
VLCFA	Very long chain fatty acid
VLDL	Very low density lipoprotein
WAT	White adipose tissue
Ypk1	Yeast protein kinase (yeast ceramide synthase)

List of figures

List of tables

Table of content

1. Introduction

1.1 Lipids as contributor to impaired insulin sensitivity in human body

Lipids play an important role in every living cell by serving as carbon source, bioactive signaling molecules and components of the cell membrane due to their amphipathic properties. Based on their complex heterogeneous structure, lipids can be classified into: (i) acylglycerols when single hydrocarbon chains, termed fatty acids (FA), are bound to glycerol, (ii) membrane localized phospholipids or (iii) sterol esters if FAs are esterified to sterols. Within each lipid subgroup the molecules differ in structure according to linked FA chain length, saturation and polar head group such as inositol, ethanolamine, choline or serine (van Meer et al., 2008). In addition, FAs can be bound to sphingosine backbones to form sphingolipids (Hannun & Obeid, 2018). Through this complex variation, lipids differ in function and influence the cellular metabolism extensively. Therefore, fine-tuning of lipid metabolism and distribution in the body is fundamental for regular physiologic metabolism.
Overweight and obesity are major public health problems of the 21st century, predominately but not exclusively in industrialized countries with excessive access to hypercaloric energy-dense and sugar-refined food coupled to sedentary lifestyle habits (Hill et al., 2012). Over the last decades the western hemisphere was characterized by an increased prevalence of obesity culture, mostly in North America (Ng et al., 2014). Thus, obesity reached 42 % among adults in the US in 2020 (Hales et al., 2020), but also China can be a recent example for correlation of food supply and obesity; indeed obesity increased from 4.2 % in 1993 to 15.7 % in 2015 in overall population, with the change from "land of famine" to a country with increased food supply. At the same time, abdominal obesity more than doubled from 20.2 % to 46.9 % (Ma et al., 2021).
Obesity is a risk factor for metabolic diseases such as type 2 diabetes (T2D) (Schnurr et al., 2020). In parallel, lifestyle and genetic predisposition factors additionally contribute to rise the incidence of insulin resistance and T2D (Barres & Zierath, 2016; Bellou et al., 2018; Manning et al., 2012; Wahl et al., 2017). T2D is a heterogeneous metabolic disease which occurs when cells exhibit impaired insulin sensitivity, i.e. insulin resistance, due to interrupted insulin signaling pathways and the pancreatic ß cells cannot secrete enough insulin to meet the increased need of insulin to counteract the body´s insulin resistance (Mastrototaro & Roden, 2021; Roden & Shulman, 2019). These alterations ultimately lead to hyperglycemia due to reduced glucose uptake, impaired glycogen synthesis and to disturbance of lipid metabolism including increased storage and delivery between organs (Roden & Shulman, 2019).

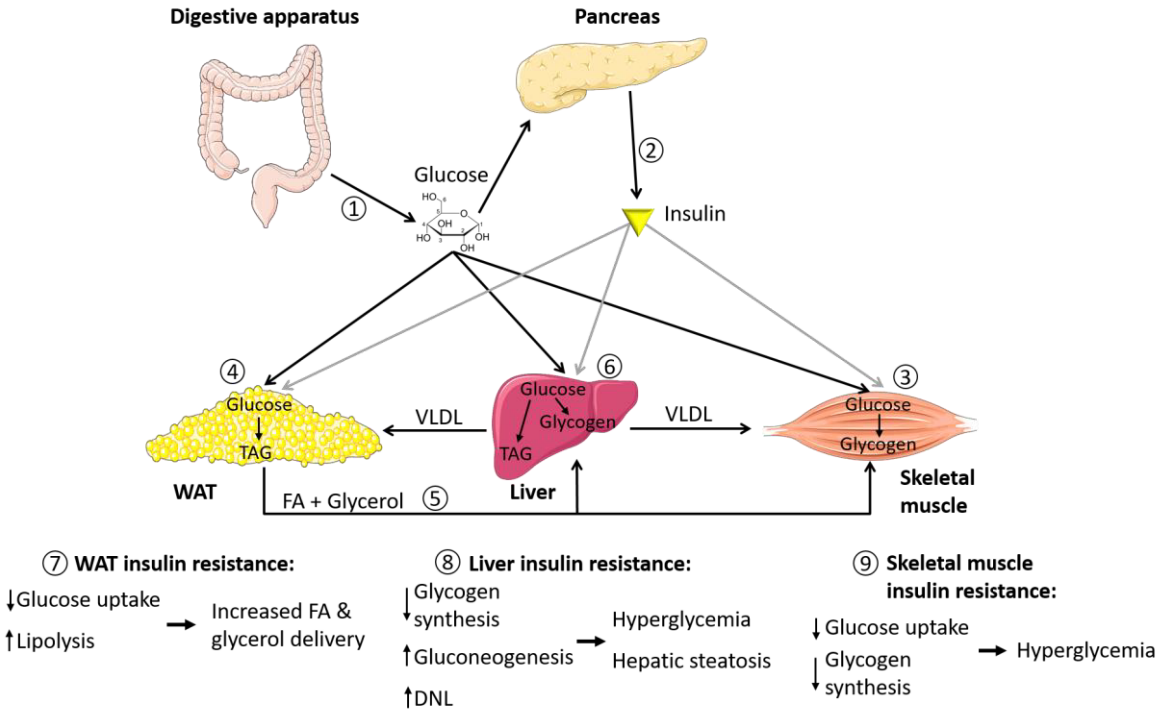

Fig. 1: Glucose uptake and development of insulin resistance in mammalian body. Digestive apparatus absorbs glucose from diet, resulting in increase of blood sugar level (1). Pancreatic ß-cells responds with insulin secretion (2), leading to glucose uptake in white adipose tissue (WAT) and skeletal muscle via glucose transporters. Glucose is utilized for energy production in skeletal muscle and excessive glucose is converted into the storage molecule glycogen (3). WAT stores the absorbed glucose in form of triacylglycerol (TAG) (4). Fatty acids (FA) and glycerol can be released from WAT by hydrolysis of TAG and delivered to muscle and liver (5). The liver responds to insulin with decreased gluconeogenesis, increased glycogen synthesis and conversion of glucose to TAG via de novo lipogenesis (DNL) (6). Insulin resistance in multiple tissues results in the disruption of insulin-regulated signaling, which can lead to reduced glucose uptake accompanied with elevated lipolysis, which leads to increased release of FA and glycerol from WAT (7). Further, insulin resistance results in reduced glycogen synthesis, increased gluconeogenesis and accumulation of TAGs driven by elevated DNL in the liver (8). Skeletal muscle tissue reacts to insulin resistance with reduced glucose uptake and impaired glycogen synthesis (9). These abnormalities in maintenance of glucose metabolism can lead to hyperglycemia and further diseases like type 2 diabetes and hepatic steatosis.

Ultimately, an altered interorgan crosstalk supports progression to T2D and tightly related nonalcoholic fatty liver disease (NAFLD) (Dewidar et al., 2020; Gancheva et al., 2018; Roden & Shulman, 2019). However, the progression from obesity to insulin resistance, T2D and NAFLD is still incompletely understood.

It is assumed that insulin resistance in adipose tissue is induced by elevated levels of pro-inflammatory cytokines such as interleukin 6 (IL-6) and tumor necrosis factor-α (Bodis & Roden, 2018), which activate the c-Jun N-terminal kinase (JNK) and the inhibitor kappa B kinase (IKK), consequently inhibiting activity of the insulin receptor substrate 1 (IRS1) by phosphorylation at serine residues (Dewidar et al., 2020; Solinas & Becattini, 2017). Obesity-induced WAT insulin resistance impairs insulin-mediated suppression of lipolysis, resulting in increased nonesterified fatty acids (NEFA) and glycerol release into blood circulation and delivery to ectopic tissues (Bodis & Roden, 2018; Petersen & Shulman,

2018). Nevertheless, studies of lipodystrophy models in mice and human support the hypothesis that adipose tissue insulin resistance can also occur without inflammation (Grundy, 2015; Lotta et al., 2017). A recent study reports that short-term overnutrition induces WAT insulin resistance through plasma membrane *sn*-1,2-diacylglycerol (DAG) accumulation, which promotes protein kinase C epsilon (PKCε) activation and impairment of insulin signaling by inhibitory phosphorylation of insulin receptor (INSR) at residue Thr^{1160} (Lyu et al., 2021). However, as a consequence of adipose tissue dysfunction enhanced rates of FA from WAT are delivered to distant tissues like skeletal muscle and liver, resulting in an excessive lipid accumulation, which can cause insulin resistance (Perry et al., 2015; Petersen & Shulman, 2018; Roden & Shulman, 2019; Szendroedi & Roden, 2009).

The skeletal muscle is one of the main glucose consuming tissues, because glucose is needed as a substrate for energy production during physical activity. In addition, the skeletal muscle stores postprandial glucose excess in the blood plasma in form of glycogen (Saatmann et al., 2021). Increased NEFA flux into skeletal muscle as consequence of disturbed WAT function or oversupply of lipids from diet, leads to increased accumulation of intramyocellular lipids, resulting in insulin resistance and further progression to T2D (Dewidar et al., 2020; Szendroedi & Roden, 2009).

Studies in humans have shown that high plasmatic NEFA levels increase the intramyocellular concentration of DAG, which is temporally related to translocation of PKCθ from cytosol to the plasma membrane and muscle insulin resistance in obese and T2D individuals (Bergman et al., 2012; Szendroedi et al., 2014). Indeed, the activated PKCθ phosphorylates IRS1 at Ser^{1101} and blunts PI3K activation, which impairs Protein kinase B 2 (AKT2) activity through decreased phosphorylation at Ser^{473}, ultimately inhibiting insulin downstream signaling. This results in disruption of inhibitory threonine phosphorylation of AS160 and subsequent reduced Rac1-mediated translocation of glucose transporter type 4 (Glut4) to the plasma membrane, which is required for glucose uptake (Shulman, 2014). The consequence of insulin resistance is a reduced storage of postprandial carbohydrates in form of glycogen in muscle due to a decreased glucose uptake (Mastrototaro & Roden, 2021; Petersen et al., 2007). Thereby ingested energy storage is diverted to hepatic triacylglycerol (TAG) synthesis, which promotes progression to NAFLD (Roden & Shulman, 2019).

The liver is the central organ for the body's energy balance. It is involved in the control of glucose, fat and protein metabolism by absorbing nutrients from the blood via the portal vein and releasing them into the bloodstream when needed (Trefts et al., 2017). The liver equilibrates the blood sugar level by importing glucose into the cells via the insulin-independent glucose transporter type 2 (Glut2); intracellularly the glucokinase (GK) convertes glucose to glucose-6-phosphate (G6P), which is either converted to glycogen by

the glycogen synthase (GS) or into the principal energy storage molecule TAG via de novo lipogenesis (DNL) (Dentin et al., 2006; Thorens, 2015). NEFAs and glycerol can also be utilized for TAG synthesis.

Stimulation of the insulin signaling pathway promotes hepatic glycogen synthesis and storage of imported glucose through GK and GS activation. Moreover, the reconversion of glycogen to glucose is suppressed by inhibition of GP, resulting in low EGP (Rothman et al., 1991).

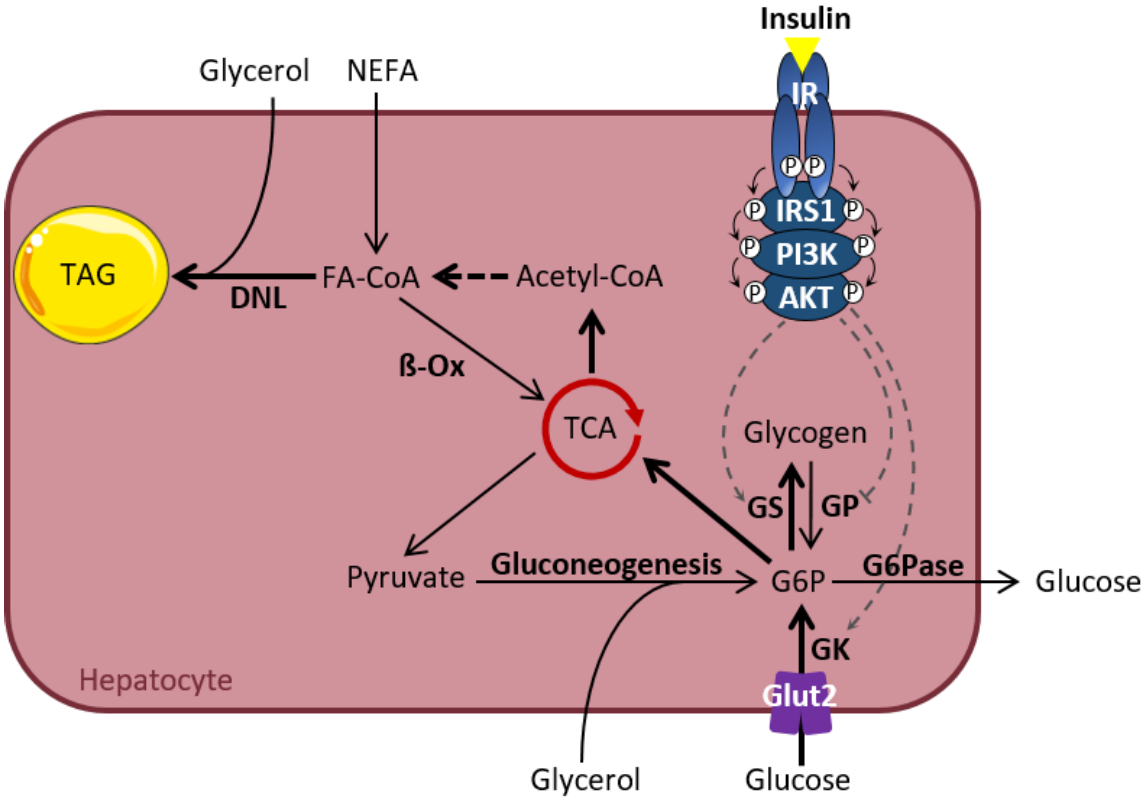

Fig. 2: Liver metabolism under insulin sensitive condition. Hepatic insulin signaling activation stimulates glucokinase (GK) activity, thus increasing conversion of insulin independent channeled glucose to glucose-6-phosphate (G6P) by the glucose transporter type 2 (Glu2). G6P is converted to glycogen via glycogen synthase (GS), whereas reconversion of glycogen to G6P by glycogen phosphorylase (GP) is suppressed and gluconeogenesis is downregulated by insulin action. Acetyl-CoA can be used as a byproduct of energy production with G6P as a substrate in the tricarboxylic acid cycle (TCA) for de novo lipogenesis (DNL). NEFA and glycerol influx is used as well for DNL with further storage in form of triacylglycerol (TAG). Under beta oxidation (ß-Ox), NEFAs are also incorporated into the TCA for energy generation.

In obese, delivery of NEFA and glycerol to the liver due to lipolysis from dysfunctional WAT or nutrient oversupply induce hepatic TAG accumulation (Roden & Shulman, 2019; Vatner et al., 2015). In conjunction with hyperglycaemia, due to reduced carbohydrate conversion in glycogen in insulin-resistant skeletal muscle, pancreatic ß-cells try to compensate for hyperglycaemia by secreting more insulin. The emerging hyperinsulinaemia promotes enhanced hepatic DNL, resulting in steatosis (Petersen et al., 2007).

Elevated cellular TAG accumulation associates with increased level of lipotoxic intermediates such as DAG and ceramides (Cer) which can cause insulin resistance in

different tissues (Apostolopoulou et al., 2018; Lyu et al., 2021; Petersen & Shulman, 2017; Szendroedi & Roden, 2009; Szendroedi et al., 2014). With regard to liver tissue, both lipid species are potentially mediators of hepatic insulin resistance by activating PKC isoforms (Jornayvaz & Shulman, 2012; Petersen et al., 2016). Early studies in rodents demonstrated a correlation between hepatic insulin resistance and increased accumulation of *sn*-1,2-DAG (Turinsky et al., 1990). Since DAG are bioactive molecules, the impairment of insulin signaling could be linked to the activation of PKC by DAG (Shmueli et al., 1993). Further studies revealed that elevated accumulation of *sn*-1,2-DAG specifically promotes activation of the PKCε isoform by translocation from cytosol to the plasma membrane, resulting in inhibition of the insulin receptor kinase (IRK) activity (Kumashiro et al., 2011; Samuel et al., 2004; Samuel et al., 2007; Samuel & Shulman, 2012). The molecular mechanism was determined by studying the *in vitro* phosphorylation of recombinant IRK. PKCε was shown to be responsible for the inactivation of IRK due to inhibitory phosphorylation at Thr^{1160}, consequently destabilizing the configuration of the catalytic unit (Petersen et al., 2016). Indeed, the activation loop of unphosphorylated IRK is in an auto-inhibitory configuration, which occludes the catalytic pocket and hinders the activation of IRS1 (Hubbard et al., 1994). Only the binding of insulin to the α-subunits of the INSR leads to a conformational change of the two β-subunits, which approach each other and undergo reciprocal phosphorylation (Gutmann et al., 2020). Through this *trans*-autophosphorylation of the side chain residues Tyr^{1158}, Tyr^{1162}, and Tyr^{1163} the activation loop adopts a configuration that activates the kinase domain and thus also downstream insulin signaling cascade (Hubbard, 1997). Translocation to the plasma membrane and activation of PKCε, due to an increased DAG level, leads to IRK phosphorylation at Thr^{1160} and electrostatic repulsion with phosphorylated Tyr^{1162} (Petersen et al., 2016). This sterically hinders the active configuration of the activation loop and impairs activation of the IRS1 adaptor protein. Further *in vivo* studies in mice with a threonine-to-alanine mutation at the homologous residue Thr^{1150} (Thr^{1150A}) displayed protection against hepatic insulin resistance induced by a high-fat diet (Petersen et al., 2016). Compared to WT mice fed with high-fat diet, the Thr^{1150A} mutant mice were shown to have functional insulin signaling, suppression of EGP, and increased hepatic glycogen production. In conclusion, these data demonstrate that Thr^{1150} phosphorylation in mice and Thr^{1160} phosphorylation in human contributes to lipid induced hepatic insulin resistance under high-fat diet conditions.

Early studies show that an increased *sn*-1,2-DAG concentration in livers of obese rats was accompanied by an increase in hepatic Cers (Turinsky et al., 1990). As bioactive signaling molecule Cers play an important role in multiple biological processes including cellular apoptosis, oxidative stress and inflammation and all these factors are associated with the progressive NAFLD (Apostolopoulou et al., 2018; Chaurasia et al., 2019; Pagadala et al.,

2012). However, it is still unclear how elevated cellular Cer levels are linked to hepatic insulin resistance, indeed existing data regarding the role of Cers in lipid-induced hepatic insulin resistance are controversial. Several studies conducted in different rodent models show that hepatic insulin resistance is not accompanied by increases in hepatic Cers (Galbo et al., 2013; Holland et al., 2007; Lee et al., 2011; Montgomery et al., 2016; Montgomery et al., 2013; Turner et al., 2013; Ussher et al., 2010). In addition, reversal of hepatic steatosis and improvement of insulin signaling have been shown to be associated with decreased hepatic DAG content, but not Cer level (Camporez et al., 2013; Camporez et al., 2015; Perry et al., 2013). Also, in human studies of obese individuals without diabetes, hepatic Cer content was not associated with abortion of the hepatic insulin signaling pathway, suggesting that hepatic Cers are rather dissociated from lipid-induced hepatic insulin resistance (Kumashiro et al., 2011; Magkos et al., 2012). In contrast, studies conducted in mice with induced increased TAG synthesis or in high fed diet rats, display hepatic insulin resistance associated with increased total hepatic Cer, DAG, and TAG levels (Jornayvaz et al., 2011; Kurek et al., 2014). Moreover, a lipidomic study of obese humans indicates a strong correlation between hepatic Cers and insulin sensitivity (Luukkonen et al., 2016).

Of note, the underlying mechanism of how Cers mediate hepatic insulin resistance is still unknown. It is proposed that Cers are able to activate PKCζ, which leads to phosphorylation of AKT pleckstrin homology (PH) domain at Thr^{34} (Bourbon et al., 2000; Powell et al., 2003). This in turn inhibits the binding to PIP3 thereby preventing activation of AKT caused by unphosphorylated Ser^{473}, ultimately resulting in abortive insulin signaling (Laplante & Sabatini, 2012; Schubert et al., 2000). However, this effect of Cers on insulin action has only been shown with cytotoxic synthetic short chain C2-cermide under non-physiological concentrations and is therefore not very conclusive.

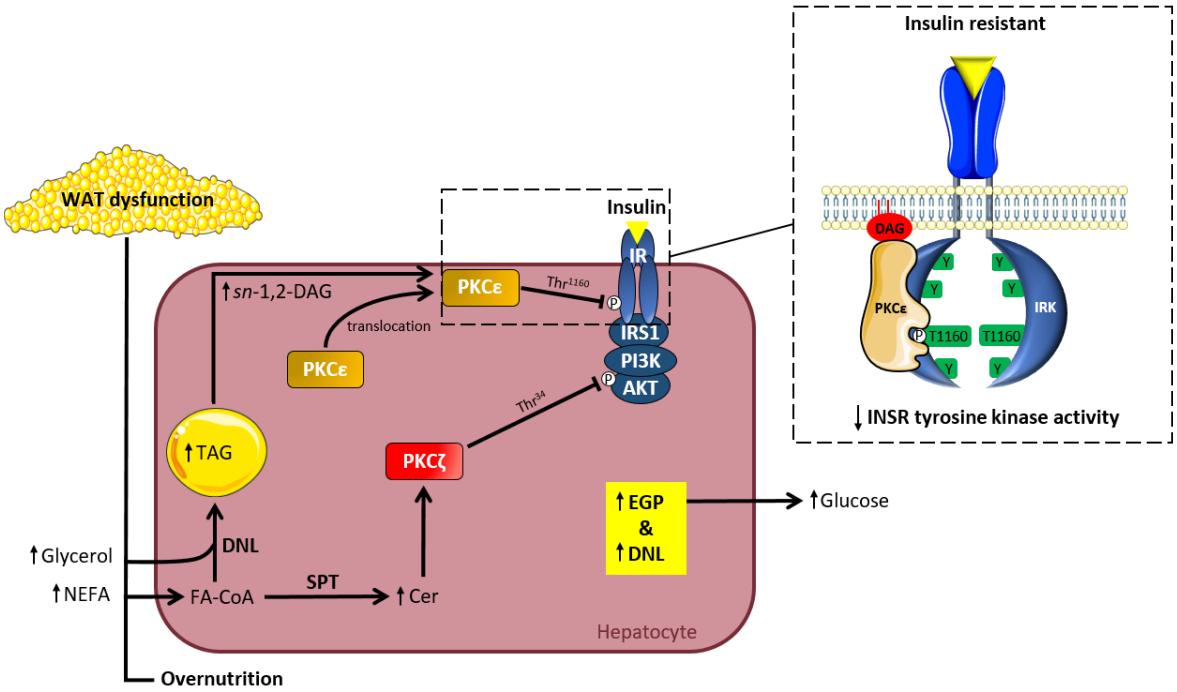

Fig. 3: Liver under insulin resistant condition. Dysfunctional WAT favors lipolysis-induced non esterified fatty acid (NEFA) and glycerol release, thereby elevates plasma circulating NEFA and glycerol levels and a shift of substrates towards the liver. Once NEFA and glycerol enter the liver, they are used for de novo lipogenesis (DNL) and promote hepatic triacylglycerol (TAG) accumulation. Overnutrition also promotes elevated TAG accumulation in the liver. Excessive TAG accumulation is accompanied with increased levels of lipotoxic intermediates such as *sn*-1,2-diacylglycerol (DAG) and ceramide (Cer), which activates protein kinase C-epsilon (PKCε) and protein kinase C-zeta (PKCζ). In detail PKCε phosphorylates the insulin receptor kinase (IRK) at side chain residue threonine 1160 (Thr^{1160}), which inhibits the tyrosine autophosphorylation and consequently the IRK activity. Cers activate PKCζ, which inhibit protein kinase B (AKT) activation. The DAG-PKCε-IRK and Cer-PKCζ-AKT axis processes in turn inhibit the insulin signaling cascade, resulting in hepatic insulin resistance with subsequently elevated endogen glucose production (EGP). Hepatic insulin resistance also enhance conversion of glucose-6-phosphate to FA, thus promotes DNL and contributes hepatic TAG storage and aggravation of hepatic insulin resistance.

It is possible that the deleterious effects of specific Cers are indirectly caused by complex mechanisms such as hepatocellular lipid oxidation, reduced very low density lipoprotein (VLDL) export, impaired activation of the FA transporter CD36 and abnormal mitochondrial function, promoting progression to steatosis (Aburasayn et al., 2016; Raichur et al., 2014; Turpin et al., 2014; Xia et al., 2015).

As central components of TAG metabolism, lipid droplets (LD) safeguard the supply of lipid metabolites for Cer and DAG biogenesis, therefore play a critical role in obesity and related diseases such as T2D and NAFLD and the mechanism of lipid storage and delivery remains of high interest (Greenberg et al., 2011; Krahmer et al., 2013).

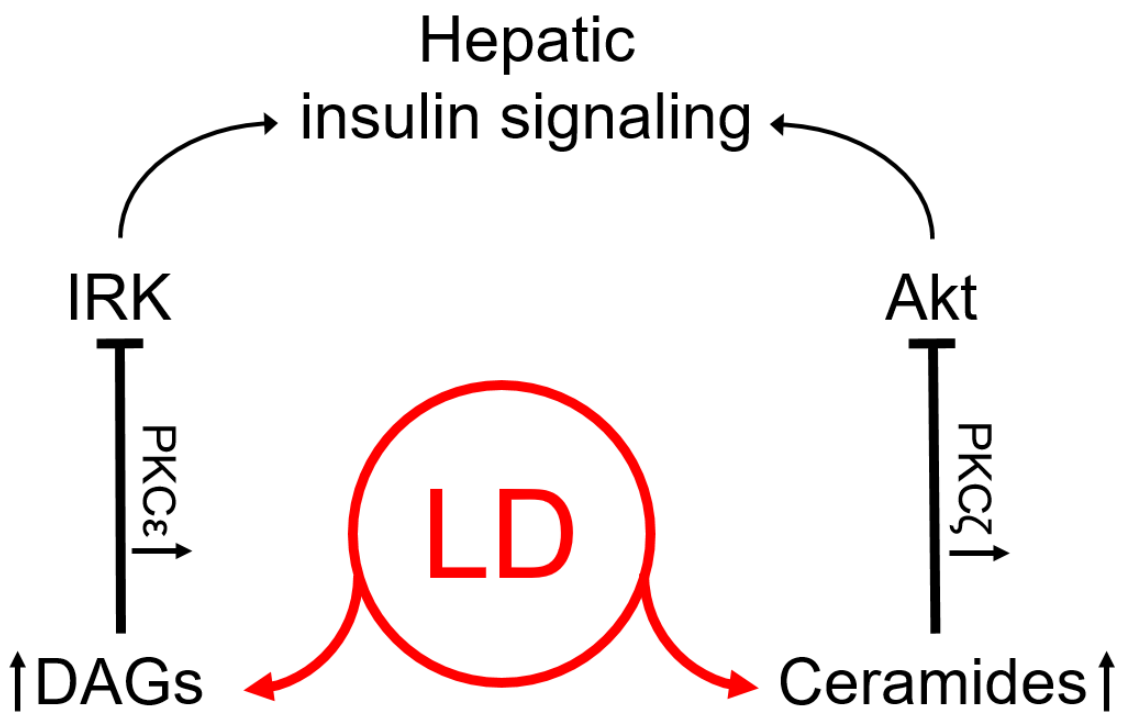

Fig. 4: Lipid droplets couple neutral lipid with sphingolipid metabolism to maintain the cellular lipid homeostasis. Lipid droplets (LD) store fatty acids, the substrate for the ceramide synthesis, in form of TAG or bound as sterol esters. Diacylglycerol (DAG) plays a major role in this context, as it serves as a precursor molecule for TAG or is released from LD through hydrolysis. Both lipids, DAGs and ceramides, interrupt insulin signaling by activating the protein kinases C epsilon and zeta (PKCε, PKCζ). PKCε inhibits the insulin receptor kinase (IRK) domain and PKCζ interrupts the activation of protein kinase B (AKT). Therefore, the maintenance of a balanced availability of the corresponding precursor molecules originating from LDs must be tightly controlled.

1.2 *Saccharomyces cerevisiae* as an alternative model organism to conduct research in lipid metabolism and lipotoxicity

The underlying mechanisms of TAG storage in LD and their link between metabolic diseases are poorly understood. The yeast *S. cerevisiae* represents a convenient *in vivo* model to investigate these mechanisms at the molecular level, since it is an easy handling organism in the laboratory. Genetic manipulations can be generated efficiently and quickly due to the yeast´s high reproduction rate. But most importantly, several cellular processes in yeast, such as lipid metabolism, are similar to those in mammalian cells. In this way, insights into genetic processes or protein functions can be adopted from the unicellular yeast organisms to higher eukaryotes (Mager & Winderickx, 2005). Of note, the mechanism of cholesterol and FA metabolism and the discovery of their regulation via acetyl-coenzyme A has been originally studied in yeast (Lynen, 1952, 1954a, 1954b), providing the basis for clinical and translational research of lipid metabolism disorders including diabetes mellitus. Other work concerning lipotoxicity has shown that excessive accumulation of lipids leads to cellular dysfunction, which can result in impaired cellular signaling, cellular stress responses and ultimately cell death (Garbarino & Sturley, 2009; Petschnigg et al., 2009; Rockenfeller

et al., 2010; Rockenfeller et al., 2018). These findings can also be transferred to humans, confirming that *S. cerevisiae* is a valuable model organism for clinical research (Kachroo et al., 2022).

1.3 Introduction to the world of lipid droplets

All eukaryotic cells are able to store neutral lipids in LDs mostly in form of TAGs but also as sterol esters and this mechanism is evolutionary conserved from yeast to human (Farese & Walther, 2009; Fujimoto & Parton, 2011; Martin & Parton, 2006; Murphy, 2001; Wilfling et al., 2014; Zhang & Liu, 2017). LDs have an important function in preventing lipotoxicity-induced cellular dysfunction and subsequent possible cell death by storing excess cytosolic free FAs (Fakas, Qiu, et al., 2011; Garbarino & Sturley, 2009; Kusminski et al., 2009; Listenberger et al., 2003; Mohammad et al., 2018; Rockenfeller et al., 2010; Rockenfeller et al., 2018). In parallel to the main function of FA storage, important lipid metabolites are released from LDs, which serve as substrate for energy generation and precursor molecule for membrane lipid biogenesis or for secondary signaling molecules involved in intracellular communication (Brady et al., 1969; Czabany et al., 2007; Rajakumari et al., 2008; Wymann & Schneiter, 2008). This insures the survival of the organism during periods of limited nutritional supply.

Compared to other organelles with bilayer membranes, LDs have a unique architecture. The neutral lipid core is sealed by a phospholipid monolayer, which controls the selective binding of proteins to the surface by its unusual properties (Beller et al., 2010; Fujimoto & Parton, 2011; Kohlwein, 2010; Rajakumari et al., 2008; Thiam, Farese, et al., 2013). According to the cell type, nutrient supply and LD life cycle, the LD coating proteins and membrane lipid composition is adapted to the respective situation, which determines the function of the LDs (Beller et al., 2010; Pol et al., 2014). LDs show diversity in size and cellular dispersion and they can either be found unbound in the cytosol or enter into a broad network with other organelles, such as the endoplasmic reticulum (ER), mitochondria, peroxisomes, vacuole (yeast) and lysosome (mammals), that ensures the coordinated exchange of lipid metabolites (Barbosa et al., 2015; Barbosa & Siniossoglou, 2017).

Of note, LDs have important contact to the ER, where LD biosynthesis and bidirectional exchange of metabolites required for phospholipid and Cer synthesis occur (Daum et al., 1998; Walther et al., 2017). In the following chapters, these mechanisms will be discussed in more details.

1.4 Lipid droplet biosynthesis

In yeast, the LD formation starts at the ER, where the responsible enzymes for the neutral lipid synthesis are located (Buhman et al., 2001; Wilfling et al., 2014). Of note, the TAG

synthesis takes place in four reactions in which three FAs are continuously bound to glycerol-3-phosphate (G3P). In the terminal step DAG and an activated FA are converted to TAG, catalyzed by the DAG acyltransferases Dga1p (orthologue of mammalian DGAT2) or Lro1p (orthologue of mammalian LCAT) (Oelkers et al., 2002; Oelkers et al., 2000; Sorger & Daum, 2002). Sterol esters are stored in LD as well and are synthesized by the acyl-coenzyme A:sterol acyltransferases (ASATs) Are1 and Are2 which are orthologues of mammalian acyl-coenzyme A:cholesterolacyltransferases (ACATs) (Jensen-Pergakes et al., 2001). A quadruple deletion of the neutral lipid synthesizing enzymes, Dga1p, Lro1p, Are1p and Are2p results in a lack of LDs with an increased sensitivity to lipotoxicity, suggesting that these proteins are essential for neutral lipid synthesis in yeast (Garbarino & Sturley, 2009). At low concentrations, neutral lipids are localized between the inner and outer leaflets of the ER membrane and at higher concentrations the LD emerge from the ER membrane into the cytosol as nascent LD (Czabany et al., 2007; Gross & Silver, 2014; Jacquier et al., 2011; Mishra et al., 2016; Ohsaki et al., 2014; Wilfling et al., 2014). At early stage, stabilizing proteins such as seipin and Pet10 (perilipin 1 in mammals) attach to the LDs and ensure that the neutral lipid cannot diffuse further into the ER membrane or be degraded prematurely (Graef, 2018). Moreover, stabilizing proteins provide vectorial budding of LD toward the cytosol (Cartwright et al., 2015; Gao et al., 2017). The stage at which certain proteins localize to the LD varies. Some coating proteins bind specifically to the ER during initial LD biosynthesis and shift to LDs in a later development stage, such as Dga1, while others, such as LD-scaffolding PAT domain proteins like perilipins appear only at matured LDs (Jacquier et al., 2011; Londos et al., 1999).

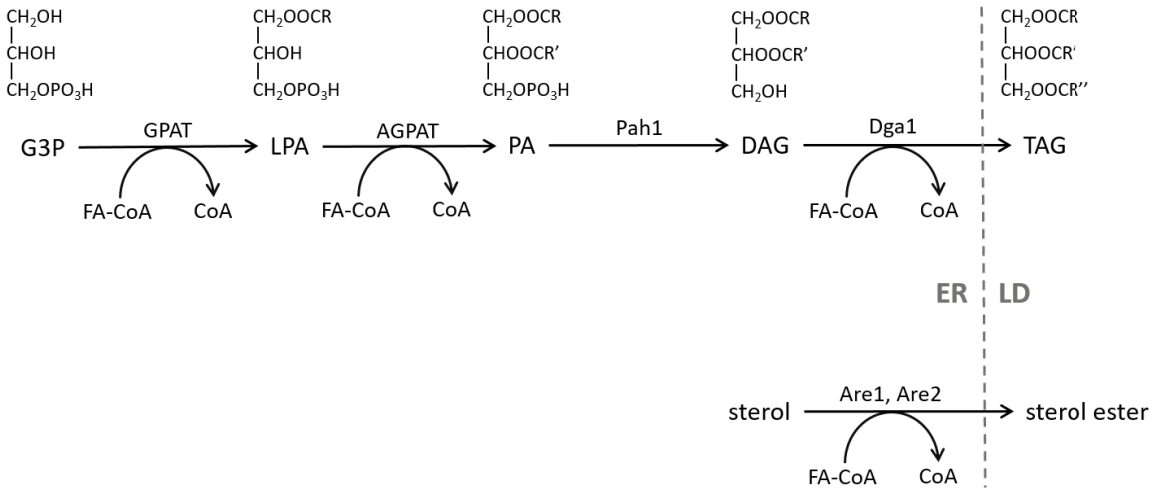

Fig. 5: Neutral lipid biosynthesis in yeast cells. Glycerol-3-phosphate (G3P) is catalyzed in serial steps of esterification with fatty acids to triacylglycerol (TAG) and stored in lipid droplet (LD). Sterols are also esterified to form sterol esters and stored in LD.

A nascent LD grows in size by either taking up more neutral lipids generated by continuous lipogenesis or by lateral fusion of LDs still located in the ER bilayer (Thiam & Foret, 2016).

In this process, coatamer proteins (COPI) residing on the LD surface play an important role by removing phospholipids, thereby increasing LD surface tension and promoting the fusion of LDs with other LD membranes (Thiam, Antonny, et al., 2013). This allows LDs to reach an average size of 0.1 µm to 0.4 µm and rarely exceed a size of 0.5 µm in diameter (Fei et al., 2011). After the growth phase, dissociation of the LD from the ER may occur, whereupon they remain in the cytosol until they are degraded by lipases or lipophagy (Athenstaedt & Daum, 2003, 2005; Kohlwein et al., 2013; van Zutphen et al., 2014).

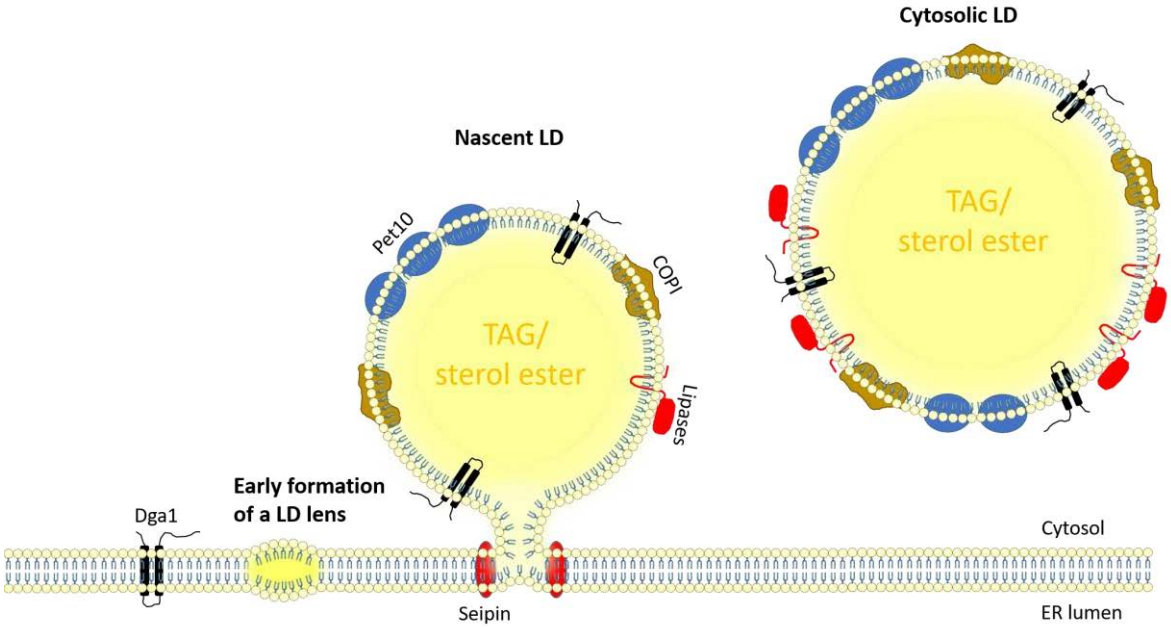

Fig. 6: Schematic model of lipid droplets biogenesis. Triacylglycerol (TAG) and sterol ester synthesis in the ER leads to neutral lipid accumulation between the ER membrane bilayer leaflets and early lipid droplet (LD) lens formation. Further neutral lipid synthesis and accumulation promotes the emergence of a nascent LD with growth toward the cytosol. At this stage, seipin prevents the lateral diffusion of neutral lipids into the ER membrane. Perilipin proteins such as Pet10 are localized to the LD membrane and block early degradation of stored lipids by LD-associated lipases. Matured LDs dissociate from the ER and remain in the cytosol until degradation. Coatamer proteins (COPI) on the LD surface promote the fusion of LD membrane with other organelle membranes.

Storage of nutrient supply in the form of neutral lipid provides a highly efficient way to channel excess lipid intermediates and to support the cell with energy or signaling processes when no nutrients are available in the environment.

1.5 Lipid droplet consumption

Besides the storage of lipids and the processes leading to growth of LD, the mechanisms that control the breakdown and mobilization of neutral lipids are equally crucial. LDs are degraded partially by lipases, which are directly located on the LD surface, or they are completely degraded in vacuoles (in yeast) or in lysosomes (in mammals) via autophagy (Graef, 2018), which can be distinguished in two forms. The first form, the macroautophagy, is featured by the new formation of a double membrane vesicle structure, the autophagosome, which expands during its formation to enclose portions of the cytoplasm,

driven by a multicomponent autophagy core machinery (Boya et al., 2013; Suzuki et al., 2007). After closure, the newly formed outer membrane of the autophagosome fuses with the vacuolar membrane and releases the neutral lipid embedded in the wrapped vesicle into the lumen of the vacuole, where it is degraded by vacuolar hydrolases (Kraft & Martens, 2012; Lamb et al., 2013). Macroautophagy mainly plays a role in the mobilization of neutral lipid in mammalian cells, such as hepatocytes (Martinez-Lopez & Singh, 2015; Singh et al., 2009). In yeast, however, it appears that during the second form of autophagy, the microautophagy, LDs are directly engulfed by the vacuolar membranes, absorbed, and degraded by vacuolar hydrolases (Uttenweiler & Mayer, 2008). Recently, it was demonstrated that lipid microautophagy, so-called lipophagy, does not contribute to LD utilization upon growth resumption. Instead, LD degradation depends on the LD-associated lipases in time of growth resumption (Ouahoud et al., 2018).

TAG degradation is mediated through hydrolysis by the LD-associated TAG lipases Tgl3p, Tgl4p (orthologue of ATGL in mammals) and Tgl5p, ensuring that stored TAG can be rapidly utilized for the synthesis of membrane lipids during periods of growth and cell proliferation (Athenstaedt & Daum, 2003, 2005; Casanovas et al., 2015; Chauhan et al., 2015; Klein et al., 2016; Kurat et al., 2006; Nickels & Broach, 1996; Sia et al., 1996). Palmitate released from LDs by TAG hydrolysis can also be incorporated into Cer synthesis catalyzed by SPT (Hanada, 2003). Release of sterols from LDs is under the control of the sterol ester lipases Tgl1p, Yep1p and Yep2p by hydrolysis of stored sterol esters (Koffel & Schneiter, 2006).

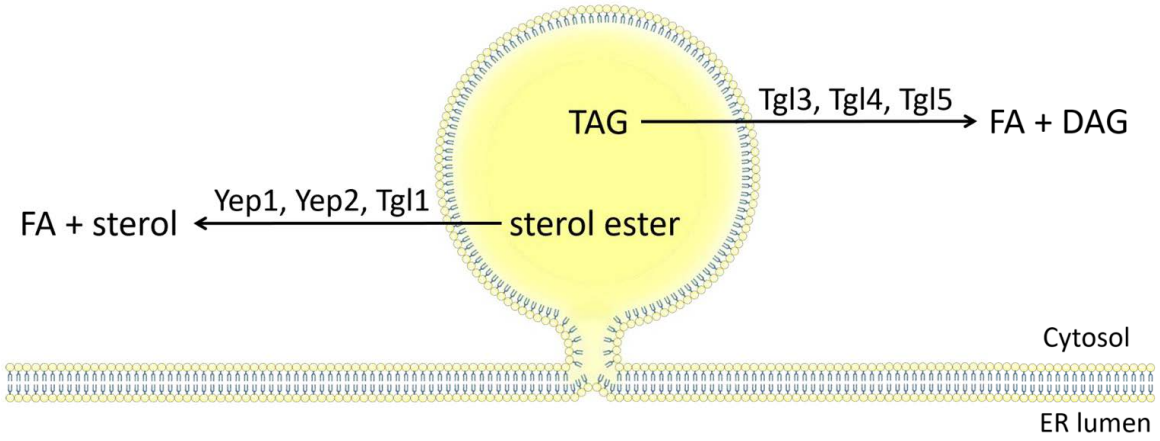

Fig. 7: Schematic illustration of lipolysis driven by triacylglycerol and sterol ester lipases. Triacylglycerol (TAG) is hydrolyzed by triacylglycerol lipases Tgl3, Tgl4 and Tgl5 to yield fatty acid (FA) and diacylglycerol (DAG). Stored sterol ester is degraded by sterol ester lipases Yep1, Yep2, Tgl1.

The lipolysis-derived intermediate product DAG, released from TAG hydrolysis, can be used for the synthesis of phospholipids via two pathways in the ER (Markgraf et al., 2014). In the phospholipid biosynthesis by the cytidine diphosphate pathway (CDP) DAG is converted to phosphatidic acid (PA) by the DAG kinase Dgk1 (Han et al., 2008). In further steps PA can be converted to the phospholipids phosphatidylinositol (PI), phosphatidylserine (PS),

phosphatidylethanolamine (PE) and phosphatidylcholine (PC) (Fakas, Konstantinou, et al., 2011). In the Kennedy pathway, ethanolamine or choline are phosphorylated and finally bound to DAG to generate PE or PC (Carman & Han, 2009). Because the accumulation of DAG is cytotoxic, mechanisms are required to mediate efficient channeling of DAG between the LDs and the ER (Fakas, Konstantinou, et al., 2011). Ice2p is an ER membrane localized protein that mediates physical contact between the LDs and the ER, thereby facilitating the channeling of DAG between the two organelles (Markgraf et al., 2014). Ice2p is the first ER protein identified in this process. In the absence of Ice2, the newly formed DAG catalyzed by TAG lipases remains on the LDs and enters a potentially futile cycle of re-esterification to TAG (Markgraf et al., 2014).

Lipolysis-released FAs can be channeled through inter-organelle contact sites to peroxisome (in yeast) or mitochondria (in mammals and yeast) for ß-oxidation and energy generation during quiescence and growth (Kohlwein et al., 2013; Pu et al., 2011; Rambold et al., 2015). Of particular interest, peroxisome protrusions, known as pexopodia, penetrates the LD core and degrade FA during the ß-oxidation, contributing to efficient energy production (Beller et al., 2010; Binns et al., 2006).

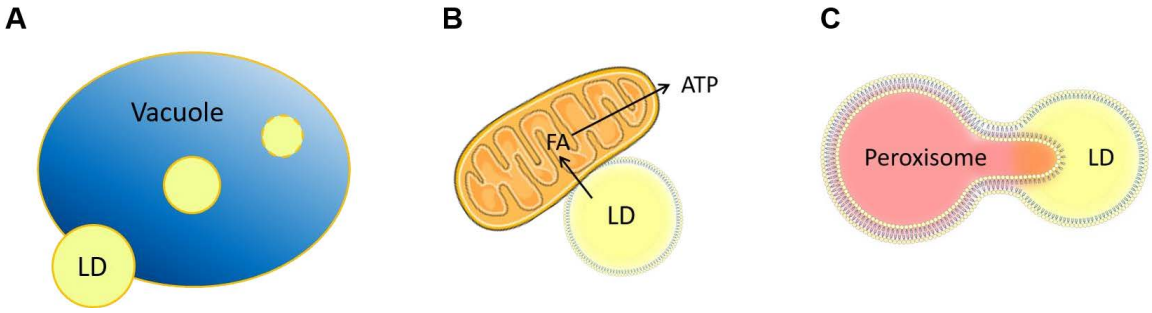

Fig. 8: Lipid droplet (LD) breakdown through LD-organelle interactions. (A) Schematic illustration of lipophagy via LD and vacuole interaction. Absorption of LD by vacuolar membrane invagination for neutral lipid degradation through vacuolar hydrolases. (B) LD-mitochondria membrane connection for channeling of liberated fatty acids (FA) into energy generation pathways. (C) Paroxysmal invasion into LD with pexopodia to support energy production efficiency by enhanced ß-oxidation.

The size and number of the LDs vary dynamically, reflecting the neutral lipids synthesis and their consumption which depends on direct degradation and the exchange of lipids between LD and connected organelles. Yeast generally accumulates large amounts of LDs when the cells enter the stationary phase, whereas lipolytic activity is enhanced during the growth phase, when the demand of membrane lipids for cell growth and division increases (Fei, Shui, et al., 2008; Kurat et al., 2009).

1.6 Sphingolipid biosynthesis

Complex sphingolipids are important components of the lipid bilayer of all eukaryotes by forming lipid rafts in combination with ergosterol (cholesterol in mammals), regulating membrane protein composition and thereby influencing signal transduction (Bagnat &

Simons, 2002; Codini et al., 2021). Various sphingolipid intermediates such as long-chain sphingoid bases (LCB), Cers and their phosphorylation derivatives, play important roles as bioactive secondary signaling molecules and growth regulators in cellular processes such as cell proliferation, differentiation, apoptosis, and heat stress (Chauhan et al., 2015; Ferguson-Yankey et al., 2002; Jenkins et al., 1997). Previous studies in yeast demonstrated that Cers influence cell growth by regulating cell cycle checkpoints and cyclin-dependent kinases upstream of the protein phosphatase 2A (PP2A) (Chauhan et al., 2015; Lucena et al., 2018; Nickels & Broach, 1996; Sia et al., 1996). Sphingolipid synthesis is tightly regulated, and impairment of sphingolipid metabolism is associated with human diseases such as T2D, cancer, heart disease, inflammation and neuropathy (Apostolopoulou et al., 2018; Ogretmen, 2018; Wittenbecher et al., 2022; Ziegler et al., 2021)

The sphingolipid synthesis begins at the cytoplasmic side of the ER, where the serine palmitoyltransferase (SPT), catalyzes the irreversible and rate-limiting step of the sphingolipid synthesis typically by condensation of palmitoyl-CoA and serine to 3-keto-dihydrosphingosine (3KDS) (Cowart & Obeid, 2007; Hanada, 2003). The SPT is a heterodimer composed of a Long-chain base 1 (Lcb1p) and Lcb2p in yeast and SPTLC1, SPTLC2 or SPTLC3 in mammalian cells (Hanada, 2003; Nagiec et al., 1994). SPT encodes proteins that are members of a subfamily of pyridoxal 5'-phosphate-dependent enzymes that catalyze the condensation of an amino acid and a carboxylic acid-CoA thioester with simultaneous decarboxylation of the amino acid (Lowther et al., 2012).

SPT in yeast requires Tsc3p (Temperature-sensitive Suppressors of Calcium Sensitive Growth mutants 3) for optimal activity (Gable et al., 2000). As stimulating subunit, Tsc3 regulates amino acid substrate selectivity by primarily promoting alanine utilization by SPT to form non-canonical 1-deoxy-3KDS and continuous synthesis of deoxy-LCB products (Ren et al., 2018). It was shown that deletion of TSC3 results in decreased incorporation of alanine and increased influx of serine into the sphingolipid synthesis pathway, which confirms that Tsc3p is responsible for an inhibitory effect of alanine on SPT utilization of serine (Ren et al., 2018). The stimulatory subunits of mammalian SPT include two isoforms of the small subunits of SPT, the ssSPTa and ssSPTb, which are defined as functionally homologous of Tsc3, although they do not share sequence homology (Han et al., 2009). Tsc3p is required for the binding of phosphatidylinositol 4-phosphate (PtdIns(4)P) phosphatase Sac1p to SPT (Han et al., 2019). Sac1p, primarily regulates the pool of PtdIns(4)P, thereby modulating substrate supply of PI to Aur1p (phosphatidylinositol:ceramide phosphoinositol transferase in yeast) in subsequent stages of sphingolipid synthesis (Brice et al., 2009; Foti et al., 2001).

However, the mechanism of regulation of SPT activity is not solely dominated by Tsc3. In yeast cells, evolutionary conserved family Orm proteins (Orm1/Orm2) have been shown to

negatively regulate SPT in response to sphingolipid availability (Breslow et al., 2010; Han et al., 2010). The ORMs bind to SPT by interacting with the first transmembrane domain 1 (TMD1) of Lcb1 and thus become components of a multimeric SPOTS complex (Han et al., 2019). The SPOTS complex is termed according to its components SPT, Orms, Tsc3 and Sac1.

In the further progress of sphingolipid biosynthesis, the 3KDS reductase Tsc10p (homolog to human KDS reductase) reduces the condensation product 3KDS through consumption of $NADPH/H^+$ to dihydrosphingosine (DHS) (Gupta et al., 2009). DHS can be converted to sphingosine-1-phosphate (S1P) by Lcb4 and Lcb5 (Nagiec et al., 1998). Moreover, DHS is converted by the C26-ceramide synthases Lag1p (homolog of human ceramide synthase 2), Lac1p (Lag1 paralog) and Lip1p (ceramide synthase subunit) to dihydroceramide (DHC) by an additional N-acetylation of a C26 acyl group (Guillas et al., 2001; Schorling et al., 2001; Vallee & Riezman, 2005). Elongation of C20 to C26 very long chain fatty acids (VLCFA) is accomplished in yeast by an ER membrane-associated system involving the elongases Elo2p and Elo3p (Oh et al., 1997). Deletion of Elo2 and Elo3 results in decreased Cer production, demonstrating the limited substrate specificity of yeast Cer synthases for C26-VLCFAs (Oh et al., 1997).

Mammalian Cers are structurally different from those of yeast. The chain length of incorporated VLCFA consists only of 26 carbons in yeast, whereas 18-24 carbons are used in mammals (Guillas et al., 2001; Levy & Futerman, 2010). In mammalian cells, several Cer synthases 1-6 (CerS 1-6) are responsible for N-acylation of DHS and sphingosine, with high specificity for the length of used acyl-CoA chain (Levy & Futerman, 2010).

All the biosynthetic steps listed so far occur *de novo* in the ER and are highly conserved from yeast to mammals (Rego et al., 2014). Differently to mammal cells, DHS in yeast can be hydroxylated to phytosphingosine (PHS) by the dihydrosphingosine C-4 hydroxylase Sur2p (Haak et al., 1997). PHS is then catalyzed to phytoceramide (PHC) by Lag1p, Lac1p via an amide bound of a C26 acyl group or to phytosphingosine-1-phosphate (PHS1P) by the PHS/DHS kinases Lcb4 and Lcb5 (Megyeri et al., 2019; Nagiec et al., 1998). PHC is converted to the complex sphingolipid inositolphosphorylceramide (IPC) via Aurp1 (Lindahl et al., 2017), which is subsequently modified to further complex sphingolipids like mannosyl-inositolphosphorylceramide (MIPC) by the regulatory subunit CSG2 and mannosyl-diinositolphosphorylceramide (M(IP)2C) by IPC1 in the Golgi (Breslow, 2013; Dickson et al., 2006). The yeast homologue of the mammalian neutral sphingomyelinase Isc1 in return catalyzes the hydrolysis of complex sphingolipids to form a specific C18:1 PHC (Clarke et al., 2006; Matmati & Hannun, 2008; Sawai et al., 2000).

In mammalian cells, Cers are converted to complex sphingolipids in the Golgi, which result in sphingomyelin (SM), glycosphingolipids, and glucosylceramides (Breslow, 2013).

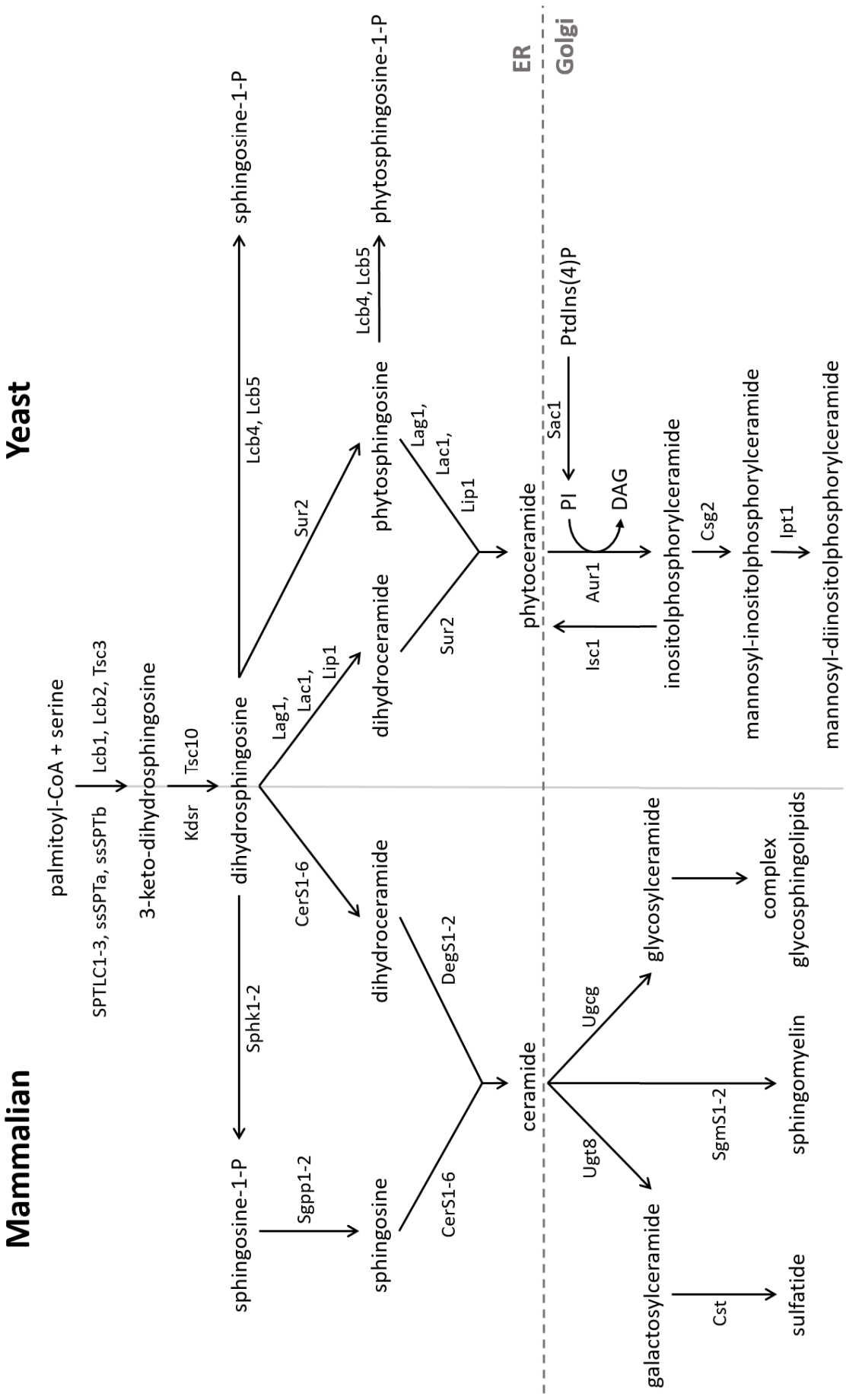
Yeast
Mammalian
palmitoyl-CoA + serine
SPTLC1-3, ssSPTa, ssSPTb
Lcb1, Lcb2, Tsc3
3-keto-dihydrosphingosine
Kdsr
Tsc10
dihydrosphingosine
sphingosine-1-P
Lcb4, Lcb5
phytosphingosine-1-P
Lcb4, Lcb5
Sur2
phytosphingosine
Lag1,
Lac1,
Lip1
dihydroceramide
Sur2
phytoceramide
ER
Golgi
Sac1
PtdIns(4)P
PI
DAG
Aur1
Isc1
inositolphosphorylceramide
Csg2
mannosyl-inositolphosphorylceramide
Ipt1
mannosyl-diinositolphosphorylceramide
Lag1,
Lac1,
Lip1
CerS1-6
dihydroceramide
DegS1-2
Sphk1-2
sphingosine-1-P
Sgpp1-2
sphingosine
CerS1-6
ceramide
Ugcg
glycosylceramide
complex
glycosphingolipids
Ugt8
SgmS1-2
sphingomyelin
galactosylceramide
Cst
sulfatide

Fig. 9: Schematic overview of mammals and yeast sphingolipid metabolism. In both yeast and mammals, the sphingolipid synthesis starts with condensation of serine and palmitoyl catalyzed by SPT to form 3-keto-dihydrosphingosine and further LCB and Cer formations occur at the ER. Cers are transported to the Golgi for complex sphingolipid synthesis and headgroup modifications.

2. Aim of this study

Obesity represents a major risk factor for type 2 diabetes and is characterized by excessive accumulation of TAGs in ectopic tissues, like muscle and liver (Markgraf et al., 2016; Schnurr et al., 2020; Shulman, 2014). At cellular level, TAGs are stored in LDs, which participate in an embracing dynamic network of functionally coupled organelles (Barbosa & Siniossoglou, 2017). LD-ER interaction plays an important role in balancing cellular lipid homeostasis, preventing aggregations of lipotoxic and diabetes-relevant lipids such as DAG and Cers (Greenberg et al., 2011; Krahmer et al., 2013). However, the dynamic interplay between LD consumption and Cer synthesis and how the pathways regulate each other remains unknown.

This work aimed to identify proteins required for sphingolipid synthesis that efficiently regulate LD consumption in order to maintain cellular lipid homeostasis. For this purpose, a flow cytometry-based method was conducted to identify proteins involved in the first steps of sphingolipid synthesis during LD consumption in *S. cerevisiae*. Furthermore, the function of the candidate protein Tsc3p, the human analogs and other LD dynamic regulating proteins were investigated with fluorescence microscopic, biochemical and cell biological methods under different conditions. Based on the results in yeast, lipid composition was investigated in ssSPTb knock-down human hepatoblastoma cell line (HepG2) to unravel if ssSPTb influences lipid induced insulin resistance in human hepatocytes.

3. Materials and Methods

3.1. Materials

3.1.1. Chemicals, consumables and equipment

3.1.1.1. Chemicals

Table 1: Chemicals used in this study

Compound	Source/Company
16% Formaldehyde (w/v), Methanol-free (PFA)	Thermo Fisher Scientific, Waltham, Massachusetts/USA
4x Laemmli sample buffer	BioRad Laboratories Inc., Hercules, California/USA
Acetic acid anhydrous	Merck, Darmstadt, Hesse/Germany
Lipofectamin 3000 Transfection Reagent	Thermo Fisher Scientific, Waltham, Massachusetts/USA
Acetone	Merck, Darmstadt, Hesse/Germany
Fetal Bovine Serum (FBS)	Merck, Darmstadt, Hesse/Germany
Agar-Agar	Roth, Karlsruhe, Baden-Wuerttemberg
Ammonium persulfate (APS)	Merck, Darmstadt, Hesse/Germany
Ampicillin sodium salt	Merck, Darmstadt, Hesse/Germany
Antibiotic-Antimycotic 100X (AA)	Thermo Fisher Scientific, Waltham, Massachusetts/USA
BODIPY FL C16	Thermo Fisher Scientific, Waltham, Massachusetts/USA
BODIPY493/503	Thermo Fisher Scientific, Waltham, Massachusetts/USA
BSA	Applichem GmbH, Darmstadt, Hesse/Germany,
Cerulenin	Merck, Darmstadt, Hesse/Germany
Chloroform	Merck, Darmstadt, Hesse/Germany
Complete supplement mixture (CSM)	MP Biomedicals, Irvine, California/USA
cOmplete tablets (Protease inhibitor)	Roche, Basel/Switzerland

CSM-His	MP Biomedicals, Irvine, California/USA
CSM-Leu	MP Biomedicals, Irvine, California/USA
CSM-Leu-Trp	MP Biomedicals, Irvine, California/USA
CSM-Leu-Ura	MP Biomedicals, Irvine, California/USA
CSM-Trp	MP Biomedicals, Irvine, California/USA
CSM-Ura	MP Biomedicals, Irvine, California/USA
D(+)-Glucose	Merck, Darmstadt, Hesse/Germany
Diemethyl sulfoxide (DMSO)	Merck, Darmstadt, Hesse/Germany
DNA gel loading dye	New England Biolabs, Ipswich, Massachusetts/USA
Ethanol	Merck, Darmstadt, Hesse/Germany
Ethyl acetate	Merck, Darmstadt, Hesse/Germany
Ether	Merck, Darmstadt, Hesse/Germany
Ethylenediaminetetraacetic acid (EDTA)	Roth,Karlsruhe, Baden-Wuerttemberg/Germany
Ethylenediaminetetraacetic acid (EGTA)	Merck, Darmstadt, Hesse/Germany
GelStar nucleic acid stain	Lonza, Basel/Switzerland
Glycerol	Merck, Darmstadt, Hesse/Germany
Glycine	Merck, Darmstadt, Hesse/Germany
Hexane	Merck, Darmstadt, Hesse/Germany
Indole-3-acetic acid (Auxin)	Merck, Darmstadt, Hesse/Germany
Lithium acetate	Merck, Darmstadt, Hesse/Germany
Luria-Bertani (LB) broth, Miller	VWR International GmbH, Damstadt, Hesse/Germany
Methanol	Merck, Darmstadt, Hesse/Germany
Methylene chloride	Merck, Darmstadt, Hesse/Germany
N'N'N'N Tetramethylethylendiamine (TEMED)	Merck, Darmstadt, Hesse/Germany

Nonidet P40 solution 10 %	Applichem GmbH, Darmstadt, Hesse/Germany
PBS tablets	Merck, Darmstadt, Hesse/Germany
PBS sterile (pH 7.4)	Merck, Darmstadt, Hesse/Germany
Phenylmethyl-sulfonyl-fluoride (PMSF)	Merck, Darmstadt, Hesse/Germany
PhosStop (Phosphatase inhibitor)	Roche, Basel/Switzerland
Phytosphingosine hydrochloride (PHS)	Merck, Darmstadt, Hesse/Germany
Skim milk powder	Merck, Darmstadt, Hesse/Germany
Sodium dodecyl sulfate (SDS) pellets	Roth, Karlsruhe, Baden-Wuerttemberg/Germany
ß-Mercaptoethanol	Merck, Darmstadt, Hesse/Germany
Sucrose	Merck, Darmstadt, Hesse/Germany
Tergitol (NP-40, 70 % H_2O	Merck, Darmstadt, Hesse/Germany
Triton-X100	Merck, Darmstadt, Hesse/Germany
0.25 % Trypsin-EDTA	Thermo Fisher Scientific, Waltham, Massachusetts/USA
Trizma base (Tris base)	Merck, Darmstadt, Hesse/Germany
Trizma hydrochloride (Tris-HCl)	Merck, Darmstadt, Hesse/Germany
Tween 20	Merck, Darmstadt, Hesse/Germany
YNB with ammonium sulfate	MP Biomedicals, Irvine, California/USA
Yeast extract peptone dextrose (YPD) broth	Merck, Darmstadt, Hesse/Germany
30% Acrylamide, 0.8% Bisacrylamide	Merck, Darmstadt, Hesse/Germany

3.1.1.2. Kits

Table 2: Kits used in this study

Kit	Company
QIAquick PCR Purification Kit:	Qiagen, Hilden, NRW/Germany

QIAquick Gel Extraction Kit:	Qiagen, Hilden, NRW/Germany
Plasmid DNA Purification Kit:	iNtRON Biotechnology, Seongnam, Gyeonggi/Republic of Korea
QuantiTect Reverse Transcription Kit:	Qiagen, Hilden, NRW/Germany
Mix2Seq Kit:	Eurofins genomics, Ebersberg, Bavaria/Germany
Lipofectamine 3000	Thermo Fisher Scientific, Waltham, Massachusetts/USA
Pierce BCA Protein Assay Kit	Thermo Fisher Scientific, Waltham, Massachusetts/USA

3.1.2. Buffers and stock solutions

Ampicillin

Stock solution: dissolved in H_2O to 100 mg/ml and stored at -20 °C.

Ammonium persulfate (APS)

For 10 % stock solution 10 mg/ml were dissolved in H_20 and stored at -20 °C.

Cerulenin

Stock solution: dissolved in ethanol to 10 mg/ml and stored at -20 °C.

EDTA

For 125 mM stock solution 36.53 mg/ml were dissolved in H_20 and stored at 4 °C.

EGTA

For 10 mM stock solution 3.8 mg/ml were dissolved in H_20 and stored at 4 °C.

Indole-3-acetic acid (Auxin)

For 5.71 mM stock solution 1 mg/ml were dissolved in ethanol and stored at -20 °C.

Myriocin

For 2.5 mM stock solution 1 mg/ml was dissolved in DMSO stored at -20 °C.

29.2 % NaCl solution

For 5 M stock solution 292 g/l were dissolved in H_2O and stored at 4 °C.

Nonidet P40

For 5 % Stock solution 10 ml 10 % Nonidet P40 solution was mixed with 10 ml H_2O and stored at 4 °C.

Phytosphingosine (PHS)

For 5.65 mM stock solution 5 mg was dissolved in 2.5 ml ethanol and stored at -20 °C.

Salmon sperm ssDNA

Stock solution: Dissolved by denaturation for 5 min at 95°C in H_2O to 2 mg/ml and stored at -20°C

Sodium dodecyl sulfate (SDS) solution

For 10 % Stock solution 10 g/l were dissolved in H_2O and stored at RT.
For 20 % Stock solution 20 g/l were dissolved in H_2O and stored at RT.

Sucrose

For 1 M Stock solution 342.3 g/l were dissolved in H_2O and stored at 4 °C

Tris buffered saline (TBS)

Tris base 20 mM (pH 7.5)
NaCl 150 mM

TBS Tween20 (TBST)

Tris base 20 mM (pH 7.5)
NaCl 150 mM
0.1 % Tween20

Total lipid extraction (TLE)

Tris-HCL 20 mM (pH 7.5)
EDTA 1 mM
EGTA 0.25 mM
Sucrose 250 mM
Protease inhibitor 1 tablet/25 ml

Tris-HCl

For 0.5 M Stock solution 60.57 g/l were dissolved in H_2O and stored at RT (adjusted to pH 6.8).

For 1 M Stock solution 121.14 g/l were dissolved in H_2O and stored at 4 °C (adjusted to pH 7.4).
For 1.5 M Stock solution 181.71 g/l were dissolved in H_2O and stored at RT (adjusted to pH 8.8).

50x TAE
242 g Tris base
57.1 ml acetic acid
100 ml 0.5 M EDTA (pH 8.0)
Fill till 1 l with H_2O

10x SDS running buffer (yeast experiments)
30 g Tris base
144 g glycine
10 g SDS
Fill till 1 l with H_2O (adjust to pH 8.3)

Premixed SDS running buffer for HepG2 experiments was ordered from BioRad (10x Tris/Glycine/SDS).

Western Blot transfer buffer (yeast experiments)
3 g Tris base
14.4 g glycine
Fill till 800 ml with H_2O
Add 200 ml methanol

Premixed Western Blot transfer buffer for HepG2 experiments were ordered from BioRad (10x Tris/Glycine). 10 % SDS (3.7 ml/l) and methanol (200 ml/l) were added prior to use.

RIPA buffer
Tris-HCl 50 mM
NaCl 150 mM
EDTA 1 mM
Nonidet P40 1 % (v/v)
SDS 0.1 % (g/v)
Protease inhibitor and PhoStop tablets were added to the solution before use.

Buffer A of isolation membrane/cytosol

Tris-HCl 20 mM

EGTA 0.25 mM

EDTA 1 mM

Sucrose 250 mM

Protease inhibitor and PhoStop tablets were added to the solution before use.

Buffer B of isolation membrane/cytosol

Tris-HCl 250 mM

EGTA 0.25 mM

EDTA 1 mM

Triton-X100 2%

Protease inhibitor and PhoStop tablets were added to the solution before use.

3.1.3. Media

Luria-Bertani (LB)

8 g LB broth powder was dissolved in 1 l with H_2O and autoclaved

Synthetic Minimal Media (SD)

6.7 g of YNB with ammonium salt with required amount of CSM and 20 g glucose was dissolved in 1 l with H_2O. Prior to autoclave the medium was adjusted to pH of 5.5.

Yeast extract peptone dextrose (YPD)

50 g of YPD broth powder was dissolved in 1 l with H_2O and autoclaved.

Agar growth plates

For pouring LB, SD or YPD plates 20 g agar were supplemented prior to autoclave.

HepG2 complete medium

Dulbecco's Modified Eagle Medium (DMEM) containing 1 g/l D-glucose, L-glutamine, 25 mM HEPES and pyruvate was supplemented with 10 % Fetal Bovine Serum (FBS) and 1 % Antibiotic-Antimycotic (AA).

3.1.4. DNA- and protein markers

Table 3: DNA marker used in this study

DNA ladder	Band length in kilo base	Company
GeneRuler 1kb	10, 8, 6, 5, 4, 3.5, 3, 2.5, 2, 1.5, 1, 0.75, 0.5, 0.25	Li-Cor Biosciences, Lincoln, Nebraska/USA

Table 4: Protein markers used in this study

Protein-Marker	Band length in kilo Dalton	Company
Chameleon Duo	260, 160, 125, 90, 70, 50, 38, 30, 25, 15, 8	Li-Cor Biosciences, Lincoln, Nebraska/USA
Blue Prestained Protein Standard, Broad Range	250, 180, 130, 95, 72, 55, 43, 34, 26, 17, 11	New England Biolabs, Ipswich, Massachusetts/USA

3.1.5. *Escherichia coli* strains

For transfection, preservation and amplification of generated plasmids the *Escherichia coli* (*E. coli*) strain MacCell competent DH5α cells with the genotype F^- Φ80*lac*ZΔM15 Δ(*lac*ZYA-*arg*F) U169 *rec*A1 *end*A1 *hsd*R17(r_k^-, m_k^+) *pho*A *sup*E44 *thi*-1 *gyr*A96 *rel*A1 λ^- (iNtRON Biotechnology, Seongnam, Gyeonggi/Republic of Korea) was used.
Vector backbone pBluescriptR carrying cDNA of human ssSPT isoforms were transformed into DH10B *E. coli* cells, which were ordered from Horizon Discovery (Waterbeach, Cambridgeshire/ United Kingdom).

3.1.6. Plasmids

The plasmids used in this study are listed in table 5. To generate plasmids carrying C-terminal green fluorescent protein (GFP)-tagged ssSPTa and ssSPTb, ssSPT isoforms were amplified from mammalian gene collection (MGC) of human Sequence-Verified cDNA (Dharmacon, Lafayette, Colorado/USA), digested with SmaI/SpeI (New England Biolabs (NEB), Ipswich, Massachusetts/USA) and ligated into the SmaI/SpeI restriction sites of a pRS415 vector, controlled by a constitutive alcohol dehydrogenase (ADH) promoter (pRS415-ADHpr-GFP). For C-terminal triple hemagglutinin (3HA)-tagged ssSPTb, ssSPTb was amplified from MGC human ssSPTb Sequence-Verified cDNA (Dharmacon). The ssSPTb PCR product was digested with SpeI/SmaI and ligated into plasmid pRS415-ADHpr-3HA which was digested the same way. To generate a plasmid carrying C-terminal GFP-tagged Tsc3, Tsc3 was amplified from genomic DNA, digested with BamHI-HF/XbaI

(NEB) and ligated into plasmid pRS415-ADHpr-GFP previously digested the same way. For plasmid carrying C-terminal 3HA-tagged Tgl3, Tgl3 was amplified from genomic DNA and digested with SpeI /HindIII and ligated into SpeI/HindIII sites of pRS415-ADHpr-3HA. Lcb1 was genomically tagged at the C-terminus using an AID-6HA-pHyg cassette amplified from pBW2744-pHyg AID 71-114-6HA (Morawska & Ulrich, 2013). Lcb1-AID-6HA tagging was integrated by homologous recombination of the PCR product AID-6HA-pHyg into SEY6210 pRS305_OsTIR_3xFLAG background strain (Robinson et al., 1988; Serbyn et al., 2020).

Table 5: Plasmids used in this study

Plasmid ID	Description	Source
133	pRS415-ADHpr	(Nguyen et al., 2012)
87	ss-RFP-HDEL	(Prinz et al., 2000)
123	pRS415-ADHpr-GFP	(Markgraf et al., 2014)
185	pRS415-ADHpr-Dga1-GFP	(Markgraf et al., 2014)
277	pRS415-ADHpr-Tgl3-3HA	This study
278	pRS415-ADHpr-Tsc3-GFP	This study
309	pRS415-ADHpr-ssSPTb-3HA	This study
310	pRS415-ADHpr-ssSPTa-GFP	This study
312	pRS415-ADHpr-ssSPTb-GFP	This study
304	pBluescriptR-ssSPTa	Horizon Discovery, Waterbeach, Cambridgeshire/ United Kingdom
305	pBluescriptR-ssSPTb	Horizon Discovery, Waterbeach, Cambridgeshire/ United Kingdom
281	pRS305_OsTIR_3xFLAG	Serbyn et al. 2020 Mol Cell
279	pBW2744- pHyg AID 71-114-6HA	Morawska 2013

3.1.7. Primers

Table 6: Primers used in this study

Primer	Alignment	Sequence
5’ Tsc3 (XbaI)	forward	5’- GCtctaga ATG ACA CAA CAT AAA AGC TCG
3’ Tsc3 (Bam-HI)	reverse	5’- CGCggatcc AAG GAA GCA ATA CTT TAG TAT

5’ ssSPTa (SpeI)	forward	5’ - GCactagt ATG GCG GGG ATG GCG CTG GCG
3’ ssSPTa (SmaI)	reverse	5’ - TCCcccggg TTG TAG TTC AAA GTA GTG
5’ ssSPTb (SpeI)	forward	5’ - GCactagt ATG GAT TTG AGG CGT GTG AAG G
3’ ssSPTb (SmaI)	reverse	5’ - TCCcccggg ATT AGA AAT TGT ACT GTG
Hs_ssSPTb_1_SG	QuantiTect Primer Assay (Primer mix validated by Qiagen, Hilden, NRW/Germany)	
Hs_TUBB_1_SG	QuantiTect Primer Assay (Primer mix validated by Qiagen, Hilden, NRW/Germany)	
5’ Lcb1 CT Knop	forward	5' - A AGT GTC AAG CAG TCC ATC CTT GCC TGT TGC CAA GAA TCT AAT AAA CGTACGCTGCAGGTCGAC
3’ Lcb1 CT Knop	reverse	5' - A TTT ATA TAT ATA TGT GCG TGT GCA TAT ACT GGC TTT CTA TTT TTA ATCGATGAATTCGAGCTCG
5’ Tgl3 (SpeI)	forward	5’ - Ggactagt ATG AAG GAA ACG GCG CAG GAA TAC
3’ Tgl3 (HindIII)	reverse	5' - CCCaagctt CCT ACT CCG TCT TGC TCT TAT TAT G
5’ GFP (HindIII)	forward	5’ - CCCaagctt ATG AGT AAA GGA GAA GAA CT
3’ GFP (XhoI)	reverse	5’ - CCGctcgag TTA TTT GTA TAG TTC ATC CAT G

3.1.8. Restriction enzymes

Table 7: Restriction enzymes used in this study

Enzyme	Company
BamHI-HF	New England Biolabs, Ipswich, Massachusetts/USA
HindIII	New England Biolabs, Ipswich, Massachusetts/USA
XhoI	New England Biolabs, Ipswich, Massachusetts/USA
SmaI	New England Biolabs, Ipswich, Massachusetts/USA
SpeI	New England Biolabs, Ipswich, Massachusetts/USA
XbaI	New England Biolabs, Ipswich, Massachusetts/USA

3.1.9. *S. cerevisiae* strains

Yeast strains used in this study are genetically identical to a BY4741 (*MAT* **a**; *his3Δ1; leu2Δ0; met15Δ0; ura3Δ0*) background, except strain SEY6210 pRS305_OsTIR_3xFLAG (table 8). Endogenous sequence-tagging was performed by homologous recombination of an integrative PCR construct (Longtine et al., 1998). As indicated, non-essential gene knock-out strains were used from a deletion library of Open Biosystems (Huntsville, Alabama/USA).

Table 8: Yeast strains used in this study

Strain ID	Genotype	Source
BY4741	*MAT* **a**; *his3Δ1 leu2Δ0 met15Δ0 ura3Δ0*	Brachmann et *al* 1998
BY4741 *csg2Δ*	*MAT* **a**; *his3Δ1*; *leu2Δ0*; *met15Δ0*; *ura3Δ0*; *CSG2::kanMX*	yeast deletion library - Open Biosystems GE Dharmacon
BY4741 *ipt1Δ*	*MAT* **a**; *his3Δ1*; *leu2Δ0*; *met15Δ0*; *ura3Δ0*; *IPT1::kanMX*	yeast deletion library - Open Biosystems GE Dharmacon
BY4741 *lac1Δ*	*MAT* **a**; *his3Δ1*; *leu2Δ0*; *met15Δ0*; *ura3Δ0*; *LAC1::kanMX*	yeast deletion library - Open Biosystems GE Dharmacon
BY4741 *lag1Δ*	*MAT* **a**; *his3Δ1*; *leu2Δ0*; *met15Δ0*; *ura3Δ0*; *LAG1::kanMX*	yeast deletion library - Open Biosystems GE Dharmacon
BY4741 *lcb3Δ*	*MAT* **a**; *his3Δ1*; *leu2Δ0*; *met15Δ0*; *ura3Δ0*; *LCB3::kanMX*	yeast deletion library - Open Biosystems GE Dharmacon
BY4741 *lcb4Δ*	*MAT* **a**; *his3Δ1*; *leu2Δ0*; *met15Δ0*; *ura3Δ0*; *LCB4::kanMX*	yeast deletion library - Open Biosystems GE Dharmacon
BY4741 *lcb5Δ*	*MAT* **a**; *his3Δ1*; *leu2Δ0*; *met15Δ0*; *ura3Δ0*; *LCB5::kanMX*	yeast deletion library - Open Biosystems GE Dharmacon
BY4741 *orm1Δ*	*MAT* **a**; *his3Δ1*; *leu2Δ0*; *met15Δ0*; *ura3Δ0*; *ORM1::kanMX*	yeast deletion library - Open Biosystems GE Dharmacon
BY4741 *orm2Δ*	*MAT* **a**; *his3Δ1*; *leu2Δ0*; *met15Δ0*; *ura3Δ0*; *ORM2::kanMX*	yeast deletion library - Open Biosystems GE Dharmacon
BY4741 *sac1Δ*	*MAT* **a**; *his3Δ1*; *leu2Δ0*; *met15Δ0*; *ura3Δ0*; *SAC1::kanMX*	yeast deletion library - Open Biosystems GE

		Dharmacon
BY4741 *scs7*Δ	*MAT* **a**; *his3*Δ*1*; *leu2*Δ*0*; *met15*Δ*0*; *ura3*Δ*0*; *SCS7::kanMX*	yeast deletion library - Open Biosystems GE Dharmacon
BY4741 *sur1*Δ	*MAT* **a**; *his3*Δ*1*; *leu2*Δ*0*; *met15*Δ*0*; *ura3*Δ*0*; *SUR1::kanMX*	yeast deletion library - Open Biosystems GE Dharmacon
BY4741 *sur2*Δ	*MAT* **a**; *his3*Δ*1*; *leu2*Δ*0*; *met15*Δ*0*; *ura3*Δ*0*; *SUR2::kanMX*	yeast deletion library - Open Biosystems GE Dharmacon
BY4741 *tgl4*Δ	*MAT* **a**; *his3*Δ*1*; *leu2*Δ*0*; *met15*Δ*0*; *ura3*Δ*0*; *TGL4::kanMX*	yeast deletion library - Open Biosystems GE Dharmacon
BY4741 *tsc3*Δ	*MAT* **a**; *his3*Δ*1*; *leu2*Δ*0*; *met15*Δ*0*; *ura3*Δ*0*; *TSC3::kanMX*	yeast deletion library - Open Biosystems GE Dharmacon
BY4741 *ydc1*Δ	*MAT* **a**; *his3*Δ*1*; *leu2*Δ*0*; *met15*Δ*0*; *ura3*Δ*0*; *YDC1::kanMX*	yeast deletion library - Open Biosystems GE Dharmacon
BY4741 *ypc1*Δ	*MAT* **a**; *his3*Δ*1*; *leu2*Δ*0*; *met15*Δ*0*; *ura3*Δ*0*; *YPC1::kanMX*	yeast deletion library - Open Biosystems GE Dharmacon
BY4741 *ysr3*Δ	*MAT* **a**; *his3*Δ*1*; *leu2*Δ*0*; *met15*Δ*0*; *ura3*Δ*0*; *YSR3::kanMX*	yeast deletion library - Open Biosystems GE Dharmacon
YDM288	*MAT* **a**; *his3*Δ*1*; *leu2*Δ*0*; *met15*Δ*0*; *ura3*Δ*0*; TGL3::3HA-KanMX	(Markgraf et al., 2014)
YDM484	*MAT* **a**; *his3*Δ*1*; *leu2*Δ*0*; *met15*Δ*0*; *ura3*Δ*0*; *TSC3::kanMX* pRS415	(Ouahoud et al., 2018)
YDM351	*MAT* **a**; *his3*Δ*1*; *leu2*Δ*0*; *met15*Δ*0*; *ura3*Δ*0*; pRS415-ADHpr-Dga1-GFP	(Markgraf et al., 2014)
YDM658	*MAT* **a**; *his3*Δ*1*; *leu2*Δ*0*; *met15*Δ*0*; *ura3*Δ*0*; pRS415	This study
YDM661	*MAT* **a**; *his3*Δ*1*; *leu2*Δ*0*; *met15*Δ*0*; *ura3*Δ*0*; *TSC3::kanMX* pRS415	This study
YDM667	*MAT* **a**; *his3*Δ*1*; *leu2*Δ*0*; *met15*Δ*0*; *ura3*Δ*0*; pRS415-ADHpr-Tgl3-3HA	This study
YDM726	SEY6210 *MAT α; leu2-3,112; ura3-52; his3-Δ200; trp1-Δ901; suc2-Δ9; lys2-801; GAL LEU2*::pRS305_OsTIR-3xFLAG	(Robinson et al., 1988; Serbyn et al., 2020)

YDM728	*MAT* **a**; *his3*Δ*1*; *leu2*Δ*0*; *met15*Δ*0*; *ura3*Δ*0*; *TSC3::kanMX* pRS415-ADHpr-Tsc3-GFP	This study
YDM731	*MAT* **a**; *his3*Δ*1*; *leu2*Δ*0*; *met15*Δ*0*; *ura3*Δ*0*; *TSC3::kanMX* pRS415-ADHpr-Dga1-GFP	This study
YDM736	*MAT* **a**; *his3*Δ*1*; *leu2*Δ*0*; *met15*Δ*0*; *ura3*Δ*0*; *TSC3::kanMX* TGL3::3HA-HIS3	This study
YDM737	*MAT* **a**; *his3*Δ*1*; *leu2*Δ*0*; *met15*Δ*0*; *ura3*Δ*0*; *TSC3::kanMX* pRS415-ADHpr-Tgl3-3HA	This study
YDM745	SEY6210 *MAT α; leu2-3,112; ura3-52; his3-Δ200; trp1-Δ901; suc2-Δ9; lys2-801; GAL LEU2*::pRS305_OsTIR-3xFLAG; Lcb1-AID-6HA	This study
YDM768	*MAT* **a**; *his3*Δ*1*; *leu2*Δ*0*; *met15*Δ*0*; *ura3*Δ*0*; pRS415-ADHpr-ssSPTb-3HA	This study
YDM770	*MAT* **a**; *his3*Δ*1*; *leu2*Δ*0*; *met15*Δ*0*; *ura3*Δ*0*; *TSC3::kanMX* pRS415-ADHpr-ssSPTb-3HA	This study
YDM771	*MAT* **a**; *his3*Δ*1*; *leu2*Δ*0*; *met15*Δ*0*; *ura3*Δ*0*; pRS415-ADHpr-ssSPTa-GFP	This study
YDM772	*MAT* **a**; *his3*Δ*1*; *leu2*Δ*0*; *met15*Δ*0*; *ura3*Δ*0*; *TSC3::kanMX* pRS415-ADHpr-ssSPTa-GFP	This study
YDM773	*MAT* **a**; *his3*Δ*1*; *leu2*Δ*0*; *met15*Δ*0*; *ura3*Δ*0*; *TRP1::HygB* pRS415-ADHpr-ssSPTa-GFP + ss-RFP-HDEL	This study
YDM774	*MAT* **a**; *his3*Δ*1*; *leu2*Δ*0*; *met15*Δ*0*; *ura3*Δ*0*; *TRP1::HygB* pRS415-ADHpr-ssSPTb-GFP + ss-RFP-HDEL	This study
YDM777	*MAT* **a**; *his3*Δ*1*; *leu2*Δ*0*; *met15*Δ*0*; *ura3*Δ*0*; *TRP1::HygB* pRS415-ADHpr-Tsc3-GFP + ss-RFP-HDEL	This study

3.1.10. Antibodies used for immunodetection

Table 9: Antibodies used in this study

Antibody	Company
IRDye 800CW Goat anti-Mouse IgG secondary Antibody	Li-Cor Biosciences, Lincoln, Nebraska/USA
Mouse Anti-HA monoclonal (16B12)	Biolegend, San Diego, California/USA
Mouse Anti-Pgk1 monoclonal	Thermo Fisher Scientific, Waltham,

(22C5D8)	Massachusetts/USA
Mouse Anti-GFP monoclonal (JL-8)	Takara Bio, Kusatsu, Shiga/Japan
Rabbit Anti-SPTSSB polyclonal	Thermo Fisher Scientific, Waltham, Massachusetts/USA
Rabbit Anti-Insulin Receptor β monoclonal (4B8)	Cell Signaling Technology, Danvers, Massachusetts/USA
Rabbit Anti-Phospho-INSR (Thr1160) polyclonal	Thermo Fisher Scientific, Waltham, Massachusetts/USA
Goat Anti-rabbit IgG (HRP-linked) secondary Antibody	Cell Signaling Technology, Danvers, Massachusetts/USA
Horse Goat Anti-mouse IgG (HRP-linked) secondary Antibody	Cell Signaling Technology, Danvers, Massachusetts/USA
Rabbit Anti-GAPDH monoclonal (14C10)	Cell Signaling Technology, Danvers, Massachusetts/USA
Rabbit Anti- Na-K-ATPase polyclonal	Cell Signaling Technology, Danvers, Massachusetts/USA
Mouse Anti-PKCε monoclonal (21/PKCε)	BD Biosciences, Franklin Lakes, NJ/USA

3.1.11. Technical equipment

Autoclave

Tuttnauer 2840EL	Tuttnauer, Breda, Norrd Brabant/Netherlands

Homogenizer

Tissue glass douncer	DWK Life Sciences, Baden-Wurttemberg/Germany
Pellet pestle motor	Kimble Chase Life Science, Vineland, NJ/USA

Imaging system

Chemie Doc XRS+	Bio-Rad Laboratories Inc., Hercules, California/USA
Odyssey CLx	Li-Cor Biosciences, Lincoln, Nebraska/USA

Incubators

Binder CB	Binder, Innsbruck, Tirol/Austria
BBD 6220	Thermo fisher scientific, Waltham, Massachusetts/USA
Innova 44	New Brunswick Scientific, Edison, NJ/USA

Power supplies

PS300B	Hoefer Inc., Holliston, Massachusetts/USA
PowerPac Basic	Bio-Rad Laboratories Inc., Hercules, California/USA

Blotting systems

TE22	Hoefer Inc., Holliston, Massachusetts/USA
Trans-Blot Turbo	Bio-Rad Laboratories Inc., Hercules, California/USA

Protein electrophoresis chambers

SE250 Mighty Small II	Hoefer Inc., Holliston, Massachusetts/USA
Mini-PROTEAN Tetra Cell	Bio-Rad Laboratories Inc., Hercules, California/USA

DNA electrophoresis chambers

HE 33 Mini Submarineo	Hoefer Inc., Holliston, Massachusetts/USA

Magnetic stirrer-heatplates

IKA Combimag Ret	IKA, Staufen, Baden-Wuerttemberg/Germany
VMS-C10	VWR, Radnor, Pennsylvania/USA

PCR

GeneAMP PCR System 9700	Applied Biosystems, Waltham, Massachusetts/USA
C1000 Touch Thermal cycler	Bio-Rad Laboratories Inc., Hercules, California/USA

RT-qPCR

StepOnePlus RT-PCR System	Applied Biosystems, Waltham, Massachusetts/USA

pH-Meter

PHM220 MeterLab	Radiometer Analytical, Lyon, Rhône-Alpes/France

Shakers

IKA Rocker 2D Basic	IKA, Staufen, Baden-Wurttemberg/Germany
Titramax 100	Heidolph, Schwabach, Bavaria/Germany
IKA Vibrax Overhead shacker	IKA, Staufen, Baden-Wuerttemberg/Germany

Sterile bench	
HERAsafe KS	Thermo fisher scientific, Waltham, Massachusetts/USA
Safety hood	
CC-30	Caspar & Co. Labora, Aachen, NRW/Germany
UV-VIS spectrophotometer	
NanoDrop 2000	Thermo fisher scientific, Waltham, Massachusetts/USA
Bio Photometer Plus	Eppendorf, Hamburg, Hamburg/Germany
Centrifuges	
Allegra X-30R	Beckman Coulter, Brea, California/USA
CompactStar CS 4	VWR, Radnor, Pennsylvania/USA
Mini Spin	Eppendorf, Hamburg, Hamburg/Germany
Z 216 MK	Hermle, Goshiem, Baden-Wuerttemberg/Germany
MIKRO 220R	Andreas Hettich GmbH & Co. KG, Tuttlingen, baden-Wuerttemberg/Germany
CVP-2	Grant Instruments, Shepreth, Cambridgeshire/ United Kingdom
Optima MAX-XP Ultracentrifuge	Beckman Coulter, Brea, California/USA
Centrifuge rotors	
Swinging-bucket tube rotor SX4400	Beckman Coulter, Brea, California/USA
Swinging-bucket microplate rotor S6096	Beckman Coulter, Brea, California/USA
TLA-55	Beckman Coulter, Brea, California/USA
Water bath	
Julabo SW 22	Julabo GmbH, Seelbach, Baden-Wuerttemberg/Germany
Flow Cytometry	
FACScalibur	BD Biosciences, Franklin Lakes, NJ/USA
HTS 96-well autosampler	BD Biosciences, Franklin Lakes, NJ/USA

Microscopes

Primovert	Carl Zeiss AG, Oberkochen, Baden-Wuerttemberg/Germany
LSM 880 Airyscan	Carl Zeiss AG, Oberkochen, Baden-Wuerttemberg/Germany

Multi-function plate reader

Infinite Pro 200	TECAN, Maennedorf, Zurich/Switzerland

Liquid Chromatography - Mass Spectrometry and Liquid Chromatography - Tandem Mass Spectrometry (LC-MS/MS)

LC-MS QQQ 6495	Agilent Technologies Inc., Santa Clara, California/USA

Heat block shaker

Thermomixer Compact	Eppendorf, Hamburg, Hamburg/Germany

3.2. Methods

3.2.1. Molecular cloning in *E. coli* and *S. cerevisiae*

3.2.1.1. Polymerase chain reaction

Amplification of gene sequences were generated by polymerase chain reaction (PCR) (Mullis & Faloona, 1987). In briefly, double strand DNA template denaturates at 98 °C by breaking of the hydrogen bounds between bases. Following cool down to 55 °C allows primers (listed in table 6) with complementary nucleic acid sequence to anneal at 3' ends on both single strand DNA templates in the gene target region. Elevating temperature to 72 °C activates thermostable DNA polymerase to elongate the gene target region from 5'-3' by condensing the dNTPs 5'-phosphate group with the 3'-hydroxy group of the template strand. Once the synthesis of new complimentary DNA strand is completed, templates are reheated to 98 °C to start a new cycle. Repeating the cycle results in exponential amplification of the gene target region. The PCR reaction mixture with a total volume of 50 µl was prepared as follows:

5x Phusion Puffer	10 µl
dNTPs (10 mM)	1 µl
Primer for. (10 µM)	2.5 µl
Primer rev. (10 µM)	2.5 µl
DNA-template	1 µl
Phusion polymerase highfidelity	0.5 µl
H2O dest.	32.5 µl

The cycling temperature program of the Thermocycler was set as follows:

0:30 min at 98 °C
0:10 min at 98 °C
0:25 min at 55 °C
2:00 min at 72 °C
7:00 min at 72 °C
} 32 x
∞ min at 4 °C

Resulting PCR products were quantified via agarose gel electrophoresis and separated from reaction components with QIAquick PCR Purification Kit. Concentration was quantified with a NanoDrop at 260 nm.

3.2.1.2. Restriction

PCR products and vectors were cleaved by restriction enzymes. Restriction enzymes used in this study are listed in table 7. The restriction enzymes recognize and bind to specific DNA sequences for hydrolyzing single strand flanks to generate sticky ends. The restriction reaction mixture was prepared as follows:

10x Cut Smart Puffer	5 µl
Restriktionsenzym (5'-end)	1 µl
Restriktionsenzym (3'-end)	1 µl
DNA sample	1 µg
H2O dest.	Add to final volume of 50 µl

After overnight incubation at required temperature, restriction enzymes were heat inactivated. Restriction products were separated via agarose gel electrophoresis, cut out from gel and extracted with QIAquick Gel Extraction Kit. Concentration was assessed with the NanoDrop at 260 nm.

3.2.1.3. Ligation

The restriction enzymes were selected to allow targeted integration of gene sequences into the multiple cloning site of vectors. Therefore, complementary sticky ends of the restriction products were catalyzed by a T_4-ligase (New England BioLab Inc., Ipswich, Massachusetts/USA). For ligation, vector and insert were taken in a molar ratio of 1:5. The reaction mixture was prepared as follows:

T_4-ligase Buffer	2.5 µl
Linearized vector	50 ng
Insert	5 fold molar of vector
T_4-ligase	1 µg
H2O dest.	Add to final volume of 25 µl

Reactions were incubated for 4 h at room temperature, followed by heat inactivation at 65 °C for 10 min and stored at 4 °C until transformation.

3.2.1.4. *E. coli* transformation

Resulting plasmids from ligation containing requested gene sequence were transformed into MacCell competent DH5α *E. coli* cells (iNtRON, Biotechnology, Seongnam, Gyeonggi/Republic of Korea). Therefore, DH5α cells were thawed and 1.5 µl of ligation product was added and incubated on ice for 30 min. The cells were heated 90 sec. at 42 °C and subsequently placed on ice for 5 min. Then, 1 ml of pre-heated LB medium was added, followed by 1 h on shacking incubator at 37 °C. Finally, 200 ml of cell mixture were spread on LB agar plates containing 100 µg/ml ampicillin. Plates were incubated at 37 °C overnight. Positive antibiotic resistance plasmid carrying colonies were picked for preculture.

3.2.1.5. Isolation of plasmid DNA

The plasmid isolation was performed with iNtRON DNA Purification Kit. For amplification of the plasmid, 5 ml LB medium containing 100 µg/ml ampicillin was inoculated with a grown DH5α colony and incubated at 37°C at 180 RPM overnight. Cells were harvested, lysed and the plasmids were purified as specified in the iNtRON DNA Purification Kit protocol.

3.2.1.6. Gene sequencing

For gene sequencing 100 ng/µl of isolated plasmids were diluted together with 10 pmol/µl of target gene primers in a Mix2Seq vial. The vial was sent to Eurofins genomics for Sanger sequencing analysis (Sanger et al 1977).

3.2.1.7. Preservation of *E. coli* strains

In case of a positive sequencing result, generated *E. coli* strains were stored as long time culture. Therefore 5 ml of LB medium containing 100 µg/ml ampicillin were inoculated with cells and incubated at 37°C. 500 µl of overnight precultured cells were mixed with 500 µl of 50 % autoclaved glycerol in a cryo vial, shocked-freezed in liquid nitrogen and stored at -80 °C.

3.2.1.8. Lithium acetate transformation of *S. cerevisiae*

The yeast strains used for transformation are genetically identical to BY4147 (*MAT* **a**; *his3Δ1; leu2Δ0; met15Δ0; ura3Δ0*) background except strain SEY6210 pRS305_OsTIR_3xFLAG and non-essential gene knock-out strains from deletion library (Open Biosystems, Huntsville, Alabama/USA) as indicated in table 8. Endogenous sequence-tagging was performed by homologous recombination of transformed integrative PCR construct (Longtine et al., 1998). For overexpression of artificial recombinant proteins, yeast cells were transformed with isolated plasmids from table 5 (Robert H. Schiestl & R. Daniel Gietz, 1989).

Overnight preculture was diluted to an optical density at 600 nm wavelength (OD_{600}) of 0.1 in 20 ml and was further grown for 3-5 h. Cells were harvested by centrifugation at 4000 RPM, washed with water and 0.1 M lithium acetate. After final centrifugation at 13000 RPM for 15 sec, the cell pellet was resuspended in 350 µl of 0.1 M lithium acetate. For each transformation 50 µl of cell suspension was mixed with 240 µl of 50 % polyethylene glycol, 36 µl of 1 M lithium acetate, 10 µl of salmon sperm single strand carrier DNA (2 mg/ml), added with 1.5 µl of isolated plasmid or 50 µl of integrative PCR construct. The solution was vortexed for 1 min and incubated for 30 min at 30 °C. After supplementation of 36 µl DMSO, cells were heat shocked at 42 °C for 15 min. Afterwards cells were centrifuged at 4000 RPM, resuspended in 100 µl water and spread to defined synthetic complete (SC) minimal medium plates. By lacking specified nutrients, auxotrophic clones carrying transformed DNA grow and can be selected. Plates were incubated for three days at 30 °C. Grown colonies were picked for preculture, followed by detecting recombinant protein expression with immunodetection or fluorescence microscopy analyses.

3.2.1.9. Culturing and preservation of *S. cerevisiae* strains

In case of positive transformation, cells were grown at 30°C shaking at 180 RPM overnight in synthetic complete (SC) growth medium containing 6.7 g/L yeast nitrogen ammonium sulfate (YNB), 20 g/L glucose and required mixture of amino acids (Complete Supplement Mixture [CSM] 0.79 g/L; CSM-leucine 0.69 g/L; CSM-leucine-tryptophan 0.64 g/L; CSM-histidine 0.77 g/L purchased from MP Biomedicals, Irvine, California/USA). Next day 700 µl

of yeast preculture were mixed with 300 µl of 50 % glycerol and stored at -80 °C for long time storage. For experiments, strains in long time culture were spread out on yeast extract peptone dextrose agar plates (Merck, Darmstadt, Hesse/Germany) or on SC media plates and incubated for three days at 30 °C until experimental procedures.

3.2.2. Cell culture of HepG2 cells

3.2.2.1. Culturing HepG2

Human hepatoblastoma cell line (HepG2) was obtained from ATCC (Manassas, Virginia/USA) and cultured in Dulbecco's Modified Eagle Medium (DMEM) containing 1 g/l D-glucose, L-glutamine, 25 mM HEPES and pyruvate and supplemented with 10 % FBS and 1 % AA (DMEM complete medium). Cells were thawed from long time storage and transferred to DMEM complete medium. After centrifugation the supernatant was discharged and the cell pellet was resuspended in DMEM complete medium. The cell suspension was transferred in a tissue culture flask. Adherent HepG2 cells were incubated overnight. On the next day the medium was discharged and replaced with fresh DMEM complete medium. Medium change was repeated every second day. When the cells reached 80 % of confluence, they were detached from the culture flask by incubating the cells in trypsin, which induces cells to lose adherence. Detached cells were washed with DMEM complete medium and the cell pellet was resuspended in DMEM complete medium. After cell count, cells were finally transferred into a new flask. Cells were passaged four times prior to experiments.

3.2.3. Experiments with *S. cerevisiae*

3.2.3.1. Flow cytometry-based assessment of lipid droplets in *S. cerevisiae*

96-well plates containing SC medium with 2 % glucose (150 µl/well) was used, which was inoculated with yeast strains of interest and precultured overnight (~12 h) by incubation at 30 °C on a shaker. On the next day, the OD_{600} was measured and cells were diluted in fresh medium to an OD_{600}=0.5. After further incubation for 24 h under the same conditions, the stationary phase of the cells was ensured by a static OD_{600} value. Once stationary phase (T0) was confirmed, half volume of the cells was fixed 30 min with 3.7 % PFA at room temperature and half volume was diluted and grown for 5 h (T5) in fresh SC containing 10 µg/ml cerulenin, which inhibits de novo FA synthesis (Omura, 1976). The incubation with cerulenin forces the cell to use only the FAs already stored in LDs without synthesizing and incorporating new ones. After 5 h incubation, the OD_{600} was measured again to ensure

viability of the cells indicated by growth. Upon centrifugation at 4000 RPM, the cells were collected, washed with phosphate buffered saline (PBS), and fixed in 3.7 % PFA.

After fixation, the LDs of the cells were stained with 150 µl BODIPY 493/503 (final concentration 1 µg/ml in PBS) for 30 min in the dark. Subsequently, the cells were washed three times with PBS and resuspended in 120 µl appropriate buffer for flow cytometry measurements (BD FACSFlow sheat fluid BD Bioscience, Franklin Lakes, NJ/USA). The BODIPY 493/503 fluorescence signal of individual cells was analyzed by using a flow cytometer coupled to a 96-well plate high throughput auto sampler (BD FACSCalibur BD Bioscience).

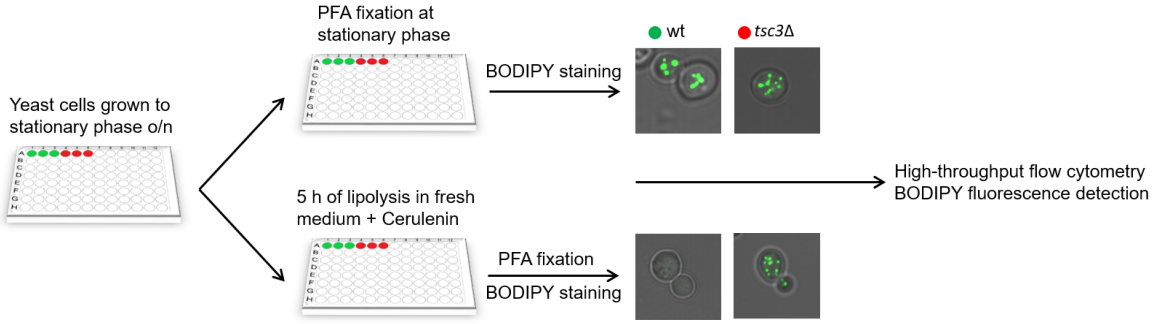

Fig. 10: Procedure of flow cytometry-based LD quantification in yeast. Wild-type and knock-out cells were grown to stationary phase to induce LD formation. LD content in stationary phase and 5 h after dilution into fresh medium containing cerulenin was quantified by flow cytometry analysis of BODIPY493/503-labeled LDs.

3.2.3.2. Fluorescence microscopy

To investigate protein localization and subcellular structures the fluorescence microscopy was used.

For localization studies in yeast cells expressing GFP-fused Tsc3p, ssSPTa and ssSPTb, an overnight preculture was harvested in stationary phase, resuspended in PBS and immediately analyzed.

For localization studies of Dga1-GFP 20 ml SC medium was inoculated with wild-type (WT) and *tsc3*Δ cells, which were grown for 48 h to reach the stationary phase. Next, cells in stationary phase were diluted to an OD_{600} of 0.5 in SC medium containing 10 µg/ml cerulenin, with and without 15 µM PHS and were grown for 5 h at 30 °C with 180 RPM shaking. Cells in stationary phase and 5 h after dilution in fresh medium were harvested and fixed with 3.7 % paraformaldehyde (PFA). Finally, cells were resuspended in PBS.

For all analysis, 1 µl cell suspension was applied to microscopy slides, covered by 0.17 mm glass. Images were captured using a confocal laser scanning microscope (LSM) 880 and processed with ImageJ 3.0.1 (Schindelin et al., 2012) or ZEN 2.3 (Carl Zeiss AG, Oberkochen, Baden-Wuerttemberg/Germany).

3.2.3.3. Growth curve

Overnight precultured cells in stationary phase were diluted to OD_{600} of 0.5 in appropriate fresh SC medium to induce growth. Yeast cells were incubated at 30 °C. Growth was detected by OD_{600} measurements at 2-h intervals until the stationary phase was reached using the Multi-function plate reader Infinite Pro 200 and the Bio Photometer Plus.
To determine statistically comparable values for the growth curves, the area under the curve (AUC) was determined using an integration method. For an equation y = f(x) with limit values a and b, the integral formula $\mathrm{AUC} = \int_b^a f(x)\,dx$ was used. The AUC was calculated by using the program GraphPad Prism 8.2.1.

3.2.3.4. Spotting assay

To investigate growth of divergent yeast strains a spotting assay was used. Overnight precultured cells were diluted to an OD_{600} of 0.5 in SC medium and were grown for 3 h at 30 °C at 180 RPM shacking. After the OD_{600} was measured, the cells were diluted to OD_{600} of 0.5 and a serial dilution of 1:10 was performed. Next, 5 µl of each dilution was transferred to SC agar plates. The cells were incubated at indicated temperatures and detected with a cell phone camera (Samsung Galaxy A3) every 24h.

3.2.3.5. Protein degradation by Auxin-inducible degron system

The auxin-inducible degron (AID) system is a method to control the cellular protein level and therefore it is useful to study the function of essential proteins *in vivo*. Through induction by the plant hormone auxin, target proteins can be rapidly degraded by the proteasome as previously described (Nishimura et al., 2009).
Plants use a unique degradation complex, SKP/Cullin/F-box (SCF), for specific degradation of AID fused target proteins induced by auxin (Salehin et al., 2015). Subsequent recruited E3 ligase ubiquitinates the target proteins for degradation through proteasome signaling. Yeast lacks the F-box transport inhibitor response 1 domain (TIR1) but shares the highly conserved SCF degradation pathway. Genomic integration of TIR1 from *Oryza sativa* (OsTIR1) allowed us to degrade AID tagged fused proteins by auxin supplementation in yeast (Morawska & Ulrich, 2013).
To investigate the physiological impact of Lcb1, the AID system was used to deplete the essential protein in a dose-dependent way. As deletion results in nonviable yeast cells, Lcb1 was genomically tagged with AID, which was expressed in an OsTIR background strain (Giaever et al., 2002). For Lcb1-AID degradation, cells in stationary phase were diluted in fresh medium supplemented with 1 mM auxin.

3.2.4. Experiments with HepG2 cells

3.2.4.1. Gene silencing in HepG2 cells

To knock-down the small subunit of serine palmitoyltransferase b (ssSPTb) gene in HepG2, the cells were treated for 48 h with 25 nm small interfering RNA (siRNA). The ssSPTb siRNA was purchased as ON-TARGETplus construct (Horizon Discovery, Waterbeach, Cambridgeshire/ United Kingdom) (Birmingham 2006 3' UTR).

The double strand (ds) siRNA consists of two 21 base pairs (bp) long RNAs strands with dinucleotide overhangs at each 3' end, forming duplex. The guide strand is designed as a revers complementary antisense to the target ssSPTb mRNA, whereas the second strand is used for construct passaging into the cell. The siRNA duplex is spliced by a cellular DICER RNase, which also initiates formation of the RNA-induced silencing complex (RISC) with the guide strand. The guide strand connects to the target ssSPTb mRNA and an endonuclease of the RISC complex degrades the mRNA. This results in translational inhibition of protein biosynthesis of ssSPTb (Elbashir et al., 2001).

For transfection, 4 x 10^5 cells were seeded in a 6 well cell culture plate (Greiner Bio-One, Solingen, NRW/Germany) and incubated overnight at 37 °C in a humidified atmosphere of 5 % CO_2. On the next day the cells reached a confluence of 70 % and were ready for transfection. The siRNA and transfection reagent were prepared as follows: 12.5 µl of 20 µM ssSPTb siRNA was mixed with 112.5 µl DMEM, 37.5 µl lipofectamin were diluted in 87.5 µl DMEM and both solutions were incubated for 5 min at RT. Afterwards, the diluted siRNA was transferred to prepared Lipofectamin solution and incubated for further 15 min at RT. The 6 well plate was taken out of the incubator, the medium was removed and 1.95 ml fresh DMEM complete medium was added prior to supplementation of 50 µl prepared siRNA-lipofectamin solution. After 48 hours, the cells were washed with preheated PBS, scraped in 1 ml PBS with a cell scraper (Sarstedt, Nuembrecht, NRW/Germany) and transferred into a 1.5 ml reaction tube (Eppendorf, Hamburg, Hamburg/Germany) for centrifugation at 1000 RPM for 5 min. The supernatant was discharged and the wet weight cell pellet was determined before experimental application or shock freezed in liquid nitrogen and storage at -80 °C.

The silencing effect of ssSPTb-siRNA was analyzed with RT-qPCR. Effect of ssSPTb-siRNA treatment on proteins of insulin signaling was analyzed with immunodetection and cellular lipid composition was analyzed with LC-MS/MS.

3.2.5. Molecular biological methods

3.2.5.1. Total protein extraction from *S. cerevisiae* cells

To investigate the expression level of proteins of interest, the total protein was extracted according to (Horvath and Riezman, 1994). Cells of an OD_{600} of 2 were harvested at 4000 RPM and resuspended in 500 µl H_2O. Cells were disrupted by addition of 75 µl Roedel mix (1.85 M NaOH, 1 M ß-mercaptoethanol, 1 mM PMSF), mixed on a vortexer and incubated on ice for 10 min. Proteins were precipitated by addition of 75 µl 100 % trichloroacetic acid (TCA) and further incubated on ice for 10 min. After centrifugation at 13000 RPM at 4 °C for 10 min, supernatant was removed and the protein pellet was washed with ice cold 100 % acetone. After centrifugation at 13000 RPM at 4 °C for 10 min, the acetone was decanted and the pellet was dried at 55 °C. Afterwards proteins were dissolved in 50 µl Laemmli buffer with 5 % ß-mercaptoethanol and kept at RT until running SDS-PAGE.

3.2.5.2. Total protein extraction from HepG2

For protein extraction, HepG2 cells were washed with phosphate-buffered saline (PBS) and harvested with a cell scraper. After centrifugation at 1000 RPM the supernatant was discharged. Cells were lysed with RiPA lysis buffer on ice for 30 min, mixing every 10 min on a vortexer. Afterwards, the suspension was centrifuged at 13000 RPM at 4 °C for 20 min to sediment chromosomal DNA and un-lysed membranes. The supernatant was transferred to a new reaction vial and the protein concentration was detected with a NanoDrop at 280 nm or with the Pierce BCA Protein Assay.

3.2.5.3. Isolation of membrane fraction vs. cytosolic fraction

To investigate proteins localized in different cellular compartment, membrane fraction was separated from cytosolic fraction via ultracentrifugation. HepG2 cells were harvested as described above (3.2.2.4) and resuspended in 300 µl buffer A followed by incubation on ice for 20 min with mixing by vortexing every 5 min. The homogenate was then centrifuged for 1 h at 100000 g at 4 °C. The clear supernatant containing cytosolic proteins was transferred to a fresh reaction tube and the protein concentration was detected prior to storage at -80 °C until experimental procedure.

The pelleted membrane fraction was resuspended in 100 µl buffer B and homogenized with a tissue grinder prior to centrifugation for 1 h at 100000 g at 4 °C. The supernatant was transferred to a fresh reaction tube and the protein concentration was detected prior to storage at -20 °C until experimental procedure.

3.2.5.4. RNA extraction from HepG2

RNA was extracted from collected HepG2 cells using the RNeasy Kit, following manufacturer's instruction. Briefly, the cells were resuspended in 350 µl RLT buffer (containing ß-mercaptoethanol), transferred to a Qiashredder spin column and centrifuged at high speed for 2 min. The lysate was mixed with 70 % ethanol, transferred to an RNeasy spin column and centrifuged for 15 sec at 10000 RPM and the flow trough was discharged. The RNA bound to the spin column was washed twice with 500 µl RPE buffer and eluted with 30 µl RNase free water. The RNA concentration was measured with NanoDrop at 260 nm.

3.2.6. Analytic biophysical methods

3.2.6.1. Agarose gel electrophoresis

The agarose gel electrophoresis method was used to separate DNA fragments. Indeed, the negatively charged phosphate of the DNA backbone migrates to the anode in a generated electric field. Based on the pore size of the agarose matrix, the DNA is then separated by size. Thus the migration speed is independent of the molecular weight of the DNA. DNA samples mixed with gel loading dye were loaded into a 5 % agarose gel and separated in an electric field. DNA was detected by intercalated fluorescent GelStar under UV irradiation.

3.2.6.2. SDS-PAGE

Using sodium dodecyl sulfate polyacrylamide gel electrophoresis (SDS-PAGE) proteins were separated according to their size (Laemmli 1970). The SDS binds uniformly to amino acid chains and creates a constant negative charge distribution proportional to the mass of the protein, causing them to migrate to the anode in a polyacrylamide gel. Based on the gel matrix, large proteins run slower than smaller proteins, resulting in separation of different sized proteins.

To separate proteins extracted from yeast, total protein of 2 OD_{600} were resolved in Laemmli buffer and boiled before loading the protein sample to the SDS gel. The 10 % SDS gel was prepared as follows:

Separating gel	Stacking gel
12.3 ml H_2O	3.075 ml H_2O
7.5 ml Tris-HCl (1.5 M, pH 8.8)	1.25 ml Tris-HCl (0.5 M, pH 6.8)
9.9 ml 30% Acrylamide, 0.8% Bisacrylamide	670 µl 30% Acrylamide, 0.8% Bisacrylamide
150 µl SDS (20 %)	25 µl SDS (20 %)
150 µl APS (10 %)	25 µl APS (10 %)
20 µl TEMED	5 µl TEMED

To separate proteins extracted from HepG2, protein sample was heated prior to loading on 4–20 % gradient Mini-PROTEAN TGX Stain-Free precast gels (BioRad Laboratories Inc., Hercules, California/USA). The gel ran in a premixed SDS running buffer till the dye reached the bottom.

3.2.6.3. Immunodetection (Western Blot)

Western Blot is used for specific detection of a protein based on immunological staining. Proteins extracted from yeast were transferred from SDS-PAGE gel to a methanol activated PVDF membrane using a Tank Blot system. Proteins were blotted using a Tris-glycine-methanol transfer buffer. After blotting, the membrane was blocked in milk 5% in Tris-buffered saline with Tween20 (TBST) and then incubated with a primary antibody, which bound to specific binding sites of protein of interest. The secondary IRDye 800CW antibody is fused to an infrared fluorescent dye which was detected with the Licor Odyssey image system.

Proteins extracted from HepG2 were transferred from SDS-PAGE gel to a methanol activated PVDF membrane using a semi-dry Blot method. Therefore proteins were blotted using a premixed Tris-glycine-methanol transfer buffer. The membrane was blocked in milk 5% in TBST and then incubated with a primary antibody followed by a secondary peroxidase fused-antibody. Protein of interest was detected by chemiluminescence of peroxide reagent and Luminol enhancer reagent (ECL).

3.2.6.4. RT-qPCR

To quantify the efficiency of silencing in HepG2 cells, the reverse transcriptase quantitative PCR was performed (RT-qPCR). Similar to conventional PCR, this involves the amplification of target genes using specific forward and reverse primers. In a first step extracted RNA (3.2.5.4) was retro-transcripted to cDNA using the QuantiTect Reverse Transcription Kit. In a second step, the ds cDNA was amplified via PCR. With every PCR cycle, the number of cDNA doubles with incorporation of SYBR green into the ds sequence.

SYBR green is a fluorescent dye, which shows low fluorescence in aquatic solutions. At the end of every amplification step the fluorescence is detected, which is proportional to the amount of the target gene cDNA. For RT-qPCR the reaction mixture with a total volume of 10 µl was prepared as follows:

SYBR green mix	5 µl
Primer for. (100 pM)	1 µl
Primer rev. (100 pM)	1 µl
cDNA (5 ng)	3 µl

The cycling temperature program of the Thermocycler was set as follows:

15:00 min at 95 °C
0:15 min at 94 °C
0:30 min at 55 °C
0:30 min at 72 °C
0:15 min at 95 °C
} 40 x
1:00 min at 55 °C

A gradient from 0.3 °C until 95 °C was running to obtain the melting curves. All gene expressions were normalized to tubulin.

3.2.6.5. LC-MS/MS lipidomic analysis

To investigate the lipidome of HepG2 cells the Liquid Chromatography - Mass Spectrometry and Liquid Chromatography - Tandem Mass Spectrometry (LC-MS/MS) was used. The analytical method of LC-MS/MS is used for the detection of single molecules in pico-molar range. This application allows the analysis of cellular lipid composition in tissues and homogeneous cell cultures. In LC-MS/MS, dissolved lipid samples are accelerated in the electrical field of an analytical Quadrocore after liquid chromatographic separation and subsequent electrospray ionization. In the Quadrocore, the separation takes place under vacuum according to the mass/charge ratio of the ions. These are detected and quantified by a secondary electron multiplier.

Cellular lipids of ssSPTb-siRNA treated HepG2 cells were extracted as follows according to Bligh and Dyer (Bligh & Dyer, 1959): 20 mg cell pellet was homogenized in 500 µl ice cold TLE buffer in a glass douncer tissue homogenizer and transferred into 3 ml ice cold chloroform/methanol (2:1, v/v). Internal standards (Avanti Polar Lipids, Birmingham, Alabama/USA) of 50 ng d17:1, 50 ng d17:0, 100 ng Cer C17 and 500 ng DAG d17:0 were added to each sample, briefly mixed by a Vortexer and incubated on ice for 10 min, followed

by 5 min overhead shacking. After addition of 1 ml ice cold chloroform and 1 ml H_20, the samples were mixed by a Vortexer. The organic chloroform phase was collected after centrifugation for 10 min at 4 °C with 4000 RPM. The extracted lipids were dried with a gentle nitrogen stream and resuspended in 400 µl. For sphingolipid measurements 1 µl of the dissolved lipids were then injected on the LC/MS/MS. The remaining sample volume was dried again under a gentle nitrogen stream and dissolved in 0.2 ml hexane/methylene chloride/ether (89:10:1, v/v) and loaded to a hexane conditioned Diol solid phase extraction (SPE) column. TAG were eluted with 5 ml hexane/methylene chloride/ether (89:10:1, v/v) and discharged. The remaining DAG and Cer was eluted with 2 ml hexane/ethyl acetate (25/75, v/v) and subsequently dried with a gentle stream of nitrogen. After resuspension of the sample in 300 µl methanol, 1 µl was injected on the LC-MS/MS for DAG and Cer measurement. These measurements were conducted by Mrs. Preuß in the Biomedical Laboratory of the German Diabetes Center in Düsseldorf.

3.2.7. Electronic data processing

3.2.7.1. Text processing programs

Text, tables and figures were created with Microsoft Word, Microsoft PowerPoint, GraphPad Prism 8.2.1 and ImageJ 1.8.0. Figures of organs are from available elements of SmartServier.

3.2.7.2. Statistical analysis

Statistical analyses of the mean, standard derivation (SD), standard error of the mean (SEM), Student's *t* test, one-way ANOVA and two-way ANOVA were performed by GraphPad Prism 8.2.1.

4. Results

4.1. Decreased LD consumption in sphingolipid synthesis-deficient yeast cells

An efficient LD consumption is essential to maintain cellular lipid homeostasis. In order to identify regulator proteins of efficient LD consumption in yeast, accumulated LDs were measured in the stationary phase (T0) and relative LD consumption was determined after 5 h of growth (T5) by measuring LD residues. To measure cellular LD content at the indicated time points T0 and T5, LDs were stained with BODIPY493/503 and its fluorescent signal was detected via flow cytometry.

To investigate whether proteins responsible for sphingolipid synthesis have an influence on LD consumption, yeast strains with deletion of sphingolipid synthesizing proteins were grown to stationary phase and then transferred into fresh medium containing 10 µg/ml cerulenin to suppress FA synthesis and *de novo* neutral lipid synthesis.

After 5 h of growth, yeast cells with a deletion of *tsc3*, the SPT-stimulating and amino acid substrate-selective protein, consumed up to 34% of stored LDs, whereas the WT cells showed 73% of LD consumption in the same time span of growth.

In addition, defective LD consumption was detectable in strains with deletions of Sac1, Csg2, and Ipt1 proteins required for terminal synthesis of complex sphingolipids. The flow cytometry measurement shows that *sac1Δ* cells have a LD consumption of 49%, *csg2Δ* cells show 61% and *ipt1Δ* cells 65% of consumed LD under same conditions as WT cells (Fig. 11A).

The measurements showed that the deletion strains tsc3 and sac1 are markedly impaired in LD consumption. Since Tsc3p and Sac1p interact directly with SPT, further flow cytometry experiments were conducted in the presence of 10 µM myriocin which inhibits the function of SPT. The results showed that myriocin-treated control cells (WT) only reduced their LD pool by 15%, whereas untreated control cells reduced their LD pool size by 75% (Fig. 11B).

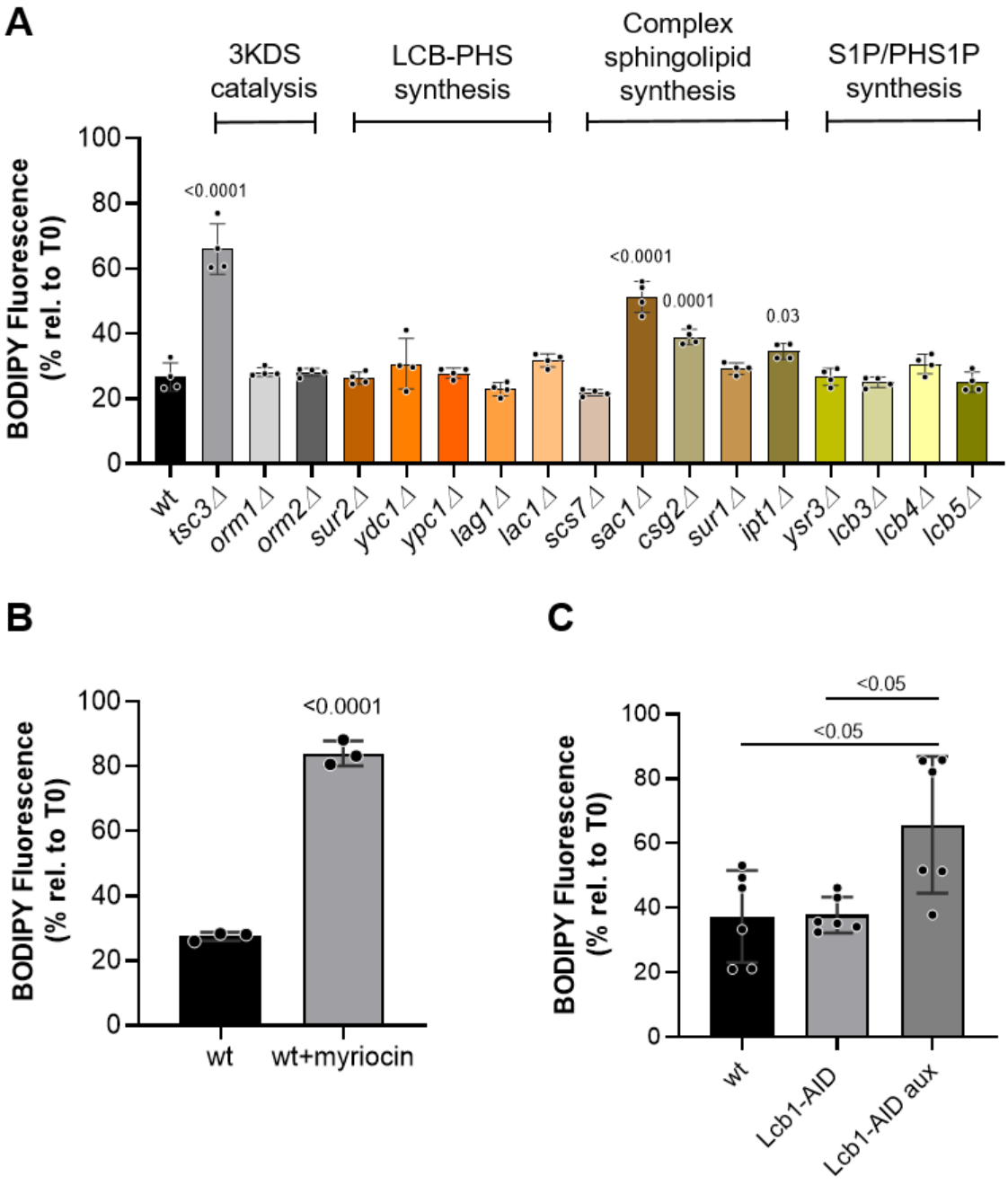

Fig. 11: LD consumption is decreased in yeast strains with deficient sphingolipid synthesis. (A) LD consumption of deletion strains in sphingolipid synthesis downstream of SPT after 5 h of growth measured by flow cytometry analysis of BODIPY493/503-labeled LDs. LD consumption is defined in percentage as the remaining amount of LDs after 5 h of growth in relation to the amount of LDs in the stationary phase (n=4, mean ± SD, one-way ANOVA, *P* value vs. WT). (B) LD consumption after 5 h of growth of WT and myriocin-treated WT cells measured by flow cytometry analysis of BODIPY493/503-labeled LDs (n=3, mean ± SD, one-way ANOVA, *P* value vs. WT). (C) LD consumption of Lcb1-AID expressing OsTIR background strains grown in SC-medium for 5 h with and without auxin measured by flow cytometry analysis of BODIPY493/503-labeled LDs (n=6, mean ± SD, one-way ANOVA).

To further analyze the effect of a direct disruption of the SPT activity on LD dynamics, the AID system was used to deplete the heterodimeric SPT-component Lcb1. Complete deletion of Lcb1 results in inviable cells (Buede et al., 1991). To circumvent this effect, the AID system to degrade Lcb1 was used in a concentration-dependent manner. For the flow

cytometry experiment, cells in the stationary phase were diluted in fresh medium containing 10 µM cerulenin and 1 mM auxin. Auxin-induced depletion of Lcb1-AID in OsTIR Lcb1-AID cells results in 28% consumed LDs after 5 hours of growth whereas auxin untreated OsTIR-Lcb1-AID cells consume 62% of LDs (Fig. 11C).

4.2. Overexpression of Tgl3p rescues LD consumption in *tsc3Δ* cells

After demonstrating that deletion of *tsc3* in yeast leads to lower LD consumption (Fig. 11A), the next step was to ensure that *tsc3Δ* does not interfere with the activity of TAG-degrading lipases; therefore, the influence of Tgl3 on LD dynamics was investigated.

First, the endogenous expression level of the yeast major lipase, Tgl3p, was determined in WT and *tsc3Δ* by immunodetection. For this purpose, WT and *tsc3Δ* cells expressing 3HA-tagged Tgl3 were grown to stationary phase and transferred to fresh medium containing 10 µg/ml cerulenin for 2.5 h. At stationary phase and after two hours of growth with cerulenin, WT and *tsc3Δ* cells expressed Tgl3-3HA, indicating that *tsc3Δ* had no effect on Tgl3 expression (Fig. 12A).

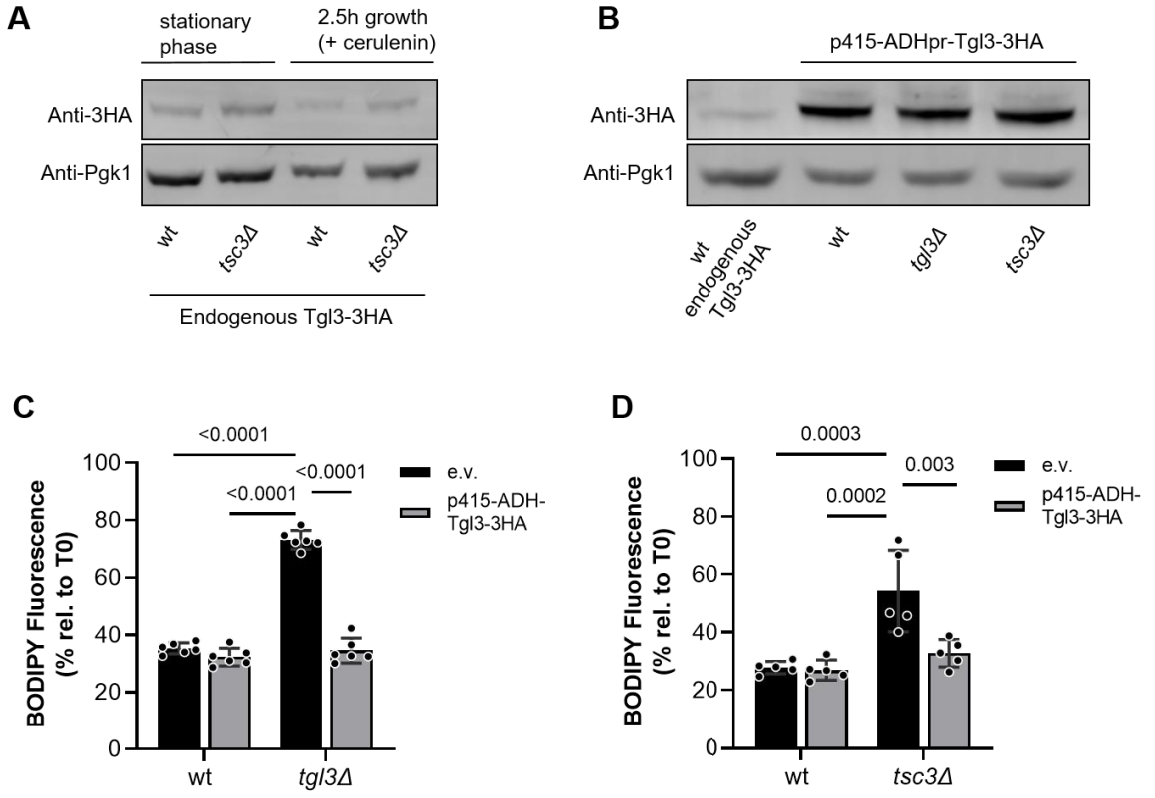

Fig. 12: Overexpression of recombinant Tgl3-3HA rescues lipid droplet consumption defect in *tgl3Δ* and *tsc3Δ* cells. (A) Immunodetection of endogen 3HA tagged Tgl3 expressed in WT and *tsc3Δ* cells in stationary phase and 2.5 h after dilution in fresh medium containing 10 µg/ml cerulenin (B). Immunodetection of overexpressed Tgl3-3HA in WT, *tgl3Δ* and *tsc3Δ* cells in stationary phase. (C) LD consumption after 5 h of growth of WT and *tgl3Δ* cells transfected with an empty vector (e.v.) or Tgl3-3HA overexpressing vector measured by flow cytometry analysis of BODIPY493/503-labeled LDs (n=6, mean ± SD, two-way ANOVA). (D) LD consumption after 5 h of growth of WT and *tsc3Δ*

cells transfected with an empty vector (e.v.) or Tgl3-3HA overexpressing vector measured by flow cytometry analysis of BODIPY493/503-labeled LDs (n=5, mean ± SD, two-way ANOVA).

Since the hydrolytic activity of Tgl3p is limited to the presence of LDs (Schmidt et al., 2013), Tgl3p was overexpressed in yeast cells to increase lipolysis. The result of immunodetection of recombinant Tgl3-3HA, overexpressed in WT, *tgl3Δ* and *tsc3Δ* cells showed an elevated level of Tgl3-3HA in these cells in stationary phase (Fig. 12B).

Flow cytometry analysis of LD consumption showed that increased lipolysis by overexpression of Tgl3-3HA did not increase the LD consumption in WT cells after 5 h of growth, but reversed the defective LD consumption in *tgl3Δ* (Fig. 12C) and *tsc3Δ* cells (Fig. 12D), indicating that the recombinant Tgl3-3HA functions as the native protein and overcomes potential reduced lipolytic activity in *tsc3Δ* cells.

4.3. Exogenous phytosphingosine rescues lipid droplet consumption in *tsc3*Δ cells

Next, LD dynamics were examined in the context of Tgl4p, the second major lipase of yeast regulated by the cyclin-dependent kinase Cdc28 (Kurat et al., 2009). It was previous shown that deletion of *tgl4* results in decreased mobilization of TAG (Athenstaedt & Daum, 2005). The flow cytometry measurement indicated a defect in LD consumption in *tgl4Δ* cells after 5 h of growth in fresh medium containing 10 µg/ml cerulenin, similar to cells with compromised sphingolipid synthesis such as *tsc3Δ* cells (Fig. 13A). It can be speculated that the impairment of sphingolipid synthesis due to myriocin or deletion of *tsc3* decreases the consumption of stored TAG by dysregulating the lipolytic activity of Tgl4.

To investigate the effect of cellular Cer levels on LD consumption in WT and *tsc3Δ* cells, the LD consumption was analyzed in the presence of the Cer-precursor PHS (Kondo et al., 2014). Flow cytometry analysis of *tsc3Δ* cells in stationary phase diluted in fresh medium containing 10 µg/ml cerulenin and 15 µM PHS indicated an increased LD consumption (14.9%) after 5 h of growth compared to *tsc3Δ* cells grown without PHS (Fig. 13B). Fluorescence microscopic analyses under the same conditions confirmed the flow cytometry results (Fig. 13C).

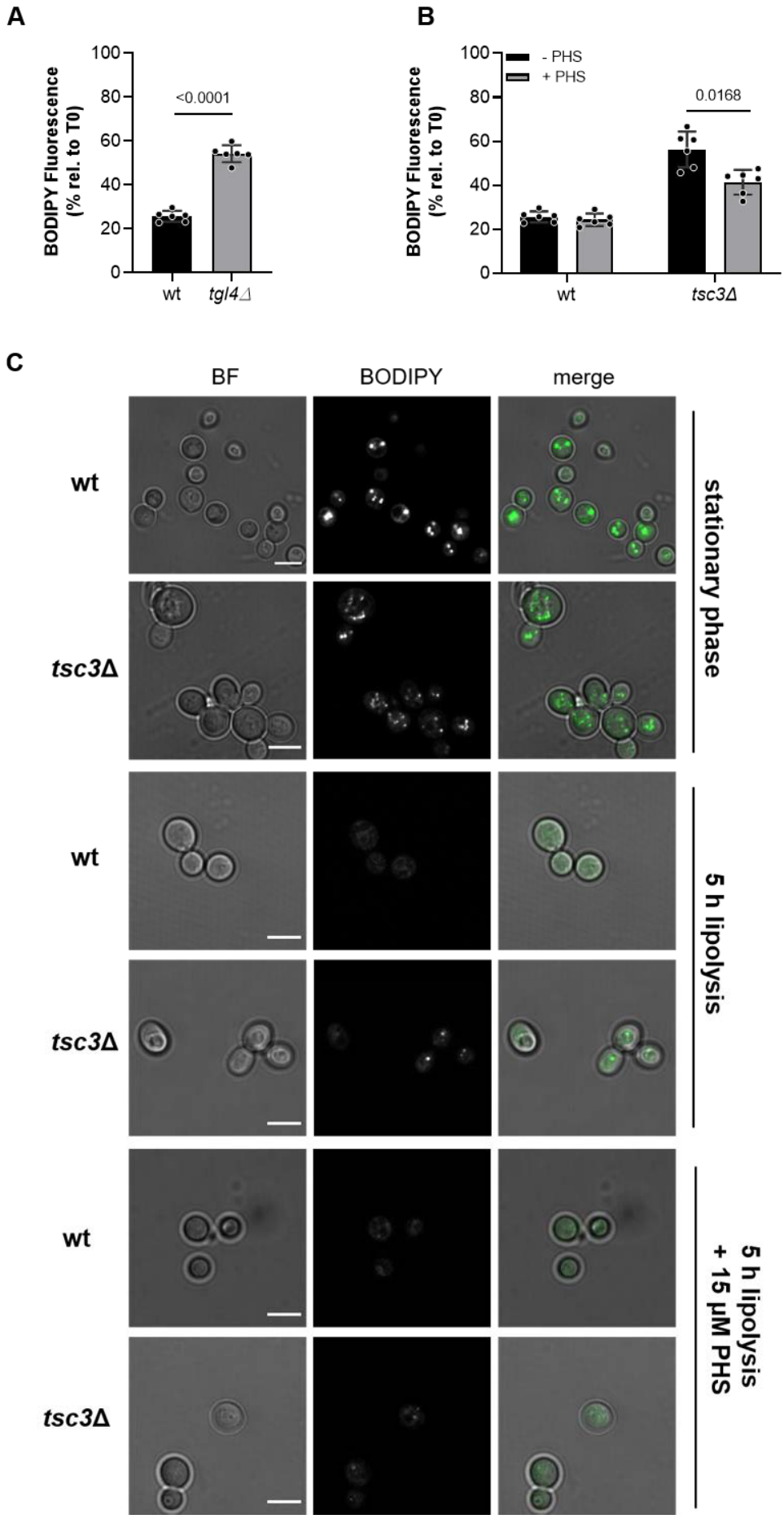
A
BODIPY Fluorescence (% rel. to T0)
100
80
60
40
20
0
<0.0001
wt
tgl4Δ
B
BODIPY Fluorescence (% rel. to T0)
- PHS
+ PHS
0.0168
wt
tsc3Δ
C
BF
BODIPY
merge
wt
tsc3Δ
stationary phase
wt
tsc3Δ
5 h lipolysis
wt
tsc3Δ
5 h lipolysis + 15 µM PHS

Fig. 13: Influence of exogenous phytosphingosine on lipid droplet consumption in yeast cells. (A) LD consumption after 5 h of growth of WT and *tgl4Δ* cells quantified by flow cytometry analysis of BODIPY493/503-labeled LDs (n=6, mean ± SD, unpaired two-tailed *t* test). (B) Flow cytometry analysis of BODIPY493/503 stained LD after 5 h of growth of WT and *tsc3Δ* cells into fresh medium containing cerulenin with and without 15 µM PHS (n=6, mean ± SD, two-way ANOVA, *P* value PHS untreated vs. PHS treatment). (C) Representative fluorescence microscopy of BODIPY493/503 stained LD in WT and *tsc3Δ* cells under same conditions as for B.

4.4. Exogenous phytosphingosine rescues growth of *tsc3*∆ cells

In the present study, a growth curve with WT and *tsc3Δ* cells was done at 30°C. Monitoring of the growth rates showed that the WT strain reached the stationary phase at OD_{600} of 6.8 after 14 h, whereas the *tsc3Δ* strain reached stationary phase only after 26 h with a lower OD_{600} of 3.2 (Fig. 14A). Addition of 15 µM PHS rescued the observed growth defect of *tsc3Δ* cells by reaching the stationary phase at OD_{600} of 6.4 (Fig. 14A).

Moreover, the effect of induced Lcb1-AID depletion on growth were analyzed. OsTIR Lcb1-AID cells in stationary phase were diluted in fresh medium with and without 1 mM auxin in combination with or without 15 µM PHS. The auxin-mediated Lcb1-depletion significantly reduced the growth of the OsTIR Lcb1-AID strain at 26 h after growth resumption and this defect was reversed by supplementation with PHS (Fig. 14B).

A spotting assay using serially diluted WT and *tsc3Δ* strains grown on substrate with and without 15 µM PHS for 48 h, confirmed the result that PHS reverses the growth defect of cells with insufficient sphingolipid synthesis even at temperatures of 37°C (Fig. 14C).

In addition, the spotting assay was conducted in WT and *tsc3Δ* cells with transfected recombinant C-terminal GFP tagged Tsc3, C-terminal GFP ssSPTa or C-terminal 3HA tagged ssSPTb, which are integrated into a pRS415 vector controlled by an ADH promoter. The spotting assay showed that overexpression of artificial Tsc3-GFP and the human ssSPTb-3HA in *tsc3Δ* cells resulted in WT-like growth (Fig. 14C). *Tsc3Δ* cells overexpressing ssSPTa-GFP failed to grow at 37°C after 48 h on substrate without supplemented 15 µM PHS (Fig. 14C).

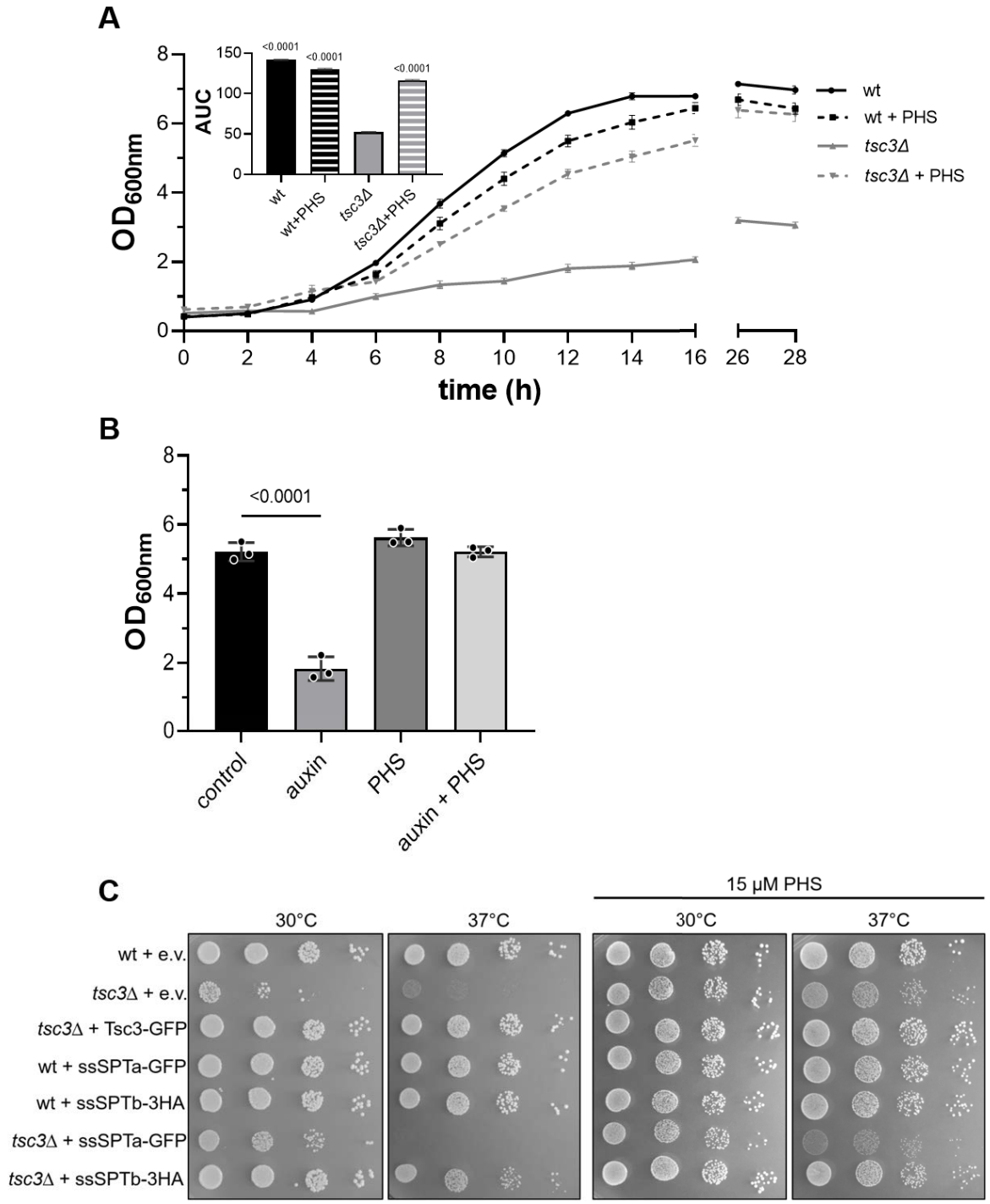

Fig. 14: Addition of phytosphingosine restores normal growth in *tsc3Δ* cells. (A) Growth of WT and *tsc3Δ* cells in the stationary phase after dilution into fresh medium containing 15 µM PHS. The insert shows the respective areas under curve (AUC) (n=9, mean ± SEM, one-way ANOVA, *P* vs. *tsc3Δ*). (B) Growth of OsTIR LCB1-AID cells 26 h after dilution into fresh medium with and without 1 mM auxin and 15 µM PHS (n=3, mean ± SD, one-way ANOVA, *P* value vs. control). (C) Representative spotting assay analyzing growth at 30°C and 37°C of indicated strains. Cells in log phase were grown for 48 h, serially diluted and spotted on growth medium plates with and without containing 15 µM PHS.

4.5. Subcellular localization of the candidate protein Tsc3p at the ER

Prior studies demonstrated co-immunoprecipitation of Tsc3p with Lcb1p and Lcb2p (Gable et al., 2000). As SPT resides in the ER membrane active in a multimeric SPOTS complex

with Tsc3p, it is hypothesized that Tsc3p also localizes at the ER membrane (Breslow, 2013; Davis et al., 2019).

First, the effect of the transfected pRS415-ADHpr-Tsc3p-GFP plasmid on LD consumption and growth in WT and *tsc3Δ* cells was tested. It was observed that the constitutively expressed Tsc3p-GFP was able to rescue the growth defect (Fig. 15A) and LD consumption (Fig. 15B) in *tsc3Δ* cells.

Laser scanning microscopic investigation with transfected WT cells in stationary phase confirmed the co-localization of Tsc3p-GFP and red fluorescent protein (RFP)-tagged HDEL (ER marker), indicating a Tsc3p localization on the perinuclear and cortical ER (Fig. 15C).

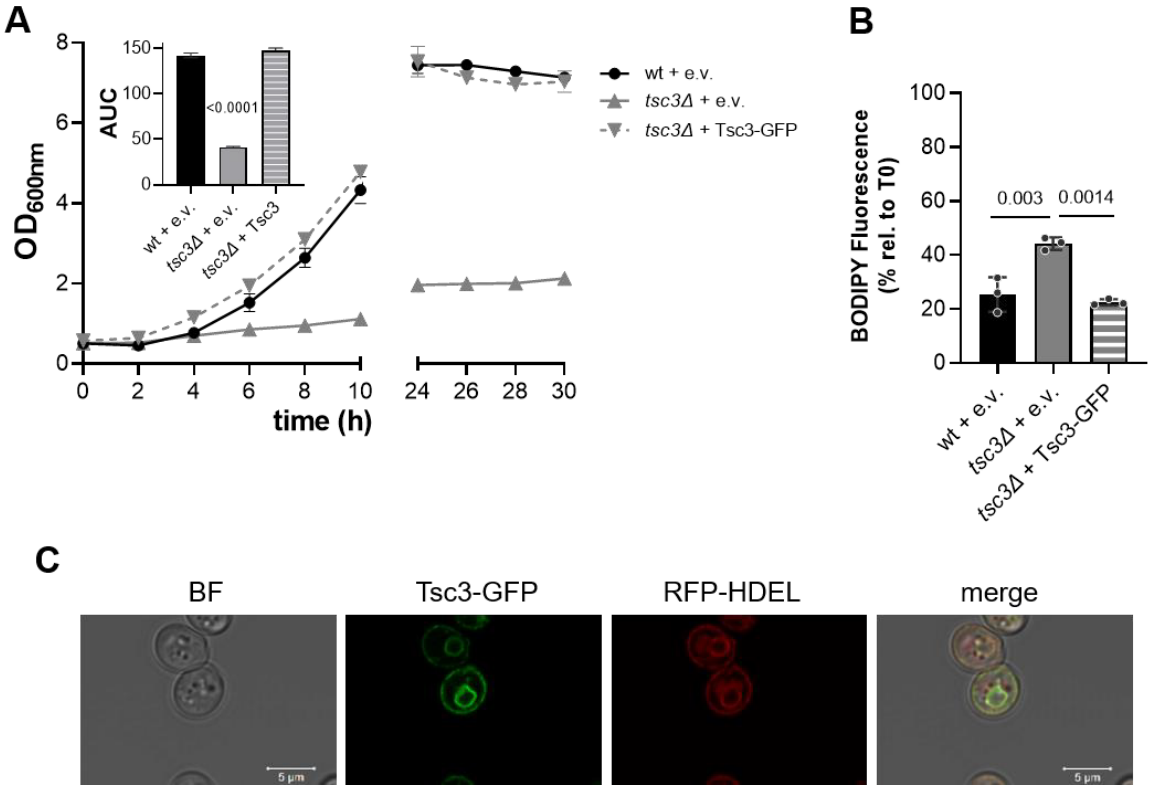

Fig. 15: Characterization of recombinant Tsc3p in yeast cells. (A) Growth progression of WT and *tsc3Δ* strains transfected with an empty vector (e.v.) or pRS415-ADHpr-Tsc3-GFP. The insert shows the respective areas under curve (AUC) (n=3, ± SEM, one-way ANOVA, *P* vs. WT + e.v.). (B) LD consumption after 5 h of growth of WT and *tsc3Δ* strains transfected with an empty vector (e.v.) or pRS415-ADHpr-Tsc3-GFP quantified by flow cytometry of BODIPY493/503 stained LDs (n=3, mean ± SD, one-way ANOVA). (C) Co-localization of Tsc3p-GFP and RFP-HDEL expressed in WT cells in stationary phase.

4.6. Human small subunits of SPT rescue defective phenotype of *tsc3*Δ cells

In mammals, two small subunits of SPT (ssSPTa and ssSPTb) have been reported to stimulate the activity of SPT (Gable et al., 2000; Han et al., 2009). To explore whether human ssSPTs resemble the function of Tsc3 in yeast, LD consumption and the growth of *tsc3Δ* cells overexpressing ssSPTa-GFP or ssSPTb-3HA was examined.

For flow cytometric investigations of the LD consumption, indicated yeast cells were grown to stationary phase and transferred into fresh medium containing 10 µg/ml cerulenin to induce growth resumption accompanied with lipolysis.

Flow cytometry measurements revealed that after 5 h of lipolysis only the ssSPTb-3HA, but not the ssSPTa-GFP rescued the LD consumption defect in *tsc3Δ* cells (Fig. 16A). Conversely, neither the overexpression of ssSPTa-GFP nor ssSPTb-3HA increased the LD consumption in WT cells (Fig. 16A). Furthermore, the overexpression of ssSPTa and ssSPTb rescued the growth defect in *tsc3Δ* cells (Fig. 16B).

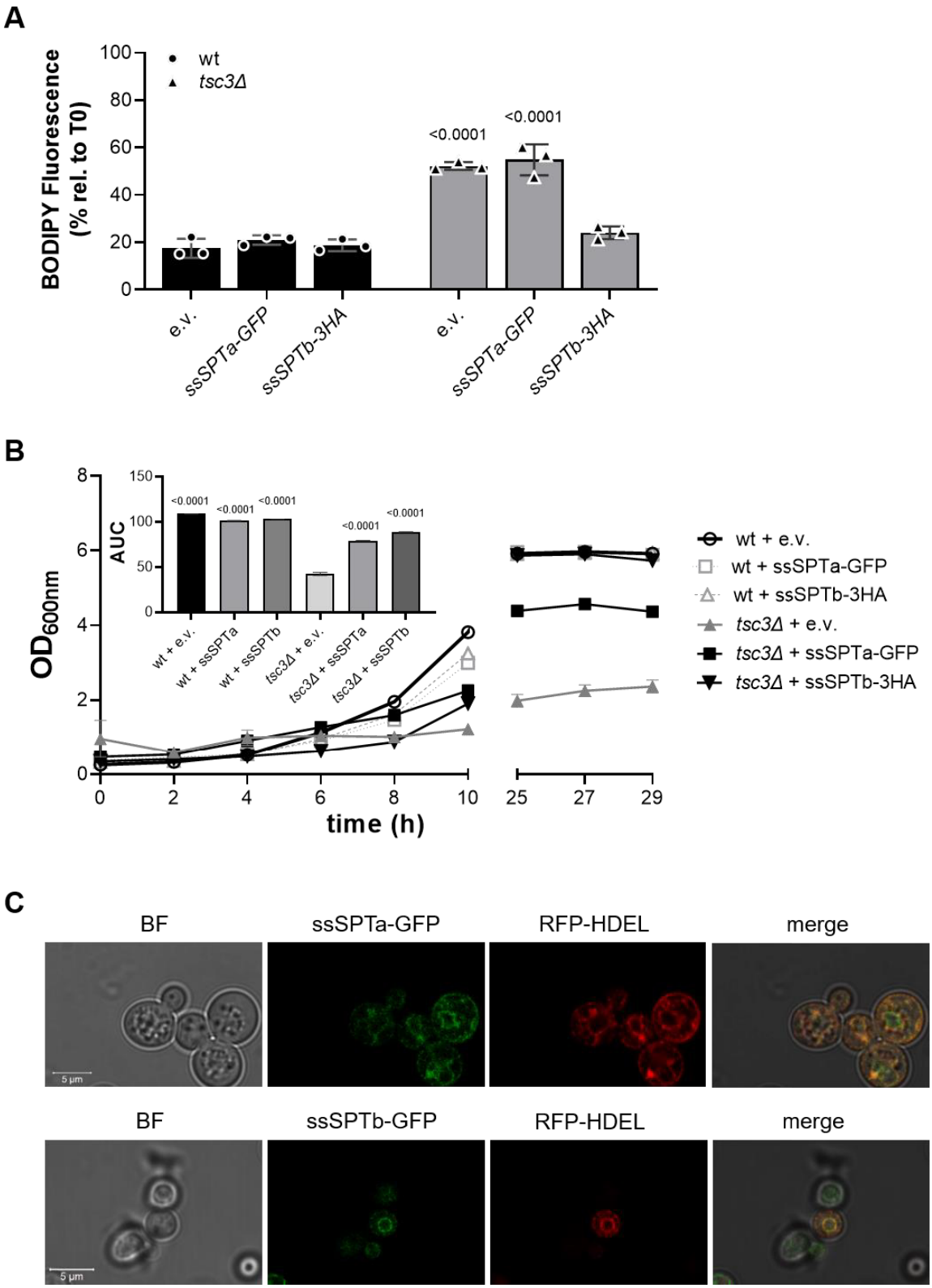

Fig. 16: Effects of recombinant human ssSPTs in *tsc3Δ* cells. LD consumption after 5 h of growth of WT and *tsc3Δ* strains, transfected with an empty vector (e.v.), pRS415-ADHpr-ssSPTb-3HA or pRS415-ADHpr-ssSPTa-GFP, after dilution from stationary phase into fresh medium containing cerulenin quantified by BODIPY493/503 stained LD flow cytometry analysis (n=3, mean ± SD, one-way ANOVA, *P* vs. WT + e.v.). (B) Growth progression including area under curve (AUC) statistics of WT and *tsc3Δ* strains transfected with an empty vector (e.v.), pRS415-ADHpr-ssSPTb-3HA or pRS415-ADHpr-ssSPTa-GFP (n=3, ± SEM, one-way ANOVA, *P* vs. *tsc3Δ* + e.v.). (C) The localization of constituent expressed ssSPTa-GFP or ssSPTb-GFP in WT cells co-expressing RFP-HDEL investigated in stadium of stationary phase by fluorescence microscopy.

Based on the rescue effects observed in the flow cytometry and growth curve analysis (Fig. 16A and B), it can be suggested that the human ssSPTs interact with the yeast SPT at the ER and stimulate its activity like Tsc3p, ameliorating the defective LD consumption and growth due to low cellular sphingolipid level.

To investigate the localization of the ssSPTs in yeast, WT cells overexpressing C-terminal GFP-tagged ssSPTa and ssSPTb together with a vector expressing RFP-ssHDEL as marker for the ER were analyzed with LSM in stationary phase. Fluorescence microscopic analysis showed that both ssSPTa-GFP and ssSPTb-GFP localized at the ER similarly to Tsc3p (Fig. 16C).

4.7. Analysis of the role of the small subunit b of the serine palmitoyltransferase in HepG2 cells

Previous studies have shown that increased intrahepatic TAG content is associated with elevated cellular DAG levels, which can cause hepatic insulin resistance via activation of the novel PKCε (Jornayvaz & Shulman, 2012; Petersen et al., 2016). Since TAGs are stored in LD and the expression of ssSPTb-3HA in *tsc3Δ* cells rescues LD consumption (Fig. 16A and B), the role of ssSPTb, functional human analog of Tsc3, in the lipid composition and insulin signaling in HepG2 cells was explored.

4.7.1. Assessment of ssSPTb-siRNA efficiency with qRT-PCR

It was hypothesized that the knock-down via siRNA of ssSPTb would lead to a decreased SPT activity, resulting in an impairment of the sphingolipid synthesis and an elevated cellular level of TAG like in *tsc3Δ* cells. To this end, a transient ssSPTb silencing was performed in HepG2 cells by using a commercial siRNA and the knock-down efficiency was determined at different time points by assessing levels of ssSPTb transcripts with qRT-PCR.

The qRT-PCR results showed that the ssSPTb transcript levels were significantly reduced by 50% 24 h and 48 h after transfection (Fig. 17A).

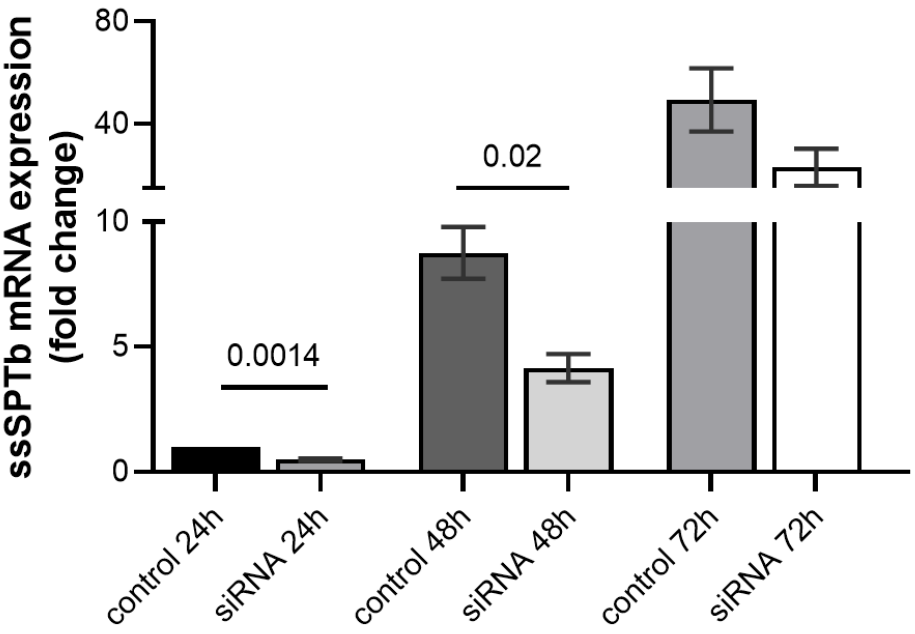

Fig. 17: Silencing efficiency of ssSPTb in HepG2 cells measured by qRT-PCR. Silencing efficiency in HepG2 cells at 24 h, 48 h and 72 h after ssSPTb-siRNA transfection (n=5, mean ± SEM, one-way ANOVA vs. control).

Unfortunately, the ssSPTb protein concentration could not be determined, because commercial polyclonal antibodies did not work. All efforts to use the standard protocol for protein detection were unsuccessful. Also, variations of the protocol, e.g. changing the concentration of dissolved antibody, different blocking solutions (milk or BSA) and changing incubation times did not lead to a meaningful detected signal. In addition, the antibody manufacturing company could not provide a result or a protocol as proof of the functioning of the antibody. Consequently, the work with the only available antibody was stopped.

4.7.2. Silencing of ssSPTb does not alter cellular lipid content in HepG2 cells

Cellular lipid composition was analyzed by LC-MS/MS in ssSPTb-silenced HepG2 cells 48 h after ssSPTb-siRNA transfection. The results of the LC-MS/MS showed no significant changes of the DAG, Cer and sphingolipid species between the untreated control group and the ssSPTb-siRNA treated group (Fig. 18A-D).

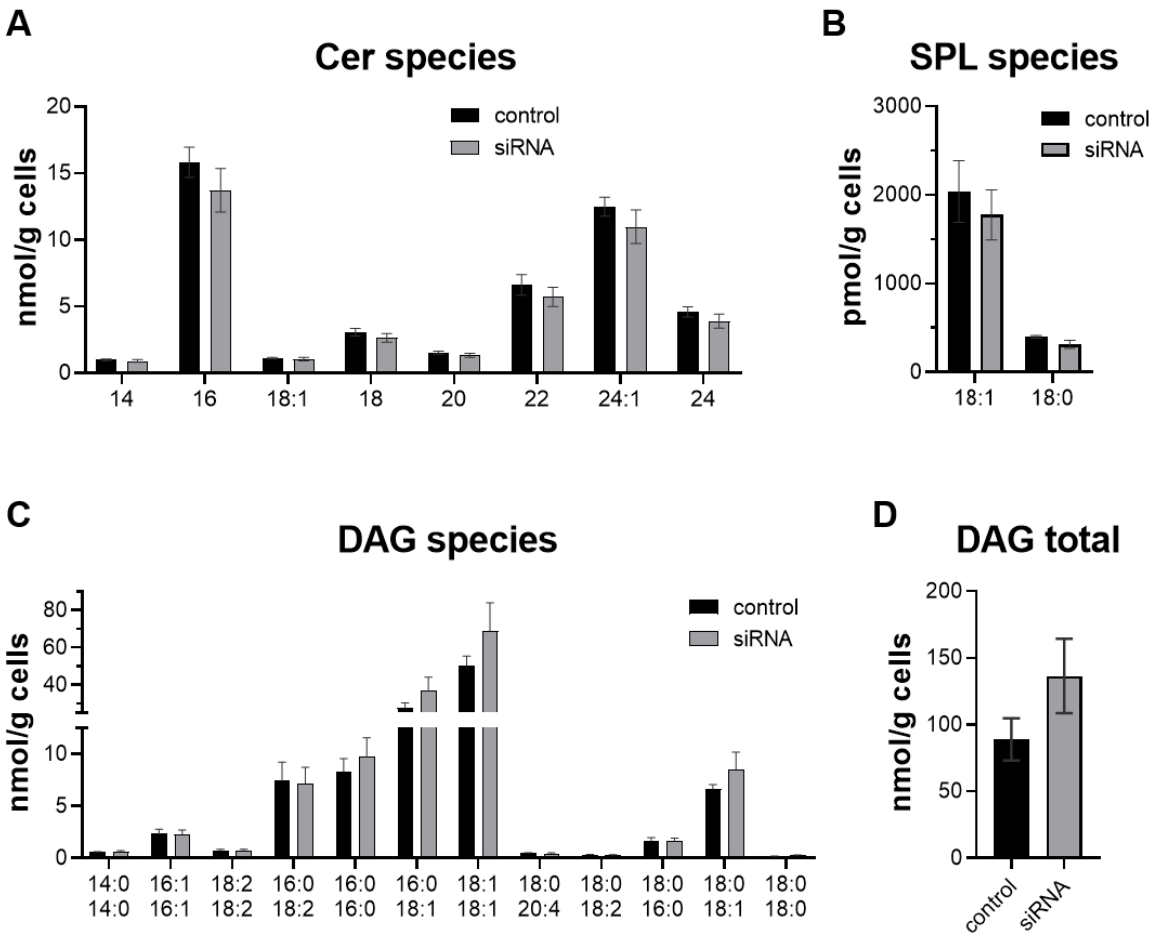

Fig. 18: Effect of siRNA-ssSPTb treatment on hepatic lipid composition in HepG2 cells. (A-D) Mass spectrometry analysis of lipid content in untreated and 48 h ssSPTb silenced HepG2 cells (SPL:sphingolipid) (n=5-7 per group, mean ± SEM).

4.7.3. Silencing of ssSPTb does not alter the insulin signaling in HepG2 cells

The DAG/PKCε insulin signaling pathway in ssSPTb silenced HepG2 cells was examined by investigations of cellular PKCε translocation and the inhibitory phosphorylation of IRK at residue Thr^{1160}. For this purpose, HepG2 cells were treated with ssSPTb-siRNA for 48 h and the proteins were extracted for immunodetection analysis.

The immunodetection results showed that ssSPTb silencing had no effect on the translocation of PKCε in HepG2 cells (Fig. 19A). Similarly, no changes in the phosphorylation status of Thr^{1160} of the IRK domain were detected (Fig. 19B).

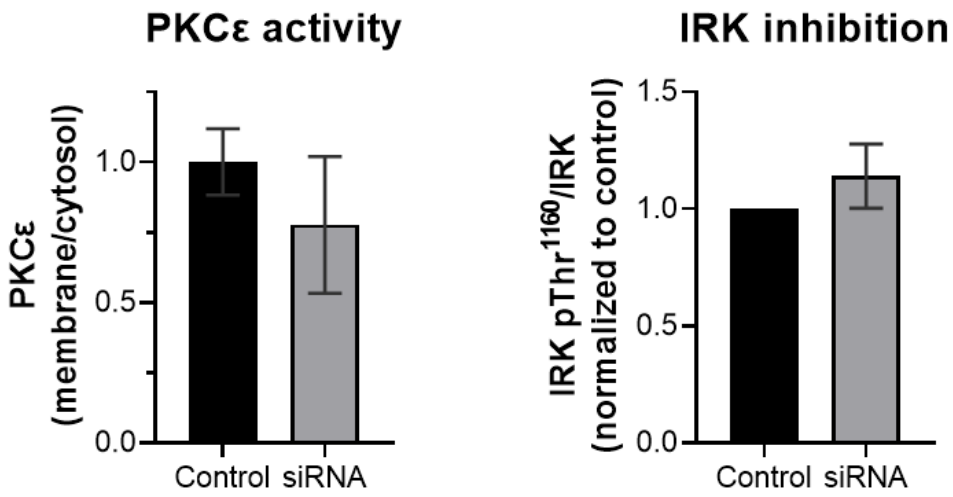

Fig. 19: Effect of ssSPTb silencing on PKCε translocation and Insulin receptor kinase phosphorylation in HepG2 cells. Immunodetection of (A) PKCε translocation [membrane/cytosol ratio] (n=3, mean ± SEM) and (B) phosphorylation of IRK pThr1160 in 48 h siRNA-ssSPTb treated HepG2 cells (n=6, mean ± SEM).

5. Discussion

The discussion of the results is structured in two sections, which refer to the two different model organisms. The first section addresses the findings of studies on *S. cerevisiae* in point-by-point fashion:

- Sphingolipid synthesis-deficiency decreases LD breakdown in yeast.
- Growth and LD dynamics under control of a common sphingolipid-regulated mechanism in yeast.

These findings on Tsc3p regulation on lipid homeostasis were further examined in human HepG2 cells and form the second section:

- Silencing of ssSPTb does not alter lipid homeostasis and insulin signaling in HepG2 cells.

5.1. Sphingolipid synthesis-deficiency decreases LD breakdown in yeast

The results of flow cytometry and fluorescence microscopy indicate that LDs are consumed during the growth phase and that Tsc3p is a regulator of LD dynamics in yeast. Deletion of *tsc3,* which encodes Tsc3, a stimulator of SPT, the first step of sphingolipid synthesis (Gable et al., 2000; Ren et al., 2018), decreases LD consumption after 5 h of growth resumption, ultimately regulating LD breakdown. Moreover, flow cytometry data of myriocin-treated yeast cells indicate that inhibition of SPT, leads to a decreased consumption of LDs. Of note, myriocin inhibits the function of the SPT (Miyake et al., 1995). Evidence from previous studies employing certain yeast mutants found that defects in the sphingolipid synthesis pathway affect lipid storage and LD biogenesis. One of them is the *lcb1-100^{ts}* mutant, which has a defect in sphingolipid biosynthesis (Nagiec et al., 1994). A genome-wide screen had shown that *lcb1-100^{ts}* cells in mid-logarithmic-phase have an elevated amount of LDs as compared to WT cells (Fei, Alfaro, et al., 2008). These results reflect the defect in LD consumption due to sphingolipid synthesis interruption observed in this work after auxin-induced degradation of Lcb1-AID.

The flow cytometry-based LD analysis of *tsc3Δ* cells, myriocin-treated cells and Lcb1-AID depleted cells indicate that disruption of total sphingolipid biosynthesis results in reduced LD consumption in yeast. These effects of defective LD consumption are also apparent in yeast mutant strains lacking genes like *sac1, csg2, and ipt1*, which are related to the sphingolipid synthesis downstream of SPT.

Furthermore, the cells in the flow cytometry experiments were exposed to cerulenin, which inhibits FA and sterol biosynthesis during growth phase (Omura, 1976). It can be concluded that the increased amount of LDs in sphingolipid biosynthesis deficient yeast cells after 5 h

growth resumption is not due to increased LD biosynthesis, but rather to reduced LD consumption.

The hypothesis of a futile cycle could explain why yeast cells with impaired sphingolipid biosynthesis exhibit disturbed LD consumption. A futile cycle of re-esterification of unused LD substrates like DAG has already been described in studies on the Ice2 protein, which is required for efficient channeling of DAG derived from LD toward the ER (Markgraf et al., 2014). In the absence of Ice2, the newly formed DAG catalyzed by TAG lipases remains on the LDs and enters a potentially futile cycle of re-esterification to TAG, resulting in a decreased LD consumption (Markgraf et al., 2014). This futile cycle prevents the accumulation of toxic levels of TAG-derived products in the cell (Markgraf et al., 2014). Among others, excessive accumulation of FAs is lipotoxic to yeast as well as human cells (Garbarino & Sturley, 2009; Rockenfeller et al., 2010; Roden & Shulman, 2019; Szendroedi et al., 2014). Disturbance of sphingolipid synthesis due to less efficient SPT in *tsc3Δ* cells may result in toxic accumulation of palmitate that is not utilized for sphingolipid synthesis. The *tsc3Δ* cells could prevent this lipotoxic effect by repetitively re-esterification of palmitate cleaved from TAG to DAG which would drive a futile cycle and ultimately suppress LD consumption (Fig 20). Future experiments on the palmitate flux in LD could provide information whether such futile cycle is indeed operative in *tsc3Δ* cells. One approach could be measurement of the ratio of TAG-bound labeled palmitate in isolated LD via mass spectrometry. In case of a futile cycle, the ratio of labeled palmitate to the number of TAGs should rise during the growth phase, as the unused palmitate would always recirculate, while other FAs are supplied to cellular processes as usual. Unfortunately, these hypotheses could not be experimentally demonstrated due to unavailability of commercial ^{13}C palmitate.

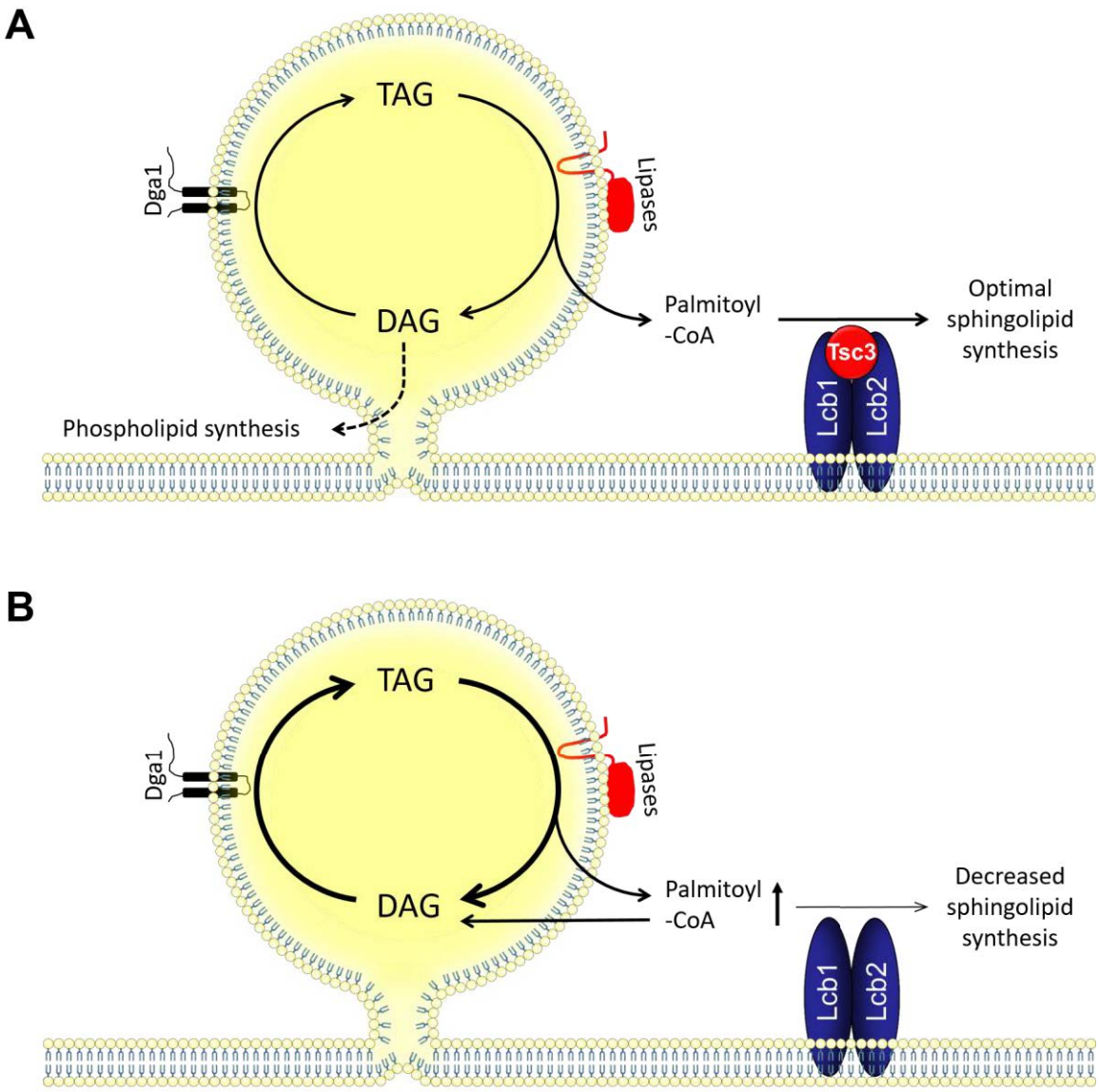

Fig. 20: Illustration of LD dynamics coupled to sphingolipid synthesis in WT and *tsc3Δ* cells. (A) Sphingolipid synthesis by utilization of palmitate released from LD in WT cells. (B) Hypothesis of the "futile cycle" where the reduction of SPT activity in *tsc3Δ* cells results in palmitate released from LDs during lipolysis and re-esterified to TAG instead of being channeled into the sphingolipid synthesis pathway.

However, the present study shows that PHS rescues LD consumption in *tsc3Δ* cells. One might speculate that this rescue effect is caused by entrance of mobilized FA into the PHC synthesis. Hence, C26 VLCFAs are condensed with PHS to yield PHC and an external addition of PHS could break a futile cycle of FA that are used for C26 elongation in *tsc3Δ* cells. In order to investigate the hypothesis of a futile cycle, the lipolytic activity of *tsc3Δ* cells was increased by overexpressing Tgl3-3HA. Tgl3p is the most relevant lipase for TAG degradation, which provides the mobilization of FA from stored TAGs for utilization in the cell (Athenstaedt & Daum, 2003; Schmidt et al., 2013). The lipolytic activity occurs in presence of LDs through hydrolysis of TAGs with variable chain lengths as substrate to receive FAs (Klein et al., 2016). If the futile cycle buffers the excessive and toxic

accumulation of unused FAs in *tsc3Δ* cells, it should also do so in the presence of increased lipolysis and increased FA release from LDs. However, our flow cytometry measurements show that overexpression of Tgl3-3HA results in a rescue of LD consumption in *tsc3Δ* but not with an increase of LD degradation in WT cells. This indicates that in WT cells the maximum potential of lipolytic activity is already reached within 5 h of growth resumption. The fact that overexpression of Tgl3p-3HA restores LD consumption in *tsc3Δ* cells indicates that the recombinant Tgl3-3HA overexpression may overcome the inhibited lipolytic activity, which would explain a decreased LD consumption in *tsc3Δ* cells, possibly due to the downregulation of other lipases residing on the LD. It remains yet unclear where palmitate, mobilized by the continuously active major lipase Tgl3p, is channeled in *tsc3Δ* cells if not utilized for sphingolipid synthesis. It can be speculated that excess released FAs are directed to alternative pathways rather than being re-esterified to TAG. Previous work indicated that yeast channels excess FAs into membrane phospholipid synthesis, resulting in increased levels of phosphatidic acid and DAG (Petschnigg et al., 2009).

In general, a valid measurement of the lipidome of *tsc3Δ* cells remains open in this work in order to pinpoint which FA or lipid species interfere with cellular mechanisms for maintenance of lipid homeostasis. Based on previous *in vitro* assays on isolated microsomes, one may assume that the SPT activity is reduced (by ~30fold) in yeast with *tsc3* deletion, although the level of total sphingolipids was ultimately not analyzed (Gable et al., 2000). According to these results, *tsc3Δ* cells are expected to have decreased sphingolipid synthesis due to reduced SPT activity. More recent studies, however, show that Tsc3p regulates the affinity of amino acids converted by SPT by preferring alanine as substrate for the production of non-canonical deoxy-sphingoid bases (Ren et al., 2018). In the absence of Tsc3p, the ratio of amino acids utilized changes in favor of an increased influx of serine into the sphingolipid pathway (Ren et al., 2018). It has been also claimed that the level of both yeast ceramides DHC and PHC is elevated and the LCB-precursor molecules DHS and PHS are decreased in *tsc3Δ* cells in comparison to WT cells (Ren et al., 2018).

Regardless of the controversial literature regarding cellular sphingolipid levels in *tsc3Δ* cells, this work shows that proteins related to complex sphingolipid formation influence LD dynamics. Deletion of Sac1, the phosphoinositide phosphatase, which hydrolysis PtdIns(4)P and thereby regulates substrate supply of PI to Aur1p for IPC synthesis, results in a decreased LD consumption in comparison to WT cells. Foti et al. already achieved similar results in a *sac1^{ts}* mutant, demonstrating that rapid inactivation of Sac1p leads to increased accumulation of cellular PtdIns(4)P, accompanied by disturbed morphology of vacuoles and an increased accumulation of LDs (Foti et al., 2001). Control of the PtdIns(4)P pool appears to be critical for maintaining normal vacuole shape and function (Foti et al.,

2001). The attached LDs in *sac1^{ts}* cells cluster around the vacuole and associate with vacuolar invaginations (Foti et al., 2001). It has been suggested that the vacuole/LDs formation may provide a transport pathway for sterol esters to the plasma membrane and it is conceivable that Sac1p is required in this process (Foti et al., 2001; Zweytick et al., 2000). One may conclude that nonfunctioning Sac1p results in increased accumulation of cellular PtdIns(4)P with disrupted vacuole shape and impaired sterol ester exchange between LD and vacuole, ultimately leading to reduced LD degradation. This also provides an explanation for the reduced LD consumption in *tsc3Δ* cells, because Tsc3p is required for Sac1p binding to SPT and ER localization of Sac1 is crucial for the efficient turnover of PtdIns(4)P (Han et al., 2019).

It is also conceivable that deletion of *tsc3* in yeast impairs LD breakdown by reduced synthesis of IPC and subsequent complex sphingolipids. This supported by studies in yeast cells treated with aureobasidin A, which prevents synthesis of IPC and its mannosylated derivatives (Epstein, Castillon, et al., 2012; Schorling et al., 2001). Nile red staining of LD is increased in WT cells treated with aureobasidin A as well as in a quadruple mutant *cSLΔ* strain that is deficient to form complex sphingolipids (Epstein, Castillon, et al., 2012). The present results on reduced LD consumption in cell lines devoid of synthesis of complex sphingolipids such as *sac1Δ csg2Δ* and *ipt1Δ*, support the conclusion that reduced synthesis of complex sphingolipids decreases LD degradation.

5.2. Growth and LD dynamics under control of a common sphingolipid-regulated mechanism in yeast

This thesis demonstrates that sphingolipid metabolism has a regulatory influence on LD dynamics with the additional potential to modulate growth in yeast. Monitoring of the growth rate of WT and *tsc3Δ* cells showed that the WT strain reaches the stationary phase faster than the *tsc3Δ* strain. This result is comparable to previous studies where it has been demonstrated that Tsc3p is essential for growth at high temperatures of 37°C (Gable et al., 2000; Han et al., 2009). The present work extends this finding of a growth defect of thermosensitive *tsc3Δ* cells to lower temperatures of 30°C. Additionally, direct interruption of the first step of sphingolipid synthesis by auxin inducible depletion of Lcb1p-AID also results in a growth defect. This confirms previous studies showing that mutation of Lcb1 (lcb1-100) impairs sphingolipid synthesis, resulting in low cellular sphingolipid levels accompanied with reduced growth (Epstein, Kirkpatrick, et al., 2012). Impaired growth is also a phenotypic hallmark of triple knockout *lcb1Δlcb2Δtsc3Δ* mutant yeast cells expressing the human LCB1–LCB2 heterodimer, which accumulates less sphingolipids due to reduced activity of SPT (Han et al., 2009; Harmon et al., 2013). Moreover, a growth defect

was detected in a thermosensitive double mutant *lac1Δlag1Δ* yeast strain, which is known for its decreased Cer synthesis (Epstein, Castillon, et al., 2012).
As in other studies on Tsc3 (Gable et al., 2000; Han et al., 2009), this work demonstrates that the addition of PHS, a Cer precursor molecule, to the growth medium reverses the growth defect in *tsc3Δ* cells, even at higher temperatures of 37°C. PHS also reverses the auxin-induced growth defect in the OsTIR LCB1-AID strain, highlighting the functional impact of sphingolipids on growth.

Previous research found an explanation for the impact of sphingolipids on growth, that providing evidence of a sphingolipid-PP2A-Swe1-Cdc28 pathway (Fig 21). Sphingolipids have already been described as regulatory molecules activating the function of the protein phosphatase 2A (PP2A) and thereby inhibiting the activity of the yeast morphogenesis checkpoint kinase Swe1 (Fishbein et al., 1993; Nickels & Broach, 1996). In detail, the regulatory subunit Cdc55 of PP2A inhibits the phosphorylation and activity of Swe1 (Harvey et al., 2011; Yang et al., 2000). Swe1 in turn regulates the G2/M transition in yeast by its inhibitory phosphorylation at side chain residue tyrosine 19 of the major cyclin-dependent kinase Cdc28 (Lew, 2003; Sia et al., 1998; Sia et al., 1996). Cdc28 is an essential regulator responsible for the cell cycle transitions in yeast (Costanzo et al., 2004). It is unclear which specific sphingolipids regulate PP2A. It is suspected that the specific Cer species C18:1 PHC serves as an activator of Cdc55, which then leads to the activation of Cdc28 by Swe1 (Matmati et al., 2009; Matmati et al., 2013). However, complimentary studies support the hypothesis that sphingolipids influence cell cycle progression coordinated by a PP2A-Swe1-Cdc28 pathway. A *tgl3Δtgl4Δ* mutant strain, which is impaired in lipolysis of TAGs shows a cell cycle delay (Chauhan et al., 2015). These cells are unable to provide adequate palmitate for sphingolipid synthesis (Chauhan et al., 2015). Interestingly, supplementation of PHS reconstitutes the cell cycle progression in *tgl3Δtgl4Δ* cells through Swe1 phosphorylation of Cdc28 regulated by PP2A and Cdc55 (Chauhan et al., 2015).

The rescue effect on the observed reconstitution of growth by supplementation of PHS may lead to the hypothesis that cell cycle progression in *tsc3Δ* mutant or cells with depleted Lcb1p is disturbed due to a low level of sphingolipids. It would be conceivable that a reduced level of sphingolipids decreases the activity of $PP2A^{Cdc55}$, which in turn leads to an enhanced activation of the cell cycle checkpoint Swe1p. Swe1p is thus able to arrest the cell cycle by an inhibitory phosphorylation of Cdc28p, ultimately abolishing cell cycle progression. At this point, immunodetection experiments on the phosphorylation status of $Cdc28^{Y19}$ could determine whether the activity of the sphingolipid-PP2A-Swe1-Cdc28 pathway is altered in *tsc3Δ* cells.

It is conceivable that the sphingolipid-PP2A-Swe1-Cdc28 pathway is also responsible for the defective LD consumption in sphingolipid synthesis deficient cells by downregulation of lipolysis (Fig 21). The yeast TAG lipase Tgl4p is phosphorylated and activated by the cyclin-dependent kinase Cdc28p which provides evidence for a direct connection between regulation of the cell cycle progression and LD breakdown (Kurat et al., 2009). In detail, Tgl4p is activated via phosphorylation at residues Thr^{675} and Ser^{890} by Cdc28p in time of G1/S transition (Kurat et al., 2009). Thus, Cdc28p is a branching point for sphingolipids regulating activity of growth and lipolysis. Of note, this study shows that cells with a deletion of the sphingolipid regulated lipase Tgl4p showed a similar defect of LD consumption as *tsc3Δ* cells.

According to Gable et al., a deletion of Tsc3 results in reduced flux of palmitate into sphingolipid synthesis (Gable et al., 2000). Thus, lack of Tsc3p could prevent efficient channeling of palmitoyl-CoA into sphingolipid biosynthesis, thereby decreasing total cellular sphingolipid level, which in turns impairs Tgl4p-controlled lipolysis indirectly by the PP2A-Swe1-Cdc28 pathway. This model is supported by the rescue of LD consumption in *tsc3Δ* cells upon addition of exogenous PHS, which should replenish cellular sphingolipid levels.

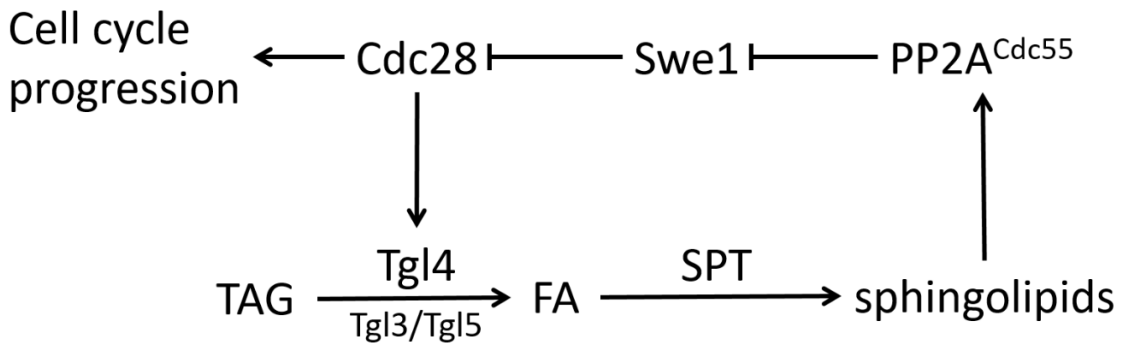

Fig. 21: Sphingolipids regulate PP2A-Swe1-Cdc28 axis in yeast. Schematic illustration of proposed mechanism of how sphingolipids control the PP2A-Swe1-Cdc28 pathway, resulting in regulation of cell cycle progression and Tgl4 driven lipolysis.

In contrast to Gable et al., elevated Cer levels are found in *tsc3Δ* cells due to increased activity of the yeast Cer synthases Ypk1 (Ren et al., 2018). This supports the concept that only a specific sphingolipid species, but not total cellular sphingolipids activate PP2A.

In line, C18:1 PHC activates $PP2A^{Cdc55}$ (Matmati et al., 2009; Matmati et al., 2013). C18:1 PHCs are formed by hydrolysis of complex sphingolipids catalyzed by Isc1 (Clarke et al., 2006; Matmati & Hannun, 2008; Sawai et al., 2000). The formation of complex sphingolipids requires a functional Sac1p, which depends on Tsc3p (Han et al., 2019). Consequently, reduced complex sphingolipid levels as well as reduced amount of C18:1 PHC should be present in *tsc3Δ* cells. However, in this hypothetical model, it remains unclear why exogenous PHS restores defective growth and LD consumption in *tsc3Δ* cells. At this point, detailed measurements of the lipid profile of *tsc3Δ* cells are essential to rule out how the

crosstalk between neutral lipid and sphingolipid metabolism regulates cellular lipid homeostasis and growth.

In conclusion, based on the data from this thesis, one may speculate that a deletion of Tsc3p leads to low levels of specific cellular sphingolipid content, which in turn inhibits the activity of Cdc28p, resulting in a decreased Tgl4p-controlled lipolysis and cell cycle progression. Due to the absence of lipidome measurements, it remains unclear which sphingolipid species exactly triggers the inhibitory effect of growth and LD consumption in yeast. Future experiments are needed to investigate which sphingolipid species is reduced in *tsc3Δ* cells and whether the activity of Cdc28p is inhibited in *tsc3Δ* cells, resulting in a cell cycle arrest accompanied with decreased lipolytic activity of Tgl4p.

5.3. Silencing of ssSPTb does not alter lipid homeostasis and insulin signaling in HepG2 cells

The present work shows that the overexpression of human ssSPTb-3HA is able to rescue the defective growth and LD consumption in *tsc3Δ* cells. Previous studies have reported that *lcb1Δlcb2Δtsc3Δ* yeast cells co-expressing either human ssSPTa or ssSPTb along with human LCB1–LCB2 show an increased SPT activity and reconstitute cellular sphingolipid level accompanied with improved growth (Han et al., 2009; Harmon et al., 2013). These results also highlight how closely the function of the human SPT and its small subunits correspond to those of yeast. Fluorescence microscopic analysis in this study supports this statement, showing that both ssSPTa-GFP and ssSPTb-GFP localize to the cortical ER similarly to the Tsc3p and SPT. Based on these findings, it is probable that human ssSPTs stimulates the sphingolipid synthesis by a co-localization in the ER and interaction with yeast SPT.

However, overexpression of human ssSPTa-GFP shows only a minor effect on growth without rescue of the LD consumption defect. It can be speculated that in our ssSPTa-GFP construct the C-terminal GFP tag (27 kDa), which is a big protein in relation to ssSPTa (8.46 kDa), interferes with activity.

Because overexpression of ssSPTb-3HA, but not ssSPTa-GFP, rescues the LD consumption and the growth of the *tsc3Δ* strain, the role of ssSPTb in the cellular lipid homeostasis in HepG2 cells was further investigated, since elevated levels of lipid intermediates like Cer and DAG are associated with hepatic insulin resistance (Apostolopoulou et al., 2018; Greenberg et al., 2011; Jornayvaz & Shulman, 2012; Krahmer et al., 2013; Luukkonen et al., 2016; Petersen et al., 2016; Roden & Shulman, 2019). Contrary to our hypothesis, knock-down of ssSPTb by siRNA did not significantly decline neither the sphingolipid synthesis nor elevates the accumulation of DAG in HepG2.

Based on the presence of structurally distinct LCBs, there is reason to believe that sphingosine backbones in mammalian cells are synthesized from acyl-CoAs other than just palmitoyl-CoA (Pruett et al., 2008). Using an *in vitro* assay with microsomes consisting of human LCB1 (hLCB1) and human LCB2a (hLCB2a), combined with one of the two ssSPT isoforms, shows that the differently combined SPT isozymes have different acyl-CoA preferences (Han et al., 2009). Microsomes with hLCB1/hLCB2a/ssSPTa are highly selective for C16-CoA and microsomes hLCB1/hLCB2a/ssSPTb have a preference for C18-CoA as a substrate for sphingolipid synthesis (Han et al., 2009). It is possible that the sphingolipid synthesis is not declined in HepG2 ssSPTb knocked-down cells because the function of the missing ssSPTb is replaced by ssSPTa. The additional fact that ssSPTb is only poorly expressed in liver tissue, which is shown in studies of HPA Tissue Gene Expression Profiles Dataset of ssSPTb from National Center for Biotechnology Information (https://www.ncbi.nlm.nih.gov/gene/165679), leads to the hypothesis that ssSPTb is not that important for sphingolipid synthesis in liver cells. This is also reflected in the low detection of ssSPTb transcript levels in HepG2 cells measured by RT-qPCR in this work.

Moreover, in this work it is shown that knock-down of ssSPTb has no effect on the translocation of PKCε from cytosol to the plasma membrane. Consequently, PKCε does not show elevated activity in HepG2 cells with ssSPTb knock-down. In addition, immunodetection does not show significant changes in inhibitory Thr^{1160} phosphorylation of the IRK domain. These results are consistent with the unchanged level of cellular DAG measured in ssSPTb-silenced HepG2 cells.

Although the present study of ssSPTb did not show an effect on cellular DAG and Cer content in HepG2 cells, previous studies have demonstrated the considerable influence of sphingolipid synthesis on lipid homeostasis maintenance and hepatic insulin resistance. Previous studies demonstrate that adenoviral mediated hLCB2 expression results in an elevated level of Cers and an inhibited insulin signaling, whereas a knock-down of hLCB3 suppresses Cer accumulation and reduces insulin resistance in HepG2 cells (Kim et al., 2020; Teng et al., 2019). Furthermore, inhibition of the SPT activity has influence on the LD consumption. It has been shown that the treatment of HepG2 cells with myriocin activates pathways of autophagy, which results in lipophagy and elevated degradation of LDs (Yang et al., 2019).This is in contrast with the present results in myriocin treated yeast cells, showing a reduced LD consumption. Further *in vivo* studies are needed to draw conclusions on how the crosstalk between neutral lipid and sphingolipid metabolism regulates cellular lipid homeostasis with regard to metabolic diseases like T2D or NAFLD.

6. Summary

This work investigates whether proteins required for sphingolipid synthesis regulate lipid droplet consumption, and thus efficient interception of lipotoxic, diabetes-relevant metabolites.

This thesis shows that Tsc3p, a stimulator of the serine palmitoyltransferase and thus of sphingolipid biosynthesis in the endoplasmic reticulum, is an essential regulator of lipid droplet consumption and ultimately of lipid droplet dynamics in yeast. Lipid droplet consumption and growth is impaired in *tsc3* deletion cells as well as in cells with deletion of proteins of the sphingolipid biosynthesis downstream of the serine palmitoyltransferase. The rescue effect of phytosphingosine on lipid droplet consumption and growth in these cells suggests that the downregulated lipolysis and attenuated growth are due to low level of sphingolipids. One conceivable mechanism regulating both triacylglycerol breakdown and growth is the sphingolipid-regulated PP2A-Swe1-Cdc28 signaling pathway, although the exact sphingolipid species involved in this regulation remains uncertain. Moreover, a continuous re-esterification of lipolysis-derived fatty acids into triacylglycerol could have a concomitant influence on deficient lipid droplet consumption.

In addition, this thesis shows that the human analog of Tsc3p, at least ssSPTb, is able to reconstitute the growth and rescue lipid droplet consumption defect in *tsc3Δ* cells, suggesting an essential role for ssSPTb in the regulation of lipid droplet dynamics in human cells. However, silencing of ssSPTb in human hepatocytes does not alter the concentration of any diacylglycerol, ceramide and sphingolipid species as well as the activity of the PKCε and the phosphorylation of the insulin receptor kinase. This suggests that the second stimulator of the serine palmitoyltransferase, ssSPTa, compensates for the absent activity of ssSPTb.

A more profound and advanced knowledge of the interplay between sphingolipid metabolism and lipid droplet dynamics in mammalian cells could be beneficial for clinical detection of diabetes subtypes and the care of people suffering from it.

7. Appendix

Table 10: Values of qRT-PCR analysis of ssSPTb transcript from ssSPTb silenced HepG2 cells.

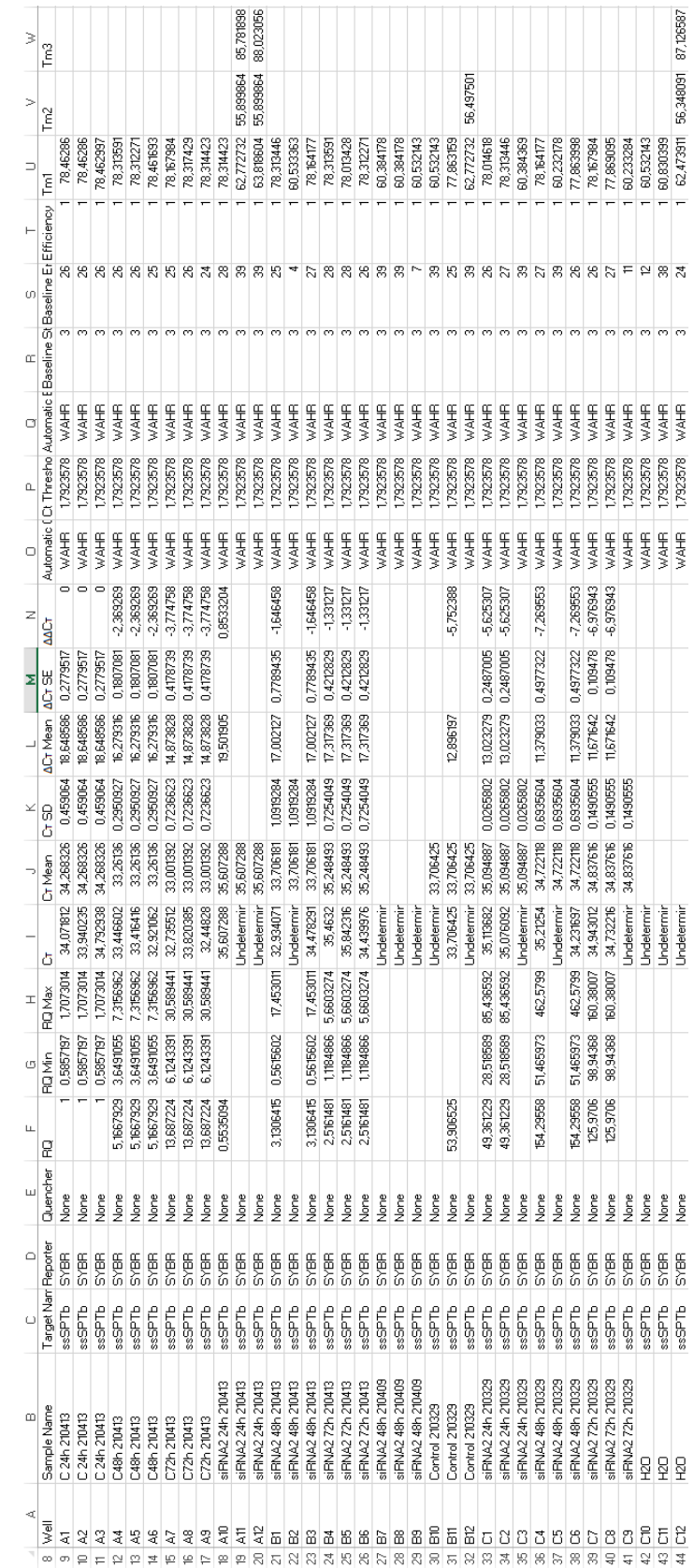

Well	Sample Name	Target Nan	Reporter	Quencher	RQ	RQ Min	RQ Max	Ct	Ct Mean	Ct SD	ΔCt Mean	ΔCt SE	ΔΔCt	Automatic	Ct Thresho	Automatic E	Baseline	Baseline St	Baseline E	Efficiency	Tm1	Tm2	Tm3
A1	C 24h 210413	ssSPTb	SYBR	None	1	0,5857197	1,7073014	34,07812	34,268326	0,459064	18,648586	0,2779517	0	WAHR	1,7923578	WAHR	3	26	1	78,46286		
A2	C 24h 210413	ssSPTb	SYBR	None	1	0,5857197	1,7073014	33,940235	34,268326	0,459064	18,648586	0,2779517	0	WAHR	1,7923578	WAHR	3	26	1	78,46286		
A3	C 24h 210413	ssSPTb	SYBR	None	1	0,5857197	1,7073014	34,732938	34,268326	0,459064	18,648586	0,2779517	0	WAHR	1,7923578	WAHR	3	26	1	78,462397		
A4	C48h 210413	ssSPTb	SYBR	None	5,1667929	3,6491055	7,3156962	33,446602	33,26136	0,2950927	16,279316	0,1807081	-2,369269	WAHR	1,7923578	WAHR	3	26	1	78,313591		
A5	C48h 210413	ssSPTb	SYBR	None	5,1667929	3,6491055	7,3156962	33,416416	33,26136	0,2950927	16,279316	0,1807081	-2,369269	WAHR	1,7923578	WAHR	3	26	1	78,312271		
A6	C48h 210413	ssSPTb	SYBR	None	5,1667929	3,6491055	7,3156962	32,921062	33,26136	0,2950927	16,279316	0,1807081	-2,369269	WAHR	1,7923578	WAHR	3	25	1	78,461693		
A7	C72h 210413	ssSPTb	SYBR	None	13,687224	6,1243391	30,589441	32,736512	33,001392	0,7236623	14,873828	0,4178739	-3,774758	WAHR	1,7923578	WAHR	3	25	1	78,167984		
A8	C72h 210413	ssSPTb	SYBR	None	13,687224	6,1243391	30,589441	33,820385	33,001392	0,7236623	14,873828	0,4178739	-3,774758	WAHR	1,7923578	WAHR	3	26	1	78,317429		
A9	C72h 210413	ssSPTb	SYBR	None	13,687224	6,1243391	30,589441	32,44828	33,001392	0,7236623	14,873828	0,4178739	-3,774758	WAHR	1,7923578	WAHR	3	24	1	78,314423		
A10	siRNA2 24h 210413	ssSPTb	SYBR	None	0,5535094			35,607288	35,607288		19,501905		0,8533204	WAHR	1,7923578	WAHR	3	28	1	78,314423		
A11	siRNA2 24h 210413	ssSPTb	SYBR	None				Undetermir	35,607288					WAHR	1,7923578	WAHR	3	39	1	62,772732	55,899864	85,781898
A12	siRNA2 24h 210413	ssSPTb	SYBR	None				Undetermir	35,607288					WAHR	1,7923578	WAHR	3	39	1	63,818604	55,899864	88,023056
B1	siRNA2 48h 210413	ssSPTb	SYBR	None	3,1306415	0,5615602	17,453011	32,934071	33,706181	1,0919284	17,002127	0,7789435	-1,646458	WAHR	1,7923578	WAHR	3	25	1	78,313446		
B2	siRNA2 48h 210413	ssSPTb	SYBR	None				Undetermir	33,706181	1,0919284				WAHR	1,7923578	WAHR	3	4	1	60,533363		
B3	siRNA2 48h 210413	ssSPTb	SYBR	None	3,1306415	0,5615602	17,453011	34,478291	33,706181	1,0919284	17,002127	0,7789435	-1,646458	WAHR	1,7923578	WAHR	3	27	1	78,164177		
B4	siRNA2 72h 210413	ssSPTb	SYBR	None	2,5161481	1,1184866	5,6603274	35,4632	35,248493	0,7254049	17,317369	0,4212829	-1,331217	WAHR	1,7923578	WAHR	3	28	1	78,313591		
B5	siRNA2 72h 210413	ssSPTb	SYBR	None	2,5161481	1,1184866	5,6603274	35,842316	35,248493	0,7254049	17,317369	0,4212829	-1,331217	WAHR	1,7923578	WAHR	3	28	1	78,013428		
B6	siRNA2 72h 210413	ssSPTb	SYBR	None	2,5161481	1,1184866	5,6603274	34,439976	35,248493	0,7254049	17,317369	0,4212829	-1,331217	WAHR	1,7923578	WAHR	3	26	1	78,312271		
B7	siRNA2 48h 210409	ssSPTb	SYBR	None				Undetermir						WAHR	1,7923578	WAHR	3	39	1	60,384178		
B8	siRNA2 48h 210409	ssSPTb	SYBR	None				Undetermir						WAHR	1,7923578	WAHR	3	39	1	60,384178		
B9	siRNA2 48h 210409	ssSPTb	SYBR	None				Undetermir						WAHR	1,7923578	WAHR	3	7	1	60,532143		
B10	Control 210329	ssSPTb	SYBR	None				Undetermir	33,706425					WAHR	1,7923578	WAHR	3	39	1	60,532143		
B11	Control 210329	ssSPTb	SYBR	None	53,906525			33,706425	33,706425		12,896197		-5,752388	WAHR	1,7923578	WAHR	3	25	1	77,863159		
B12	Control 210329	ssSPTb	SYBR	None				Undetermir	33,706425					WAHR	1,7923578	WAHR	3	39	1	62,772732	56,497501	
C1	siRNA2 24h 210329	ssSPTb	SYBR	None	49,361229	28,518589	85,436592	35,113682	35,094887	0,0265802	13,023279	0,2467005	-5,625307	WAHR	1,7923578	WAHR	3	26	1	78,014618		
C2	siRNA2 24h 210329	ssSPTb	SYBR	None	49,361229	28,518589	85,436592	35,076092	35,094887	0,0265802	13,023279	0,2487005	-5,625307	WAHR	1,7923578	WAHR	3	27	1	78,313446		
C3	siRNA2 24h 210329	ssSPTb	SYBR	None				Undetermir	35,094887	0,0265802				WAHR	1,7923578	WAHR	3	39	1	60,384369		
C4	siRNA2 48h 210329	ssSPTb	SYBR	None	154,29658	51,465973	462,5799	35,21254	34,722118	0,6935604	11,379033	0,4977322	-7,269553	WAHR	1,7923578	WAHR	3	27	1	78,164177		
C5	siRNA2 48h 210329	ssSPTb	SYBR	None				Undetermir	34,722118	0,6935604				WAHR	1,7923578	WAHR	3	39	1	60,232178		
C6	siRNA2 48h 210329	ssSPTb	SYBR	None	154,29658	51,465973	462,5799	34,223697	34,722118	0,6935604	11,379033	0,4977322	-7,269553	WAHR	1,7923578	WAHR	3	26	1	77,863398		
C7	siRNA2 72h 210329	ssSPTb	SYBR	None	125,9706	98,94368	160,38007	34,943012	34,837616	0,1490555	11,671642	0,1094778	-6,976943	WAHR	1,7923578	WAHR	3	26	1	78,167984		
C8	siRNA2 72h 210329	ssSPTb	SYBR	None	125,9706	98,94368	160,38007	34,732216	34,837616	0,1490555	11,671642	0,1094778	-6,976943	WAHR	1,7923578	WAHR	3	27	1	77,869095		
C9	siRNA2 72h 210329	ssSPTb	SYBR	None				Undetermir	34,837616	0,1490555				WAHR	1,7923578	WAHR	3	11	1	60,233284		
C10	H2O	ssSPTb	SYBR	None				Undetermir						WAHR	1,7923578	WAHR	3	12	1	60,532143		
C11	H2O	ssSPTb	SYBR	None				Undetermir						WAHR	1,7923578	WAHR	3	38	1	60,830399		
C12	H2O	ssSPTb	SYBR	None				Undetermir						WAHR	1,7923578	WAHR	3	24	1	62,473911	56,348091	87,126587

Table 11: Values of qRT-PCR analysis of tubulin transcript from ssSPTb silenced HepG2 cells.

	A	B	C	D	E	F	G	H	I	J	K	L	M	N	O	P	Q	R	S	T	U	V	W
1	Well	Sample Name	Target Nar	Reporter	Quencher	RQ	RQ Min	RQ Max	Cr	Cr Mean	Cr SD	ΔCr Mean	ΔCr SE	ΔΔCr	Automatic	Ct Threshc	Automatic	Baseline S	Baseline E	Efficiency	Tm1	Tm2	Tm3
2	D1	C 24h 210413	Tubulin	SYBR	None				15,73962	15,61974	0,145023				WAHR	0,391927	WAHR	3	10	1	81,3017		
3	D2	C 24h 210413	Tubulin	SYBR	None				15,45854	15,61974	0,145023				WAHR	0,391927	WAHR	3	8	1	81,15228		
4	D3	C 24h 210413	Tubulin	SYBR	None				15,66106	15,61974	0,145023				WAHR	0,391927	WAHR	3	10	1	81,15238		
5	D4	C48h 210413	Tubulin	SYBR	None				16,87976	16,98204	0,104339				WAHR	0,391927	WAHR	3	11	1	81,15238		
6	D5	C48h 210413	Tubulin	SYBR	None				17,08832	16,98204	0,104339				WAHR	0,391927	WAHR	3	12	1	81,15129		
7	D6	C48h 210413	Tubulin	SYBR	None				16,97805	16,98204	0,104339				WAHR	0,391927	WAHR	3	10	1	81,15129		
8	D7	C72h 210413	Tubulin	SYBR	None				18,12421	18,12757	0,012984				WAHR	0,391927	WAHR	3	11	1	81,15686		
9	D8	C72h 210413	Tubulin	SYBR	None				18,1419	18,12757	0,012984				WAHR	0,391927	WAHR	3	12	1	81,15686		
10	D9	C72h 210413	Tubulin	SYBR	None				18,11659	18,12757	0,012984				WAHR	0,391927	WAHR	3	11	1	81,15362		
11	D10	siRNA2 24h 210413	Tubulin	SYBR	None				16,00922	16,10538	0,201042				WAHR	0,391927	WAHR	3	10	1	81,15362		
12	D11	siRNA2 24h 210413	Tubulin	SYBR	None				15,97048	16,10538	0,201042				WAHR	0,391927	WAHR	3	10	1	81,00078		
13	D12	siRNA2 24h 210413	Tubulin	SYBR	None				16,33644	16,10538	0,201042				WAHR	0,391927	WAHR	3	12	1	81,15018		
14	E1	siRNA2 48h 210413	Tubulin	SYBR	None				16,7864	16,70405	0,178319				WAHR	0,391927	WAHR	3	12	1	81,3017		
15	E2	siRNA2 48h 210413	Tubulin	SYBR	None				16,49944	16,70405	0,178319				WAHR	0,391927	WAHR	3	11	1	81,3017		
16	E3	siRNA2 48h 210413	Tubulin	SYBR	None				16,82632	16,70405	0,178319				WAHR	0,391927	WAHR	3	10	1	81,15238		
17	E4	siRNA2 72h 210413	Tubulin	SYBR	None				18,02062	17,93113	0,078902				WAHR	0,391927	WAHR	3	12	1	81,30179		
18	E5	siRNA2 72h 210413	Tubulin	SYBR	None				17,87159	17,93113	0,078902				WAHR	0,391927	WAHR	3	12	1	81,30071		
19	E6	siRNA2 72h 210413	Tubulin	SYBR	None				17,90118	17,93113	0,078902				WAHR	0,391927	WAHR	3	11	1	81,30071		
20	E7	siRNA2 48h 210409	Tubulin	SYBR	None				37,07651	33,62566	3,04589				WAHR	0,391927	WAHR	3	30	1	72,19023		
21	E8	siRNA2 48h 210409	Tubulin	SYBR	None				31,31189	33,62566	3,04589				WAHR	0,391927	WAHR	3	25	1	81,00742		
22	E9	siRNA2 48h 210409	Tubulin	SYBR	None				32,48857	33,62566	3,04589				WAHR	0,391927	WAHR	3	26	1	80,85475		
23	E10	Control 210329	Tubulin	SYBR	None				20,93877	20,81023	0,117376				WAHR	0,391927	WAHR	3	14	1	81,00418		
24	E11	Control 210329	Tubulin	SYBR	None				20,70875	20,81023	0,117376				WAHR	0,391927	WAHR	3	16	1	80,85136		
25	E12	Control 210329	Tubulin	SYBR	None				20,78316	20,81023	0,117376				WAHR	0,391927	WAHR	3	15	1	81,00078		
26	F1	siRNA2 24h 210329	Tubulin	SYBR	None				22,54265	22,07161	0,42953				WAHR	0,391927	WAHR	3	18	1	81,15228		
27	F2	siRNA2 24h 210329	Tubulin	SYBR	None				21,7016	22,07161	0,42953				WAHR	0,391927	WAHR	3	17	1	81,15228		
28	F3	siRNA2 24h 210329	Tubulin	SYBR	None				21,97058	22,07161	0,42953				WAHR	0,391927	WAHR	3	17	1	81,15238		
29	F4	siRNA2 48h 210329	Tubulin	SYBR	None				23,27643	23,34308	0,147217				WAHR	0,391927	WAHR	3	18	1	81,15238		
30	F5	siRNA2 48h 210329	Tubulin	SYBR	None				23,24098	23,34308	0,147217				WAHR	0,391927	WAHR	3	16	1	81,15129		
31	F6	siRNA2 48h 210329	Tubulin	SYBR	None				23,51184	23,34308	0,147217				WAHR	0,391927	WAHR	3	16	1	81,15129		
32	F7	siRNA2 72h 210329	Tubulin	SYBR	None				23,15168	23,16597	0,051283				WAHR	0,391927	WAHR	3	14	1	81,15686		
33	F8	siRNA2 72h 210329	Tubulin	SYBR	None				23,22289	23,16597	0,051283				WAHR	0,391927	WAHR	3	17	1	81,15686		
34	F9	siRNA2 72h 210329	Tubulin	SYBR	None				23,12335	23,16597	0,051283				WAHR	0,391927	WAHR	3	16	1	81,00418		
35	F10	H2O	Tubulin	SYBR	None				35,75892	35,30113	1,167764				WAHR	0,391927	WAHR	3	31	1	75,17638		
36	F11	H2O	Tubulin	SYBR	None				33,97383	35,30113	1,167764				WAHR	0,391927	WAHR	3	29	1	72,93262		
37	F12	H2O	Tubulin	SYBR	None				36,17064	35,30113	1,167764				WAHR	0,391927	WAHR	3	29	1	71,58794		

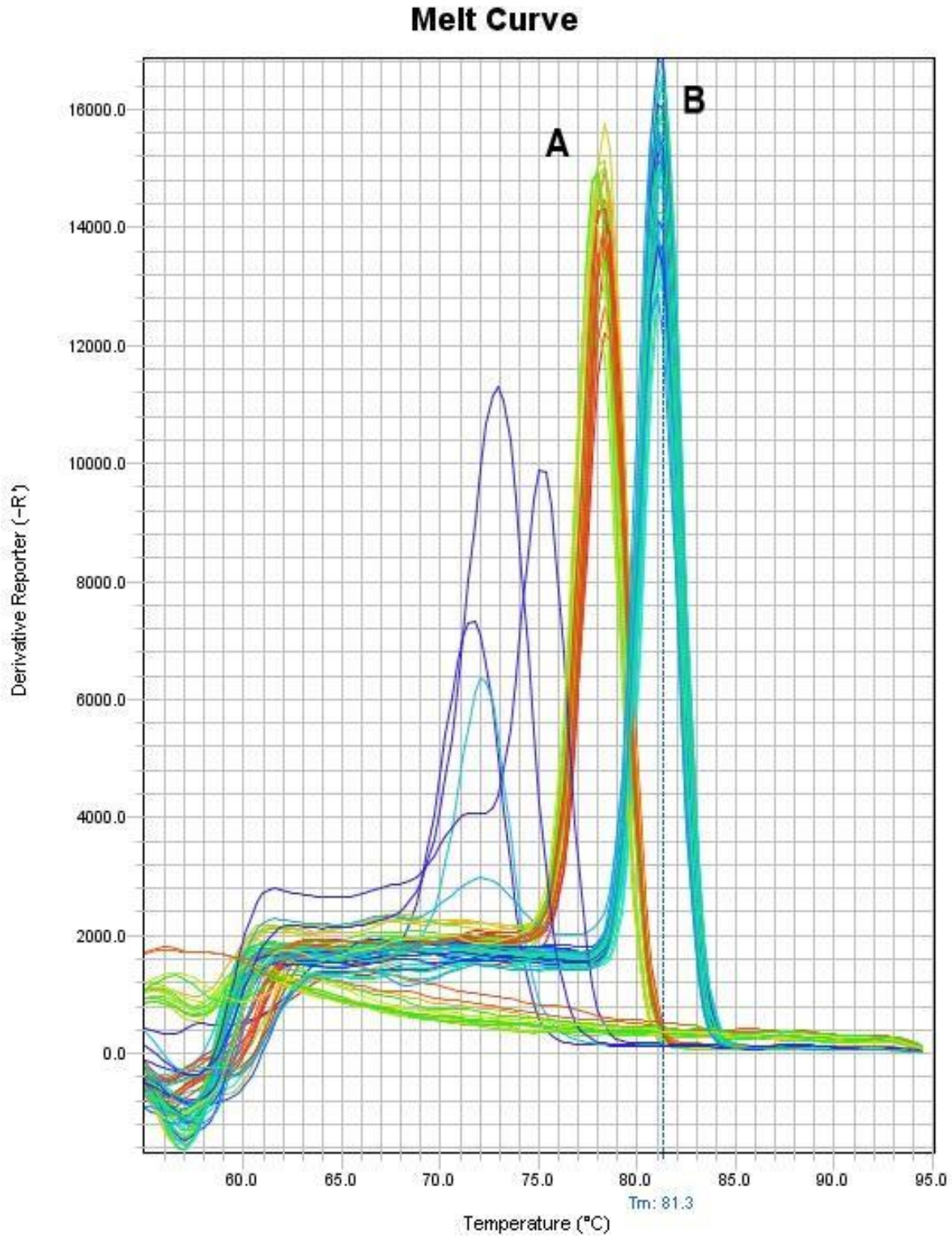

Fig. 22: Melting curve analysis of ssSPTb and tubulin amplicons of ssSPTb silenced HepG2 cells measured by qRT-PCR. Assessed is the Dissociation of (A) ssSPTb DNA amplicon and (B) tubulin DNA amplicon during heating.

8. Literature

Aburasayn, H., Al Batran, R., & Ussher, J. R. (2016). Targeting ceramide metabolism in obesity. *Am J Physiol Endocrinol Metab*, *311*(2), E423-435. https://doi.org/10.1152/ajpendo.00133.2016

Apostolopoulou, M., Gordillo, R., Koliaki, C., Gancheva, S., Jelenik, T., De Filippo, E., Herder, C., Markgraf, D., Jankowiak, F., Esposito, I., Schlensak, M., Scherer, P. E., & Roden, M. (2018). Specific Hepatic Sphingolipids Relate to Insulin Resistance, Oxidative Stress, and Inflammation in Nonalcoholic Steatohepatitis. *Diabetes Care*, *41*(6), 1235-1243. https://doi.org/10.2337/dc17-1318

Athenstaedt, K., & Daum, G. (2003). YMR313c/TGL3 encodes a novel triacylglycerol lipase located in lipid particles of Saccharomyces cerevisiae. *J Biol Chem*, *278*(26), 23317-23323. https://doi.org/10.1074/jbc.M302577200

Athenstaedt, K., & Daum, G. (2005). Tgl4p and Tgl5p, two triacylglycerol lipases of the yeast Saccharomyces cerevisiae are localized to lipid particles. *J Biol Chem*, *280*(45), 37301-37309. https://doi.org/10.1074/jbc.M507261200

Bagnat, M., & Simons, K. (2002). Lipid rafts in protein sorting and cell polarity in budding yeast Saccharomyces cerevisiae. *Biol Chem*, *383*(10), 1475-1480. https://doi.org/10.1515/BC.2002.169

Barbosa, A. D., Savage, D. B., & Siniossoglou, S. (2015). Lipid droplet-organelle interactions: emerging roles in lipid metabolism. *Curr Opin Cell Biol*, *35*, 91-97. https://doi.org/10.1016/j.ceb.2015.04.017

Barbosa, A. D., & Siniossoglou, S. (2017). Function of lipid droplet-organelle interactions in lipid homeostasis. *Biochim Biophys Acta Mol Cell Res*, *1864*(9), 1459-1468. https://doi.org/10.1016/j.bbamcr.2017.04.001

Barres, R., & Zierath, J. R. (2016). The role of diet and exercise in the transgenerational epigenetic landscape of T2DM. *Nat Rev Endocrinol*, *12*(8), 441-451. https://doi.org/10.1038/nrendo.2016.87

Beller, M., Thiel, K., Thul, P. J., & Jackle, H. (2010). Lipid droplets: a dynamic organelle moves into focus. *FEBS Lett*, *584*(11), 2176-2182. https://doi.org/10.1016/j.febslet.2010.03.022

Bellou, V., Belbasis, L., Tzoulaki, I., & Evangelou, E. (2018). Risk factors for type 2 diabetes mellitus: An exposure-wide umbrella review of meta-analyses. *PLoS One*, *13*(3), e0194127. https://doi.org/10.1371/journal.pone.0194127

Bergman, B. C., Hunerdosse, D. M., Kerege, A., Playdon, M. C., & Perreault, L. (2012). Localisation and composition of skeletal muscle diacylglycerol predicts insulin resistance in humans. *Diabetologia*, *55*(4), 1140-1150. https://doi.org/10.1007/s00125-011-2419-7

Binns, D., Januszewski, T., Chen, Y., Hill, J., Markin, V. S., Zhao, Y., Gilpin, C., Chapman, K. D., Anderson, R. G., & Goodman, J. M. (2006). An intimate collaboration between peroxisomes and lipid bodies. *J Cell Biol*, *173*(5), 719-731. https://doi.org/10.1083/jcb.200511125

Bligh, E. G., & Dyer, W. J. (1959). A rapid method of total lipid extraction and purification. *Can J Biochem Physiol*, *37*(8), 911-917. https://doi.org/10.1139/o59-099

Bodis, K., & Roden, M. (2018). Energy metabolism of white adipose tissue and insulin resistance in humans. *Eur J Clin Invest*, *48*(11), e13017. https://doi.org/10.1111/eci.13017

Bourbon, N. A., Yun, J., & Kester, M. (2000). Ceramide directly activates protein kinase C zeta to regulate a stress-activated protein kinase signaling complex. *J Biol Chem*, *275*(45), 35617-35623. https://doi.org/10.1074/jbc.M007346200

Boya, P., Reggiori, F., & Codogno, P. (2013). Emerging regulation and functions of autophagy. *Nat Cell Biol*, *15*(7), 713-720. https://doi.org/10.1038/ncb2788

Brady, R. N., Di Mari, S. J., & Snell, E. E. (1969). Biosynthesis of sphingolipid bases. 3. Isolation and characterization of ketonic intermediates in the synthesis of

sphingosine and dihydrosphingosine by cell-free extracts of Hansenula ciferri. *J Biol Chem*, *244*(2), 491-496. https://www.ncbi.nlm.nih.gov/pubmed/4388074

Breslow, D. K. (2013). Sphingolipid homeostasis in the endoplasmic reticulum and beyond. *Cold Spring Harb Perspect Biol*, *5*(4), a013326. https://doi.org/10.1101/cshperspect.a013326

Breslow, D. K., Collins, S. R., Bodenmiller, B., Aebersold, R., Simons, K., Shevchenko, A., Ejsing, C. S., & Weissman, J. S. (2010). Orm family proteins mediate sphingolipid homeostasis. *Nature*, *463*(7284), 1048-1053. https://doi.org/10.1038/nature08787

Brice, S. E., Alford, C. W., & Cowart, L. A. (2009). Modulation of sphingolipid metabolism by the phosphatidylinositol-4-phosphate phosphatase Sac1p through regulation of phosphatidylinositol in Saccharomyces cerevisiae. *J Biol Chem*, *284*(12), 7588-7596. https://doi.org/10.1074/jbc.M808325200

Buede, R., Rinker-Schaffer, C., Pinto, W. J., Lester, R. L., & Dickson, R. C. (1991). Cloning and characterization of LCB1, a Saccharomyces gene required for biosynthesis of the long-chain base component of sphingolipids. *J Bacteriol*, *173*(14), 4325-4332. https://doi.org/10.1128/jb.173.14.4325-4332.1991

Buhman, K. K., Chen, H. C., & Farese, R. V., Jr. (2001). The enzymes of neutral lipid synthesis. *J Biol Chem*, *276*(44), 40369-40372. https://doi.org/10.1074/jbc.R100050200

Camporez, J. P., Jornayvaz, F. R., Petersen, M. C., Pesta, D., Guigni, B. A., Serr, J., Zhang, D., Kahn, M., Samuel, V. T., Jurczak, M. J., & Shulman, G. I. (2013). Cellular mechanisms by which FGF21 improves insulin sensitivity in male mice. *Endocrinology*, *154*(9), 3099-3109. https://doi.org/10.1210/en.2013-1191

Camporez, J. P. G., Kanda, S., Petersen, M. C., Jornayvaz, F. R., Samuel, V. T., Bhanot, S., Petersen, K. F., Jurczak, M. J., & Shulman, G. I. (2015). ApoA5 knockdown improves whole-body insulin sensitivity in high-fat-fed mice by reducing ectopic lipid content. *J Lipid Res*, *56*(3), 526-536. https://doi.org/10.1194/jlr.M054080

Carman, G. M., & Han, G. S. (2009). Regulation of phospholipid synthesis in yeast. *J Lipid Res*, *50 Suppl*, S69-73. https://doi.org/10.1194/jlr.R800043-JLR200

Cartwright, B. R., Binns, D. D., Hilton, C. L., Han, S., Gao, Q., & Goodman, J. M. (2015). Seipin performs dissectible functions in promoting lipid droplet biogenesis and regulating droplet morphology. *Mol Biol Cell*, *26*(4), 726-739. https://doi.org/10.1091/mbc.E14-08-1303

Casanovas, A., Sprenger, R. R., Tarasov, K., Ruckerbauer, D. E., Hannibal-Bach, H. K., Zanghellini, J., Jensen, O. N., & Ejsing, C. S. (2015). Quantitative analysis of proteome and lipidome dynamics reveals functional regulation of global lipid metabolism. *Chem Biol*, *22*(3), 412-425. https://doi.org/10.1016/j.chembiol.2015.02.007

Chauhan, N., Visram, M., Cristobal-Sarramian, A., Sarkleti, F., & Kohlwein, S. D. (2015). Morphogenesis checkpoint kinase Swe1 is the executor of lipolysis-dependent cell-cycle progression. *Proc Natl Acad Sci U S A*, *112*(10), E1077-1085. https://doi.org/10.1073/pnas.1423175112

Chaurasia, B., Tippetts, T. S., Mayoral Monibas, R., Liu, J., Li, Y., Wang, L., Wilkerson, J. L., Sweeney, C. R., Pereira, R. F., Sumida, D. H., Maschek, J. A., Cox, J. E., Kaddai, V., Lancaster, G. I., Siddique, M. M., Poss, A., Pearson, M., Satapati, S., Zhou, H., . . . Summers, S. A. (2019). Targeting a ceramide double bond improves insulin resistance and hepatic steatosis. *Science*, *365*(6451), 386-392. https://doi.org/10.1126/science.aav3722

Clarke, C. J., Snook, C. F., Tani, M., Matmati, N., Marchesini, N., & Hannun, Y. A. (2006). The extended family of neutral sphingomyelinases. *Biochemistry*, *45*(38), 11247-11256. https://doi.org/10.1021/bi061307z

Codini, M., Garcia-Gil, M., & Albi, E. (2021). Cholesterol and Sphingolipid Enriched Lipid Rafts as Therapeutic Targets in Cancer. *Int J Mol Sci*, *22*(2). https://doi.org/10.3390/ijms22020726

Costanzo, M., Nishikawa, J. L., Tang, X., Millman, J. S., Schub, O., Breitkreuz, K., Dewar, D., Rupes, I., Andrews, B., & Tyers, M. (2004). CDK activity antagonizes Whi5, an

inhibitor of G1/S transcription in yeast. *Cell*, *117*(7), 899-913. https://doi.org/10.1016/j.cell.2004.05.024

Cowart, L. A., & Obeid, L. M. (2007). Yeast sphingolipids: recent developments in understanding biosynthesis, regulation, and function. *Biochim Biophys Acta*, *1771*(3), 421-431. https://doi.org/10.1016/j.bbalip.2006.08.005

Czabany, T., Athenstaedt, K., & Daum, G. (2007). Synthesis, storage and degradation of neutral lipids in yeast. *Biochim Biophys Acta*, *1771*(3), 299-309. https://doi.org/10.1016/j.bbalip.2006.07.001

Daum, G., Lees, N. D., Bard, M., & Dickson, R. (1998). Biochemistry, cell biology and molecular biology of lipids of Saccharomyces cerevisiae. *Yeast*, *14*(16), 1471-1510. https://doi.org/10.1002/(SICI)1097-0061(199812)14:16<1471::AID-YEA353>3.0.CO;2-Y

Davis, D. L., Gable, K., Suemitsu, J., Dunn, T. M., & Wattenberg, B. W. (2019). The ORMDL/Orm-serine palmitoyltransferase (SPT) complex is directly regulated by ceramide: Reconstitution of SPT regulation in isolated membranes. *J Biol Chem*, *294*(13), 5146-5156. https://doi.org/10.1074/jbc.RA118.007291

Dentin, R., Denechaud, P. D., Benhamed, F., Girard, J., & Postic, C. (2006). Hepatic gene regulation by glucose and polyunsaturated fatty acids: a role for ChREBP. *J Nutr*, *136*(5), 1145-1149. https://doi.org/10.1093/jn/136.5.1145

Dewidar, B., Kahl, S., Pafili, K., & Roden, M. (2020). Metabolic liver disease in diabetes - From mechanisms to clinical trials. *Metabolism*, *111S*, 154299. https://doi.org/10.1016/j.metabol.2020.154299

Dickson, R. C., Sumanasekera, C., & Lester, R. L. (2006). Functions and metabolism of sphingolipids in Saccharomyces cerevisiae. *Prog Lipid Res*, *45*(6), 447-465. https://doi.org/10.1016/j.plipres.2006.03.004

Elbashir, S. M., Harborth, J., Lendeckel, W., Yalcin, A., Weber, K., & Tuschl, T. (2001). Duplexes of 21-nucleotide RNAs mediate RNA interference in cultured mammalian cells. *Nature*, *411*(6836), 494-498. https://doi.org/10.1038/35078107

Epstein, S., Castillon, G. A., Qin, Y., & Riezman, H. (2012). An essential function of sphingolipids in yeast cell division. *Mol Microbiol*, *84*(6), 1018-1032. https://doi.org/10.1111/j.1365-2958.2012.08087.x

Epstein, S., Kirkpatrick, C. L., Castillon, G. A., Muniz, M., Riezman, I., David, F. P. A., Wollheim, C. B., & Riezman, H. (2012). Activation of the unfolded protein response pathway causes ceramide accumulation in yeast and INS-1E insulinoma cells. *J Lipid Res*, *53*(3), 412-420. https://doi.org/10.1194/jlr.M022186

Fakas, S., Konstantinou, C., & Carman, G. M. (2011). DGK1-encoded diacylglycerol kinase activity is required for phospholipid synthesis during growth resumption from stationary phase in Saccharomyces cerevisiae. *J Biol Chem*, *286*(2), 1464-1474. https://doi.org/10.1074/jbc.M110.194308

Fakas, S., Qiu, Y., Dixon, J. L., Han, G. S., Ruggles, K. V., Garbarino, J., Sturley, S. L., & Carman, G. M. (2011). Phosphatidate phosphatase activity plays key role in protection against fatty acid-induced toxicity in yeast. *J Biol Chem*, *286*(33), 29074-29085. https://doi.org/10.1074/jbc.M111.258798

Farese, R. V., Jr., & Walther, T. C. (2009). Lipid droplets finally get a little R-E-S-P-E-C-T. *Cell*, *139*(5), 855-860. https://doi.org/10.1016/j.cell.2009.11.005

Fei, W., Alfaro, G., Muthusamy, B. P., Klaassen, Z., Graham, T. R., Yang, H., & Beh, C. T. (2008). Genome-wide analysis of sterol-lipid storage and trafficking in Saccharomyces cerevisiae. *Eukaryot Cell*, *7*(2), 401-414. https://doi.org/10.1128/EC.00386-07

Fei, W., Shui, G., Gaeta, B., Du, X., Kuerschner, L., Li, P., Brown, A. J., Wenk, M. R., Parton, R. G., & Yang, H. (2008). Fld1p, a functional homologue of human seipin, regulates the size of lipid droplets in yeast. *J Cell Biol*, *180*(3), 473-482. https://doi.org/10.1083/jcb.200711136

Fei, W., Shui, G., Zhang, Y., Krahmer, N., Ferguson, C., Kapterian, T. S., Lin, R. C., Dawes, I. W., Brown, A. J., Li, P., Huang, X., Parton, R. G., Wenk, M. R., Walther, T. C., & Yang, H. (2011). A role for phosphatidic acid in the formation of "supersized" lipid

droplets. *PLoS Genet*, *7*(7), e1002201. https://doi.org/10.1371/journal.pgen.1002201

Ferguson-Yankey, S. R., Skrzypek, M. S., Lester, R. L., & Dickson, R. C. (2002). Mutant analysis reveals complex regulation of sphingolipid long chain base phosphates and long chain bases during heat stress in yeast. *Yeast*, *19*(7), 573-586. https://doi.org/10.1002/yea.861

Fishbein, J. D., Dobrowsky, R. T., Bielawska, A., Garrett, S., & Hannun, Y. A. (1993). Ceramide-mediated growth inhibition and CAPP are conserved in Saccharomyces cerevisiae. *J Biol Chem*, *268*(13), 9255-9261. https://www.ncbi.nlm.nih.gov/pubmed/8387486

Foti, M., Audhya, A., & Emr, S. D. (2001). Sac1 lipid phosphatase and Stt4 phosphatidylinositol 4-kinase regulate a pool of phosphatidylinositol 4-phosphate that functions in the control of the actin cytoskeleton and vacuole morphology. *Mol Biol Cell*, *12*(8), 2396-2411. https://doi.org/10.1091/mbc.12.8.2396

Fujimoto, T., & Parton, R. G. (2011). Not just fat: the structure and function of the lipid droplet. *Cold Spring Harb Perspect Biol*, *3*(3). https://doi.org/10.1101/cshperspect.a004838

Gable, K., Slife, H., Bacikova, D., Monaghan, E., & Dunn, T. M. (2000). Tsc3p is an 80-amino acid protein associated with serine palmitoyltransferase and required for optimal enzyme activity. *J Biol Chem*, *275*(11), 7597-7603. https://doi.org/10.1074/jbc.275.11.7597

Galbo, T., Perry, R. J., Jurczak, M. J., Camporez, J. P., Alves, T. C., Kahn, M., Guigni, B. A., Serr, J., Zhang, D., Bhanot, S., Samuel, V. T., & Shulman, G. I. (2013). Saturated and unsaturated fat induce hepatic insulin resistance independently of TLR-4 signaling and ceramide synthesis in vivo. *Proc Natl Acad Sci U S A*, *110*(31), 12780-12785. https://doi.org/10.1073/pnas.1311176110

Gancheva, S., Jelenik, T., Alvarez-Hernandez, E., & Roden, M. (2018). Interorgan Metabolic Crosstalk in Human Insulin Resistance. *Physiol Rev*, *98*(3), 1371-1415. https://doi.org/10.1152/physrev.00015.2017

Gao, Q., Binns, D. D., Kinch, L. N., Grishin, N. V., Ortiz, N., Chen, X., & Goodman, J. M. (2017). Pet10p is a yeast perilipin that stabilizes lipid droplets and promotes their assembly. *J Cell Biol*, *216*(10), 3199-3217. https://doi.org/10.1083/jcb.201610013

Garbarino, J., & Sturley, S. L. (2009). Saturated with fat: new perspectives on lipotoxicity. *Curr Opin Clin Nutr Metab Care*, *12*(2), 110-116. https://doi.org/10.1097/MCO.0b013e32832182ee

Giaever, G., Chu, A. M., Ni, L., Connelly, C., Riles, L., Veronneau, S., Dow, S., Lucau-Danila, A., Anderson, K., Andre, B., Arkin, A. P., Astromoff, A., El-Bakkoury, M., Bangham, R., Benito, R., Brachat, S., Campanaro, S., Curtiss, M., Davis, K., . . . Johnston, M. (2002). Functional profiling of the Saccharomyces cerevisiae genome. *Nature*, *418*(6896), 387-391. https://doi.org/10.1038/nature00935

Graef, M. (2018). Lipid droplet-mediated lipid and protein homeostasis in budding yeast. *FEBS Lett*, *592*(8), 1291-1303. https://doi.org/10.1002/1873-3468.12996

Greenberg, A. S., Coleman, R. A., Kraemer, F. B., McManaman, J. L., Obin, M. S., Puri, V., Yan, Q. W., Miyoshi, H., & Mashek, D. G. (2011). The role of lipid droplets in metabolic disease in rodents and humans. *J Clin Invest*, *121*(6), 2102-2110. https://doi.org/10.1172/JCI46069

Gross, D. A., & Silver, D. L. (2014). Cytosolic lipid droplets: from mechanisms of fat storage to disease. *Crit Rev Biochem Mol Biol*, *49*(4), 304-326. https://doi.org/10.3109/10409238.2014.931337

Grundy, S. M. (2015). Adipose tissue and metabolic syndrome: too much, too little or neither. *Eur J Clin Invest*, *45*(11), 1209-1217. https://doi.org/10.1111/eci.12519

Guillas, I., Kirchman, P. A., Chuard, R., Pfefferli, M., Jiang, J. C., Jazwinski, S. M., & Conzelmann, A. (2001). C26-CoA-dependent ceramide synthesis of Saccharomyces cerevisiae is operated by Lag1p and Lac1p. *EMBO J*, *20*(11), 2655-2665. https://doi.org/10.1093/emboj/20.11.2655

Gupta, S. D., Gable, K., Han, G., Borovitskaya, A., Selby, L., Dunn, T. M., & Harmon, J. M. (2009). Tsc10p and FVT1: topologically distinct short-chain reductases required for long-chain base synthesis in yeast and mammals. *J Lipid Res*, *50*(8), 1630-1640. https://doi.org/10.1194/jlr.M800580-JLR200

Gutmann, T., Schafer, I. B., Poojari, C., Brankatschk, B., Vattulainen, I., Strauss, M., & Coskun, U. (2020). Cryo-EM structure of the complete and ligand-saturated insulin receptor ectodomain. *J Cell Biol*, *219*(1). https://doi.org/10.1083/jcb.201907210

Haak, D., Gable, K., Beeler, T., & Dunn, T. (1997). Hydroxylation of Saccharomyces cerevisiae ceramides requires Sur2p and Scs7p. *J Biol Chem*, *272*(47), 29704-29710. https://doi.org/10.1074/jbc.272.47.29704

Hales, C. M., Carroll, M. D., Fryar, C. D., & Ogden, C. L. (2020). Prevalence of Obesity and Severe Obesity Among Adults: United States, 2017-2018. *NCHS Data Brief*(360), 1-8. https://www.ncbi.nlm.nih.gov/pubmed/32487284

Han, G., Gupta, S. D., Gable, K., Bacikova, D., Sengupta, N., Somashekarappa, N., Proia, R. L., Harmon, J. M., & Dunn, T. M. (2019). The ORMs interact with transmembrane domain 1 of Lcb1 and regulate serine palmitoyltransferase oligomerization, activity and localization. *Biochim Biophys Acta Mol Cell Biol Lipids*, *1864*(3), 245-259. https://doi.org/10.1016/j.bbalip.2018.11.007

Han, G., Gupta, S. D., Gable, K., Niranjanakumari, S., Moitra, P., Eichler, F., Brown, R. H., Jr., Harmon, J. M., & Dunn, T. M. (2009). Identification of small subunits of mammalian serine palmitoyltransferase that confer distinct acyl-CoA substrate specificities. *Proc Natl Acad Sci U S A*, *106*(20), 8186-8191. https://doi.org/10.1073/pnas.0811269106

Han, G. S., O'Hara, L., Siniossoglou, S., & Carman, G. M. (2008). Characterization of the yeast DGK1-encoded CTP-dependent diacylglycerol kinase. *J Biol Chem*, *283*(29), 20443-20453. https://doi.org/10.1074/jbc.M802866200

Han, S., Lone, M. A., Schneiter, R., & Chang, A. (2010). Orm1 and Orm2 are conserved endoplasmic reticulum membrane proteins regulating lipid homeostasis and protein quality control. *Proc Natl Acad Sci U S A*, *107*(13), 5851-5856. https://doi.org/10.1073/pnas.0911617107

Hanada, K. (2003). Serine palmitoyltransferase, a key enzyme of sphingolipid metabolism. *Biochim Biophys Acta*, *1632*(1-3), 16-30. https://doi.org/10.1016/s1388-1981(03)00059-3

Hannun, Y. A., & Obeid, L. M. (2018). Author Correction: Sphingolipids and their metabolism in physiology and disease. *Nat Rev Mol Cell Biol*, *19*(10), 673. https://doi.org/10.1038/s41580-018-0046-6

Harmon, J. M., Bacikova, D., Gable, K., Gupta, S. D., Han, G., Sengupta, N., Somashekarappa, N., & Dunn, T. M. (2013). Topological and functional characterization of the ssSPTs, small activating subunits of serine palmitoyltransferase. *J Biol Chem*, *288*(14), 10144-10153. https://doi.org/10.1074/jbc.M113.451526

Harvey, S. L., Enciso, G., Dephoure, N., Gygi, S. P., Gunawardena, J., & Kellogg, D. R. (2011). A phosphatase threshold sets the level of Cdk1 activity in early mitosis in budding yeast. *Mol Biol Cell*, *22*(19), 3595-3608. https://doi.org/10.1091/mbc.E11-04-0340

Hill, J. O., Wyatt, H. R., & Peters, J. C. (2012). Energy balance and obesity. *Circulation*, *126*(1), 126-132. https://doi.org/10.1161/CIRCULATIONAHA.111.087213

Holland, W. L., Brozinick, J. T., Wang, L. P., Hawkins, E. D., Sargent, K. M., Liu, Y., Narra, K., Hoehn, K. L., Knotts, T. A., Siesky, A., Nelson, D. H., Karathanasis, S. K., Fontenot, G. K., Birnbaum, M. J., & Summers, S. A. (2007). Inhibition of ceramide synthesis ameliorates glucocorticoid-, saturated-fat-, and obesity-induced insulin resistance. *Cell Metab*, *5*(3), 167-179. https://doi.org/10.1016/j.cmet.2007.01.002

Hubbard, S. R. (1997). Crystal structure of the activated insulin receptor tyrosine kinase in complex with peptide substrate and ATP analog. *EMBO J*, *16*(18), 5572-5581. https://doi.org/10.1093/emboj/16.18.5572

Hubbard, S. R., Wei, L., Ellis, L., & Hendrickson, W. A. (1994). Crystal structure of the tyrosine kinase domain of the human insulin receptor. *Nature*, *372*(6508), 746-754. https://doi.org/10.1038/372746a0

Jacquier, N., Choudhary, V., Mari, M., Toulmay, A., Reggiori, F., & Schneiter, R. (2011). Lipid droplets are functionally connected to the endoplasmic reticulum in Saccharomyces cerevisiae. *J Cell Sci*, *124*(Pt 14), 2424-2437. https://doi.org/10.1242/jcs.076836

Jenkins, G. M., Richards, A., Wahl, T., Mao, C., Obeid, L., & Hannun, Y. (1997). Involvement of yeast sphingolipids in the heat stress response of Saccharomyces cerevisiae. *J Biol Chem*, *272*(51), 32566-32572. https://doi.org/10.1074/jbc.272.51.32566

Jensen-Pergakes, K., Guo, Z., Giattina, M., Sturley, S. L., & Bard, M. (2001). Transcriptional regulation of the two sterol esterification genes in the yeast Saccharomyces cerevisiae. *J Bacteriol*, *183*(17), 4950-4957. https://doi.org/10.1128/JB.183.17.4950-4957.2001

Jornayvaz, F. R., Birkenfeld, A. L., Jurczak, M. J., Kanda, S., Guigni, B. A., Jiang, D. C., Zhang, D., Lee, H. Y., Samuel, V. T., & Shulman, G. I. (2011). Hepatic insulin resistance in mice with hepatic overexpression of diacylglycerol acyltransferase 2. *Proc Natl Acad Sci U S A*, *108*(14), 5748-5752. https://doi.org/10.1073/pnas.1103451108

Jornayvaz, F. R., & Shulman, G. I. (2012). Diacylglycerol activation of protein kinase Cepsilon and hepatic insulin resistance. *Cell Metab*, *15*(5), 574-584. https://doi.org/10.1016/j.cmet.2012.03.005

Kachroo, A. H., Vandeloo, M., Greco, B. M., & Abdullah, M. (2022). Humanized yeast to model human biology, disease and evolution. *Dis Model Mech*, *15*(6). https://doi.org/10.1242/dmm.049309

Kim, G. T., Kim, S. J., Park, S. H., Lee, D., & Park, T. S. (2020). Hepatic Expression of the Serine Palmitoyltransferase Subunit Sptlc2 Reduces Lipid Droplets in the Liver by Activating VLDL Secretion. *J Lipid Atheroscler*, *9*(2), 291-303. https://doi.org/10.12997/jla.2020.9.2.291

Klein, I., Klug, L., Schmidt, C., Zandl, M., Korber, M., Daum, G., & Athenstaedt, K. (2016). Regulation of the yeast triacylglycerol lipases Tgl4p and Tgl5p by the presence/absence of nonpolar lipids. *Mol Biol Cell*, *27*(13), 2014-2024. https://doi.org/10.1091/mbc.E15-09-0633

Koffel, R., & Schneiter, R. (2006). Yeh1 constitutes the major steryl ester hydrolase under heme-deficient conditions in Saccharomyces cerevisiae. *Eukaryot Cell*, *5*(7), 1018-1025. https://doi.org/10.1128/EC.00002-06

Kohlwein, S. D. (2010). Triacylglycerol homeostasis: insights from yeast. *J Biol Chem*, *285*(21), 15663-15667. https://doi.org/10.1074/jbc.R110.118356

Kohlwein, S. D., Veenhuis, M., & van der Klei, I. J. (2013). Lipid droplets and peroxisomes: key players in cellular lipid homeostasis or a matter of fat--store 'em up or burn 'em down. *Genetics*, *193*(1), 1-50. https://doi.org/10.1534/genetics.112.143362

Kondo, N., Ohno, Y., Yamagata, M., Obara, T., Seki, N., Kitamura, T., Naganuma, T., & Kihara, A. (2014). Identification of the phytosphingosine metabolic pathway leading to odd-numbered fatty acids. *Nat Commun*, *5*, 5338. https://doi.org/10.1038/ncomms6338

Kraft, C., & Martens, S. (2012). Mechanisms and regulation of autophagosome formation. *Curr Opin Cell Biol*, *24*(4), 496-501. https://doi.org/10.1016/j.ceb.2012.05.001

Krahmer, N., Farese, R. V., Jr., & Walther, T. C. (2013). Balancing the fat: lipid droplets and human disease. *EMBO Mol Med*, *5*(7), 973-983. https://doi.org/10.1002/emmm.201100671

Kumashiro, N., Erion, D. M., Zhang, D., Kahn, M., Beddow, S. A., Chu, X., Still, C. D., Gerhard, G. S., Han, X., Dziura, J., Petersen, K. F., Samuel, V. T., & Shulman, G. I. (2011). Cellular mechanism of insulin resistance in nonalcoholic fatty liver disease. *Proc Natl Acad Sci U S A*, *108*(39), 16381-16385. https://doi.org/10.1073/pnas.1113359108

Kurat, C. F., Natter, K., Petschnigg, J., Wolinski, H., Scheuringer, K., Scholz, H., Zimmermann, R., Leber, R., Zechner, R., & Kohlwein, S. D. (2006). Obese yeast: triglyceride lipolysis is functionally conserved from mammals to yeast. *J Biol Chem*, *281*(1), 491-500. https://doi.org/10.1074/jbc.M508414200

Kurat, C. F., Wolinski, H., Petschnigg, J., Kaluarachchi, S., Andrews, B., Natter, K., & Kohlwein, S. D. (2009). Cdk1/Cdc28-dependent activation of the major triacylglycerol lipase Tgl4 in yeast links lipolysis to cell-cycle progression. *Mol Cell*, *33*(1), 53-63. https://doi.org/10.1016/j.molcel.2008.12.019

Kurek, K., Piotrowska, D. M., Wiesiolek-Kurek, P., Lukaszuk, B., Chabowski, A., Gorski, J., & Zendzian-Piotrowska, M. (2014). Inhibition of ceramide de novo synthesis reduces liver lipid accumulation in rats with nonalcoholic fatty liver disease. *Liver Int*, *34*(7), 1074-1083. https://doi.org/10.1111/liv.12331

Kusminski, C. M., Shetty, S., Orci, L., Unger, R. H., & Scherer, P. E. (2009). Diabetes and apoptosis: lipotoxicity. *Apoptosis*, *14*(12), 1484-1495. https://doi.org/10.1007/s10495-009-0352-8

Lamb, C. A., Yoshimori, T., & Tooze, S. A. (2013). The autophagosome: origins unknown, biogenesis complex. *Nat Rev Mol Cell Biol*, *14*(12), 759-774. https://doi.org/10.1038/nrm3696

Laplante, M., & Sabatini, D. M. (2012). mTOR signaling in growth control and disease. *Cell*, *149*(2), 274-293. https://doi.org/10.1016/j.cell.2012.03.017

Lee, H. Y., Birkenfeld, A. L., Jornayvaz, F. R., Jurczak, M. J., Kanda, S., Popov, V., Frederick, D. W., Zhang, D., Guigni, B., Bharadwaj, K. G., Choi, C. S., Goldberg, I. J., Park, J. H., Petersen, K. F., Samuel, V. T., & Shulman, G. I. (2011). Apolipoprotein CIII overexpressing mice are predisposed to diet-induced hepatic steatosis and hepatic insulin resistance. *Hepatology*, *54*(5), 1650-1660. https://doi.org/10.1002/hep.24571

Levy, M., & Futerman, A. H. (2010). Mammalian ceramide synthases. *IUBMB Life*, *62*(5), 347-356. https://doi.org/10.1002/iub.319

Lew, D. J. (2003). The morphogenesis checkpoint: how yeast cells watch their figures. *Curr Opin Cell Biol*, *15*(6), 648-653. https://doi.org/10.1016/j.ceb.2003.09.001

Lindahl, L., Santos, A. X., Olsson, H., Olsson, L., & Bettiga, M. (2017). Membrane engineering of S. cerevisiae targeting sphingolipid metabolism. *Sci Rep*, *7*, 41868. https://doi.org/10.1038/srep41868

Listenberger, L. L., Han, X., Lewis, S. E., Cases, S., Farese, R. V., Jr., Ory, D. S., & Schaffer, J. E. (2003). Triglyceride accumulation protects against fatty acid-induced lipotoxicity. *Proc Natl Acad Sci U S A*, *100*(6), 3077-3082. https://doi.org/10.1073/pnas.0630588100

Londos, C., Brasaemle, D. L., Schultz, C. J., Segrest, J. P., & Kimmel, A. R. (1999). Perilipins, ADRP, and other proteins that associate with intracellular neutral lipid droplets in animal cells. *Semin Cell Dev Biol*, *10*(1), 51-58. https://doi.org/10.1006/scdb.1998.0275

Longtine, M. S., McKenzie, A., 3rd, Demarini, D. J., Shah, N. G., Wach, A., Brachat, A., Philippsen, P., & Pringle, J. R. (1998). Additional modules for versatile and economical PCR-based gene deletion and modification in Saccharomyces cerevisiae. *Yeast*, *14*(10), 953-961. https://doi.org/10.1002/(SICI)1097-0061(199807)14:10<953::AID-YEA293>3.0.CO;2-U

Lotta, L. A., Gulati, P., Day, F. R., Payne, F., Ongen, H., van de Bunt, M., Gaulton, K. J., Eicher, J. D., Sharp, S. J., Luan, J., De Lucia Rolfe, E., Stewart, I. D., Wheeler, E., Willems, S. M., Adams, C., Yaghootkar, H., Consortium, E. P.-I., Cambridge, F. C., Forouhi, N. G., . . . Scott, R. A. (2017). Integrative genomic analysis implicates limited peripheral adipose storage capacity in the pathogenesis of human insulin resistance. *Nat Genet*, *49*(1), 17-26. https://doi.org/10.1038/ng.3714

Lowther, J., Naismith, J. H., Dunn, T. M., & Campopiano, D. J. (2012). Structural, mechanistic and regulatory studies of serine palmitoyltransferase. *Biochem Soc Trans*, *40*(3), 547-554. https://doi.org/10.1042/BST20110769

Lucena, R., Alcaide-Gavilan, M., Schubert, K., He, M., Domnauer, M. G., Marquer, C., Klose, C., Surma, M. A., & Kellogg, D. R. (2018). Cell Size and Growth Rate Are Modulated by TORC2-Dependent Signals. *Curr Biol*, *28*(2), 196-210 e194. https://doi.org/10.1016/j.cub.2017.11.069

Luukkonen, P. K., Zhou, Y., Sadevirta, S., Leivonen, M., Arola, J., Oresic, M., Hyotylainen, T., & Yki-Jarvinen, H. (2016). Hepatic ceramides dissociate steatosis and insulin resistance in patients with non-alcoholic fatty liver disease. *J Hepatol*, *64*(5), 1167-1175. https://doi.org/10.1016/j.jhep.2016.01.002

Lynen, F. (1952). Acetyl coenzyme A and the fatty acid cycle. *Harvey Lect*, *48*, 210-244. https://www.ncbi.nlm.nih.gov/pubmed/13142486

Lynen, F. (1954a). [Fatty acid cycles]. *Expos Annu Biochim Med*, *16*, 31-51. https://www.ncbi.nlm.nih.gov/pubmed/13231847 (Cycle des acides gras.)

Lynen, F. (1954b). Participation of coenzyme A in the oxidation of fat. *Nature*, *174*(4438), 962-965. https://doi.org/10.1038/174962a0

Lyu, K., Zhang, D., Song, J., Li, X., Perry, R. J., Samuel, V. T., & Shulman, G. I. (2021). Short-term overnutrition induces white adipose tissue insulin resistance through sn-1,2-diacylglycerol/PKCepsilon/insulin receptor Thr1160 phosphorylation. *JCI Insight*, *6*(4). https://doi.org/10.1172/jci.insight.139946

Ma, S., Xi, B., Yang, L., Sun, J., Zhao, M., & Bovet, P. (2021). Trends in the prevalence of overweight, obesity, and abdominal obesity among Chinese adults between 1993 and 2015. *Int J Obes (Lond)*, *45*(2), 427-437. https://doi.org/10.1038/s41366-020-00698-x

Mager, W. H., & Winderickx, J. (2005). Yeast as a model for medical and medicinal research. *Trends Pharmacol Sci*, *26*(5), 265-273. https://doi.org/10.1016/j.tips.2005.03.004

Magkos, F., Su, X., Bradley, D., Fabbrini, E., Conte, C., Eagon, J. C., Varela, J. E., Brunt, E. M., Patterson, B. W., & Klein, S. (2012). Intrahepatic diacylglycerol content is associated with hepatic insulin resistance in obese subjects. *Gastroenterology*, *142*(7), 1444-1446 e1442. https://doi.org/10.1053/j.gastro.2012.03.003

Manning, A. K., Hivert, M. F., Scott, R. A., Grimsby, J. L., Bouatia-Naji, N., Chen, H., Rybin, D., Liu, C. T., Bielak, L. F., Prokopenko, I., Amin, N., Barnes, D., Cadby, G., Hottenga, J. J., Ingelsson, E., Jackson, A. U., Johnson, T., Kanoni, S., Ladenvall, C., . . . Langenberg, C. (2012). A genome-wide approach accounting for body mass index identifies genetic variants influencing fasting glycemic traits and insulin resistance. *Nat Genet*, *44*(6), 659-669. https://doi.org/10.1038/ng.2274

Markgraf, D. F., Al-Hasani, H., & Lehr, S. (2016). Lipidomics-Reshaping the Analysis and Perception of Type 2 Diabetes. *Int J Mol Sci*, *17*(11). https://doi.org/10.3390/ijms17111841

Markgraf, D. F., Klemm, R. W., Junker, M., Hannibal-Bach, H. K., Ejsing, C. S., & Rapoport, T. A. (2014). An ER protein functionally couples neutral lipid metabolism on lipid droplets to membrane lipid synthesis in the ER. *Cell Rep*, *6*(1), 44-55. https://doi.org/10.1016/j.celrep.2013.11.046

Martin, S., & Parton, R. G. (2006). Lipid droplets: a unified view of a dynamic organelle. *Nat Rev Mol Cell Biol*, *7*(5), 373-378. https://doi.org/10.1038/nrm1912

Martinez-Lopez, N., & Singh, R. (2015). Autophagy and Lipid Droplets in the Liver. *Annu Rev Nutr*, *35*, 215-237. https://doi.org/10.1146/annurev-nutr-071813-105336

Mastrototaro, L., & Roden, M. (2021). Insulin resistance and insulin sensitizing agents. *Metabolism*, *125*, 154892. https://doi.org/10.1016/j.metabol.2021.154892

Matmati, N., & Hannun, Y. A. (2008). Thematic review series: sphingolipids. ISC1 (inositol phosphosphingolipid-phospholipase C), the yeast homologue of neutral sphingomyelinases. *J Lipid Res*, *49*(5), 922-928. https://doi.org/10.1194/jlr.R800004-JLR200

Matmati, N., Kitagaki, H., Montefusco, D., Mohanty, B. K., & Hannun, Y. A. (2009). Hydroxyurea sensitivity reveals a role for ISC1 in the regulation of G2/M. *J Biol Chem*, *284*(13), 8241-8246. https://doi.org/10.1074/jbc.M900004200

Matmati, N., Metelli, A., Tripathi, K., Yan, S., Mohanty, B. K., & Hannun, Y. A. (2013). Identification of C18:1-phytoceramide as the candidate lipid mediator for hydroxyurea resistance in yeast. *J Biol Chem*, *288*(24), 17272-17284. https://doi.org/10.1074/jbc.M112.444802

Megyeri, M., Prasad, R., Volpert, G., Sliwa-Gonzalez, A., Haribowo, A. G., Aguilera-Romero, A., Riezman, H., Barral, Y., Futerman, A. H., & Schuldiner, M. (2019). Yeast ceramide synthases, Lag1 and Lac1, have distinct substrate specificity. *J Cell Sci*, *132*(12). https://doi.org/10.1242/jcs.228411

Mishra, S., Khaddaj, R., Cottier, S., Stradalova, V., Jacob, C., & Schneiter, R. (2016). Mature lipid droplets are accessible to ER luminal proteins. *J Cell Sci*, *129*(20), 3803-3815. https://doi.org/10.1242/jcs.189191

Miyake, Y., Kozutsumi, Y., Nakamura, S., Fujita, T., & Kawasaki, T. (1995). Serine palmitoyltransferase is the primary target of a sphingosine-like immunosuppressant, ISP-1/myriocin. *Biochem Biophys Res Commun*, *211*(2), 396-403. https://doi.org/10.1006/bbrc.1995.1827

Mohammad, K., Dakik, P., Medkour, Y., McAuley, M., Mitrofanova, D., & Titorenko, V. I. (2018). Yeast Cells Exposed to Exogenous Palmitoleic Acid Either Adapt to Stress and Survive or Commit to Regulated Liponecrosis and Die. *Oxid Med Cell Longev*, *2018*, 3074769. https://doi.org/10.1155/2018/3074769

Montgomery, M. K., Brown, S. H., Lim, X. Y., Fiveash, C. E., Osborne, B., Bentley, N. L., Braude, J. P., Mitchell, T. W., Coster, A. C., Don, A. S., Cooney, G. J., Schmitz-Peiffer, C., & Turner, N. (2016). Regulation of glucose homeostasis and insulin action by ceramide acyl-chain length: A beneficial role for very long-chain sphingolipid species. *Biochim Biophys Acta*, *1861*(11), 1828-1839. https://doi.org/10.1016/j.bbalip.2016.08.016

Montgomery, M. K., Hallahan, N. L., Brown, S. H., Liu, M., Mitchell, T. W., Cooney, G. J., & Turner, N. (2013). Mouse strain-dependent variation in obesity and glucose homeostasis in response to high-fat feeding. *Diabetologia*, *56*(5), 1129-1139. https://doi.org/10.1007/s00125-013-2846-8

Morawska, M., & Ulrich, H. D. (2013). An expanded tool kit for the auxin-inducible degron system in budding yeast. *Yeast*, *30*(9), 341-351. https://doi.org/10.1002/yea.2967

Mullis, K. B., & Faloona, F. A. (1987). Specific synthesis of DNA in vitro via a polymerase-catalyzed chain reaction. *Methods Enzymol*, *155*, 335-350. https://doi.org/10.1016/0076-6879(87)55023-6

Murphy, D. J. (2001). The biogenesis and functions of lipid bodies in animals, plants and microorganisms. *Prog Lipid Res*, *40*(5), 325-438. https://doi.org/10.1016/s0163-7827(01)00013-3

Nagiec, M. M., Baltisberger, J. A., Wells, G. B., Lester, R. L., & Dickson, R. C. (1994). The LCB2 gene of Saccharomyces and the related LCB1 gene encode subunits of serine palmitoyltransferase, the initial enzyme in sphingolipid synthesis. *Proc Natl Acad Sci U S A*, *91*(17), 7899-7902. https://doi.org/10.1073/pnas.91.17.7899

Nagiec, M. M., Skrzypek, M., Nagiec, E. E., Lester, R. L., & Dickson, R. C. (1998). The LCB4 (YOR171c) and LCB5 (YLR260w) genes of Saccharomyces encode sphingoid long chain base kinases. *J Biol Chem*, *273*(31), 19437-19442. https://doi.org/10.1074/jbc.273.31.19437

Ng, M., Fleming, T., Robinson, M., Thomson, B., Graetz, N., Margono, C., Mullany, E. C., Biryukov, S., Abbafati, C., Abera, S. F., Abraham, J. P., Abu-Rmeileh, N. M., Achoki, T., AlBuhairan, F. S., Alemu, Z. A., Alfonso, R., Ali, M. K., Ali, R., Guzman, N. A., . . . Gakidou, E. (2014). Global, regional, and national prevalence of overweight and obesity in children and adults during 1980-2013: a systematic analysis for the Global Burden of Disease Study 2013. *Lancet*, *384*(9945), 766-781. https://doi.org/10.1016/S0140-6736(14)60460-8

Nguyen, T. T., Lewandowska, A., Choi, J. Y., Markgraf, D. F., Junker, M., Bilgin, M., Ejsing, C. S., Voelker, D. R., Rapoport, T. A., & Shaw, J. M. (2012). Gem1 and ERMES do not directly affect phosphatidylserine transport from ER to mitochondria or

mitochondrial inheritance. *Traffic*, *13*(6), 880-890. https://doi.org/10.1111/j.1600-0854.2012.01352.x

Nickels, J. T., & Broach, J. R. (1996). A ceramide-activated protein phosphatase mediates ceramide-induced G1 arrest of Saccharomyces cerevisiae. *Genes Dev*, *10*(4), 382-394. https://doi.org/10.1101/gad.10.4.382

Nishimura, K., Fukagawa, T., Takisawa, H., Kakimoto, T., & Kanemaki, M. (2009). An auxin-based degron system for the rapid depletion of proteins in nonplant cells. *Nat Methods*, *6*(12), 917-922. https://doi.org/10.1038/nmeth.1401

Oelkers, P., Cromley, D., Padamsee, M., Billheimer, J. T., & Sturley, S. L. (2002). The DGA1 gene determines a second triglyceride synthetic pathway in yeast. *J Biol Chem*, *277*(11), 8877-8881. https://doi.org/10.1074/jbc.M111646200

Oelkers, P., Tinkelenberg, A., Erdeniz, N., Cromley, D., Billheimer, J. T., & Sturley, S. L. (2000). A lecithin cholesterol acyltransferase-like gene mediates diacylglycerol esterification in yeast. *J Biol Chem*, *275*(21), 15609-15612. https://doi.org/10.1074/jbc.C000144200

Ogretmen, B. (2018). Sphingolipid metabolism in cancer signalling and therapy. *Nat Rev Cancer*, *18*(1), 33-50. https://doi.org/10.1038/nrc.2017.96

Oh, C. S., Toke, D. A., Mandala, S., & Martin, C. E. (1997). ELO2 and ELO3, homologues of the Saccharomyces cerevisiae ELO1 gene, function in fatty acid elongation and are required for sphingolipid formation. *J Biol Chem*, *272*(28), 17376-17384. https://doi.org/10.1074/jbc.272.28.17376

Ohsaki, Y., Suzuki, M., & Fujimoto, T. (2014). Open questions in lipid droplet biology. *Chem Biol*, *21*(1), 86-96. https://doi.org/10.1016/j.chembiol.2013.08.009

Omura, S. (1976). The antibiotic cerulenin, a novel tool for biochemistry as an inhibitor of fatty acid synthesis. *Bacteriol Rev*, *40*(3), 681-697. https://doi.org/10.1128/br.40.3.681-697.1976

Ouahoud, S., Fiet, M. D., Martinez-Montanes, F., Ejsing, C. S., Kuss, O., Roden, M., & Markgraf, D. F. (2018). Lipid droplet consumption is functionally coupled to vacuole homeostasis independent of lipophagy. *J Cell Sci*, *131*(11). https://doi.org/10.1242/jcs.213876

Pagadala, M., Kasumov, T., McCullough, A. J., Zein, N. N., & Kirwan, J. P. (2012). Role of ceramides in nonalcoholic fatty liver disease. *Trends Endocrinol Metab*, *23*(8), 365-371. https://doi.org/10.1016/j.tem.2012.04.005

Perry, R. J., Camporez, J. G., Kursawe, R., Titchenell, P. M., Zhang, D., Perry, C. J., Jurczak, M. J., Abudukadier, A., Han, M. S., Zhang, X. M., Ruan, H. B., Yang, X., Caprio, S., Kaech, S. M., Sul, H. S., Birnbaum, M. J., Davis, R. J., Cline, G. W., Petersen, K. F., & Shulman, G. I. (2015). Hepatic acetyl CoA links adipose tissue inflammation to hepatic insulin resistance and type 2 diabetes. *Cell*, *160*(4), 745-758. https://doi.org/10.1016/j.cell.2015.01.012

Perry, R. J., Kim, T., Zhang, X. M., Lee, H. Y., Pesta, D., Popov, V. B., Zhang, D., Rahimi, Y., Jurczak, M. J., Cline, G. W., Spiegel, D. A., & Shulman, G. I. (2013). Reversal of hypertriglyceridemia, fatty liver disease, and insulin resistance by a liver-targeted mitochondrial uncoupler. *Cell Metab*, *18*(5), 740-748. https://doi.org/10.1016/j.cmet.2013.10.004

Petersen, K. F., Dufour, S., Savage, D. B., Bilz, S., Solomon, G., Yonemitsu, S., Cline, G. W., Befroy, D., Zemany, L., Kahn, B. B., Papademetris, X., Rothman, D. L., & Shulman, G. I. (2007). The role of skeletal muscle insulin resistance in the pathogenesis of the metabolic syndrome. *Proc Natl Acad Sci U S A*, *104*(31), 12587-12594. https://doi.org/10.1073/pnas.0705408104

Petersen, M. C., Madiraju, A. K., Gassaway, B. M., Marcel, M., Nasiri, A. R., Butrico, G., Marcucci, M. J., Zhang, D., Abulizi, A., Zhang, X. M., Philbrick, W., Hubbard, S. R., Jurczak, M. J., Samuel, V. T., Rinehart, J., & Shulman, G. I. (2016). Insulin receptor Thr1160 phosphorylation mediates lipid-induced hepatic insulin resistance. *J Clin Invest*, *126*(11), 4361-4371. https://doi.org/10.1172/JCI86013

Petersen, M. C., & Shulman, G. I. (2017). Roles of Diacylglycerols and Ceramides in Hepatic Insulin Resistance. *Trends Pharmacol Sci*, *38*(7), 649-665. https://doi.org/10.1016/j.tips.2017.04.004

Petersen, M. C., & Shulman, G. I. (2018). Mechanisms of Insulin Action and Insulin Resistance. *Physiol Rev*, *98*(4), 2133-2223. https://doi.org/10.1152/physrev.00063.2017

Petschnigg, J., Wolinski, H., Kolb, D., Zellnig, G., Kurat, C. F., Natter, K., & Kohlwein, S. D. (2009). Good fat, essential cellular requirements for triacylglycerol synthesis to maintain membrane homeostasis in yeast. *J Biol Chem*, *284*(45), 30981-30993. https://doi.org/10.1074/jbc.M109.024752

Pol, A., Gross, S. P., & Parton, R. G. (2014). Review: biogenesis of the multifunctional lipid droplet: lipids, proteins, and sites. *J Cell Biol*, *204*(5), 635-646. https://doi.org/10.1083/jcb.201311051

Powell, D. J., Hajduch, E., Kular, G., & Hundal, H. S. (2003). Ceramide disables 3-phosphoinositide binding to the pleckstrin homology domain of protein kinase B (PKB)/Akt by a PKCzeta-dependent mechanism. *Mol Cell Biol*, *23*(21), 7794-7808. https://doi.org/10.1128/MCB.23.21.7794-7808.2003

Prinz, W. A., Grzyb, L., Veenhuis, M., Kahana, J. A., Silver, P. A., & Rapoport, T. A. (2000). Mutants affecting the structure of the cortical endoplasmic reticulum in Saccharomyces cerevisiae. *J Cell Biol*, *150*(3), 461-474. https://doi.org/10.1083/jcb.150.3.461

Pruett, S. T., Bushnev, A., Hagedorn, K., Adiga, M., Haynes, C. A., Sullards, M. C., Liotta, D. C., & Merrill, A. H., Jr. (2008). Biodiversity of sphingoid bases ("sphingosines") and related amino alcohols. *J Lipid Res*, *49*(8), 1621-1639. https://doi.org/10.1194/jlr.R800012-JLR200

Pu, J., Ha, C. W., Zhang, S., Jung, J. P., Huh, W. K., & Liu, P. (2011). Interactomic study on interaction between lipid droplets and mitochondria. *Protein Cell*, *2*(6), 487-496. https://doi.org/10.1007/s13238-011-1061-y

Raichur, S., Wang, S. T., Chan, P. W., Li, Y., Ching, J., Chaurasia, B., Dogra, S., Ohman, M. K., Takeda, K., Sugii, S., Pewzner-Jung, Y., Futerman, A. H., & Summers, S. A. (2014). CerS2 Haploinsufficiency Inhibits beta-Oxidation and Confers Susceptibility to Diet-Induced Steatohepatitis and Insulin Resistance. *Cell Metab*, *20*(5), 919. https://doi.org/10.1016/j.cmet.2014.10.007

Rajakumari, S., Grillitsch, K., & Daum, G. (2008). Synthesis and turnover of non-polar lipids in yeast. *Prog Lipid Res*, *47*(3), 157-171. https://doi.org/10.1016/j.plipres.2008.01.001

Rambold, A. S., Cohen, S., & Lippincott-Schwartz, J. (2015). Fatty acid trafficking in starved cells: regulation by lipid droplet lipolysis, autophagy, and mitochondrial fusion dynamics. *Dev Cell*, *32*(6), 678-692. https://doi.org/10.1016/j.devcel.2015.01.029

Rego, A., Trindade, D., Chaves, S. R., Manon, S., Costa, V., Sousa, M. J., & Corte-Real, M. (2014). The yeast model system as a tool towards the understanding of apoptosis regulation by sphingolipids. *FEMS Yeast Res*, *14*(1), 160-178. https://doi.org/10.1111/1567-1364.12096

Ren, J., Saied, E. M., Zhong, A., Snider, J., Ruiz, C., Arenz, C., Obeid, L. M., Girnun, G. D., & Hannun, Y. A. (2018). Tsc3 regulates SPT amino acid choice in Saccharomyces cerevisiae by promoting alanine in the sphingolipid pathway. *J Lipid Res*, *59*(11), 2126-2139. https://doi.org/10.1194/jlr.M088195

Robinson, J. S., Klionsky, D. J., Banta, L. M., & Emr, S. D. (1988). Protein sorting in Saccharomyces cerevisiae: isolation of mutants defective in the delivery and processing of multiple vacuolar hydrolases. *Mol Cell Biol*, *8*(11), 4936-4948. https://doi.org/10.1128/mcb.8.11.4936-4948.1988

Rockenfeller, P., Ring, J., Muschett, V., Beranek, A., Buettner, S., Carmona-Gutierrez, D., Eisenberg, T., Khoury, C., Rechberger, G., Kohlwein, S. D., Kroemer, G., & Madeo, F. (2010). Fatty acids trigger mitochondrion-dependent necrosis. *Cell Cycle*, *9*(14), 2836-2842. https://doi.org/10.4161/cc.9.14.12267

Rockenfeller, P., Smolnig, M., Diessl, J., Bashir, M., Schmiedhofer, V., Knittelfelder, O., Ring, J., Franz, J., Foessl, I., Khan, M. J., Rost, R., Graier, W. F., Kroemer, G., Zimmermann, A., Carmona-Gutierrez, D., Eisenberg, T., Buttner, S., Sigrist, S. J., Kuhnlein, R. P., . . . Madeo, F. (2018). Diacylglycerol triggers Rim101 pathway-dependent necrosis in yeast: a model for lipotoxicity. *Cell Death Differ*, *25*(4), 767-783. https://doi.org/10.1038/s41418-017-0014-2

Roden, M., & Shulman, G. I. (2019). The integrative biology of type 2 diabetes. *Nature*, *576*(7785), 51-60. https://doi.org/10.1038/s41586-019-1797-8

Rothman, D. L., Magnusson, I., Katz, L. D., Shulman, R. G., & Shulman, G. I. (1991). Quantitation of hepatic glycogenolysis and gluconeogenesis in fasting humans with 13C NMR. *Science*, *254*(5031), 573-576. https://doi.org/10.1126/science.1948033

Saatmann, N., Zaharia, O. P., Loenneke, J. P., Roden, M., & Pesta, D. H. (2021). Effects of Blood Flow Restriction Exercise and Possible Applications in Type 2 Diabetes. *Trends Endocrinol Metab*, *32*(2), 106-117. https://doi.org/10.1016/j.tem.2020.11.010

Salehin, M., Bagchi, R., & Estelle, M. (2015). SCFTIR1/AFB-based auxin perception: mechanism and role in plant growth and development. *Plant Cell*, *27*(1), 9-19. https://doi.org/10.1105/tpc.114.133744

Samuel, V. T., Liu, Z. X., Qu, X., Elder, B. D., Bilz, S., Befroy, D., Romanelli, A. J., & Shulman, G. I. (2004). Mechanism of hepatic insulin resistance in non-alcoholic fatty liver disease. *J Biol Chem*, *279*(31), 32345-32353. https://doi.org/10.1074/jbc.M313478200

Samuel, V. T., Liu, Z. X., Wang, A., Beddow, S. A., Geisler, J. G., Kahn, M., Zhang, X. M., Monia, B. P., Bhanot, S., & Shulman, G. I. (2007). Inhibition of protein kinase Cepsilon prevents hepatic insulin resistance in nonalcoholic fatty liver disease. *J Clin Invest*, *117*(3), 739-745. https://doi.org/10.1172/JCI30400

Samuel, V. T., & Shulman, G. I. (2012). Mechanisms for insulin resistance: common threads and missing links. *Cell*, *148*(5), 852-871. https://doi.org/10.1016/j.cell.2012.02.017

Sawai, H., Okamoto, Y., Luberto, C., Mao, C., Bielawska, A., Domae, N., & Hannun, Y. A. (2000). Identification of ISC1 (YER019w) as inositol phosphosphingolipid phospholipase C in Saccharomyces cerevisiae. *J Biol Chem*, *275*(50), 39793-39798. https://doi.org/10.1074/jbc.M007721200

Schindelin, J., Arganda-Carreras, I., Frise, E., Kaynig, V., Longair, M., Pietzsch, T., Preibisch, S., Rueden, C., Saalfeld, S., Schmid, B., Tinevez, J. Y., White, D. J., Hartenstein, V., Eliceiri, K., Tomancak, P., & Cardona, A. (2012). Fiji: an open-source platform for biological-image analysis. *Nat Methods*, *9*(7), 676-682. https://doi.org/10.1038/nmeth.2019

Schmidt, C., Athenstaedt, K., Koch, B., Ploier, B., & Daum, G. (2013). Regulation of the yeast triacylglycerol lipase TGl3p by formation of nonpolar lipids. *J Biol Chem*, *288*(27), 19939-19948. https://doi.org/10.1074/jbc.M113.459610

Schnurr, T. M., Jakupovic, H., Carrasquilla, G. D., Angquist, L., Grarup, N., Sorensen, T. I. A., Tjonneland, A., Overvad, K., Pedersen, O., Hansen, T., & Kilpelainen, T. O. (2020). Obesity, unfavourable lifestyle and genetic risk of type 2 diabetes: a case-cohort study. *Diabetologia*, *63*(7), 1324-1332. https://doi.org/10.1007/s00125-020-05140-5

Schorling, S., Vallee, B., Barz, W. P., Riezman, H., & Oesterhelt, D. (2001). Lag1p and Lac1p are essential for the Acyl-CoA-dependent ceramide synthase reaction in Saccharomyces cerevisae. *Mol Biol Cell*, *12*(11), 3417-3427. https://doi.org/10.1091/mbc.12.11.3417

Schubert, K. M., Scheid, M. P., & Duronio, V. (2000). Ceramide inhibits protein kinase B/Akt by promoting dephosphorylation of serine 473. *J Biol Chem*, *275*(18), 13330-13335. https://doi.org/10.1074/jbc.275.18.13330

Serbyn, N., Noireterre, A., Bagdiul, I., Plank, M., Michel, A. H., Loewith, R., Kornmann, B., & Stutz, F. (2020). The Aspartic Protease Ddi1 Contributes to DNA-Protein Crosslink Repair in Yeast. *Mol Cell*, *77*(5), 1066-1079 e1069. https://doi.org/10.1016/j.molcel.2019.12.007

Shmueli, E., Alberti, K. G., & Record, C. O. (1993). Diacylglycerol/protein kinase C signalling: a mechanism for insulin resistance? *J Intern Med*, *234*(4), 397-400. https://doi.org/10.1111/j.1365-2796.1993.tb00761.x

Shulman, G. I. (2014). Ectopic fat in insulin resistance, dyslipidemia, and cardiometabolic disease. *N Engl J Med*, *371*(23), 2237-2238. https://doi.org/10.1056/NEJMc1412427

Sia, R. A., Bardes, E. S., & Lew, D. J. (1998). Control of Swe1p degradation by the morphogenesis checkpoint. *EMBO J*, *17*(22), 6678-6688. https://doi.org/10.1093/emboj/17.22.6678

Sia, R. A., Herald, H. A., & Lew, D. J. (1996). Cdc28 tyrosine phosphorylation and the morphogenesis checkpoint in budding yeast. *Mol Biol Cell*, *7*(11), 1657-1666. https://doi.org/10.1091/mbc.7.11.1657

Singh, R., Kaushik, S., Wang, Y., Xiang, Y., Novak, I., Komatsu, M., Tanaka, K., Cuervo, A. M., & Czaja, M. J. (2009). Autophagy regulates lipid metabolism. *Nature*, *458*(7242), 1131-1135. https://doi.org/10.1038/nature07976

Solinas, G., & Becattini, B. (2017). JNK at the crossroad of obesity, insulin resistance, and cell stress response. *Mol Metab*, *6*(2), 174-184. https://doi.org/10.1016/j.molmet.2016.12.001

Sorger, D., & Daum, G. (2002). Synthesis of triacylglycerols by the acyl-coenzyme A:diacyl-glycerol acyltransferase Dga1p in lipid particles of the yeast Saccharomyces cerevisiae. *J Bacteriol*, *184*(2), 519-524. https://doi.org/10.1128/JB.184.2.519-524.2002

Suzuki, K., Kubota, Y., Sekito, T., & Ohsumi, Y. (2007). Hierarchy of Atg proteins in pre-autophagosomal structure organization. *Genes Cells*, *12*(2), 209-218. https://doi.org/10.1111/j.1365-2443.2007.01050.x

Szendroedi, J., & Roden, M. (2009). Ectopic lipids and organ function. *Curr Opin Lipidol*, *20*(1), 50-56. https://doi.org/10.1097/mol.0b013e328321b3a8

Szendroedi, J., Yoshimura, T., Phielix, E., Koliaki, C., Marcucci, M., Zhang, D., Jelenik, T., Muller, J., Herder, C., Nowotny, P., Shulman, G. I., & Roden, M. (2014). Role of diacylglycerol activation of PKCtheta in lipid-induced muscle insulin resistance in humans. *Proc Natl Acad Sci U S A*, *111*(26), 9597-9602. https://doi.org/10.1073/pnas.1409229111

Teng, W., Li, Y., Du, M., Lei, X., Xie, S., & Ren, F. (2019). Sulforaphane Prevents Hepatic Insulin Resistance by Blocking Serine Palmitoyltransferase 3-Mediated Ceramide Biosynthesis. *Nutrients*, *11*(5). https://doi.org/10.3390/nu11051185

Thiam, A. R., Antonny, B., Wang, J., Delacotte, J., Wilfling, F., Walther, T. C., Beck, R., Rothman, J. E., & Pincet, F. (2013). COPI buds 60-nm lipid droplets from reconstituted water-phospholipid-triacylglyceride interfaces, suggesting a tension clamp function. *Proc Natl Acad Sci U S A*, *110*(33), 13244-13249. https://doi.org/10.1073/pnas.1307685110

Thiam, A. R., Farese, R. V., Jr., & Walther, T. C. (2013). The biophysics and cell biology of lipid droplets. *Nat Rev Mol Cell Biol*, *14*(12), 775-786. https://doi.org/10.1038/nrm3699

Thiam, A. R., & Foret, L. (2016). The physics of lipid droplet nucleation, growth and budding. *Biochim Biophys Acta*, *1861*(8 Pt A), 715-722. https://doi.org/10.1016/j.bbalip.2016.04.018

Thorens, B. (2015). GLUT2, glucose sensing and glucose homeostasis. *Diabetologia*, *58*(2), 221-232. https://doi.org/10.1007/s00125-014-3451-1

Trefts, E., Gannon, M., & Wasserman, D. H. (2017). The liver. *Curr Biol*, *27*(21), R1147-R1151. https://doi.org/10.1016/j.cub.2017.09.019

Turinsky, J., O'Sullivan, D. M., & Bayly, B. P. (1990). 1,2-Diacylglycerol and ceramide levels in insulin-resistant tissues of the rat in vivo. *J Biol Chem*, *265*(28), 16880-16885. https://www.ncbi.nlm.nih.gov/pubmed/2211599

Turner, N., Kowalski, G. M., Leslie, S. J., Risis, S., Yang, C., Lee-Young, R. S., Babb, J. R., Meikle, P. J., Lancaster, G. I., Henstridge, D. C., White, P. J., Kraegen, E. W., Marette, A., Cooney, G. J., Febbraio, M. A., & Bruce, C. R. (2013). Distinct patterns

of tissue-specific lipid accumulation during the induction of insulin resistance in mice by high-fat feeding. *Diabetologia*, *56*(7), 1638-1648. https://doi.org/10.1007/s00125-013-2913-1

Turpin, S. M., Nicholls, H. T., Willmes, D. M., Mourier, A., Brodesser, S., Wunderlich, C. M., Mauer, J., Xu, E., Hammerschmidt, P., Bronneke, H. S., Trifunovic, A., LoSasso, G., Wunderlich, F. T., Kornfeld, J. W., Bluher, M., Kronke, M., & Bruning, J. C. (2014). Obesity-induced CerS6-dependent C16:0 ceramide production promotes weight gain and glucose intolerance. *Cell Metab*, *20*(4), 678-686. https://doi.org/10.1016/j.cmet.2014.08.002

Ussher, J. R., Koves, T. R., Cadete, V. J., Zhang, L., Jaswal, J. S., Swyrd, S. J., Lopaschuk, D. G., Proctor, S. D., Keung, W., Muoio, D. M., & Lopaschuk, G. D. (2010). Inhibition of de novo ceramide synthesis reverses diet-induced insulin resistance and enhances whole-body oxygen consumption. *Diabetes*, *59*(10), 2453-2464. https://doi.org/10.2337/db09-1293

Uttenweiler, A., & Mayer, A. (2008). Microautophagy in the yeast Saccharomyces cerevisiae. *Methods Mol Biol*, *445*, 245-259. https://doi.org/10.1007/978-1-59745-157-4_16

Vallee, B., & Riezman, H. (2005). Lip1p: a novel subunit of acyl-CoA ceramide synthase. *EMBO J*, *24*(4), 730-741. https://doi.org/10.1038/sj.emboj.7600562

van Meer, G., Voelker, D. R., & Feigenson, G. W. (2008). Membrane lipids: where they are and how they behave. *Nat Rev Mol Cell Biol*, *9*(2), 112-124. https://doi.org/10.1038/nrm2330

van Zutphen, T., Todde, V., de Boer, R., Kreim, M., Hofbauer, H. F., Wolinski, H., Veenhuis, M., van der Klei, I. J., & Kohlwein, S. D. (2014). Lipid droplet autophagy in the yeast Saccharomyces cerevisiae. *Mol Biol Cell*, *25*(2), 290-301. https://doi.org/10.1091/mbc.E13-08-0448

Vatner, D. F., Majumdar, S. K., Kumashiro, N., Petersen, M. C., Rahimi, Y., Gattu, A. K., Bears, M., Camporez, J. P., Cline, G. W., Jurczak, M. J., Samuel, V. T., & Shulman, G. I. (2015). Insulin-independent regulation of hepatic triglyceride synthesis by fatty acids. *Proc Natl Acad Sci U S A*, *112*(4), 1143-1148. https://doi.org/10.1073/pnas.1423952112

Wahl, S., Drong, A., Lehne, B., Loh, M., Scott, W. R., Kunze, S., Tsai, P. C., Ried, J. S., Zhang, W., Yang, Y., Tan, S., Fiorito, G., Franke, L., Guarrera, S., Kasela, S., Kriebel, J., Richmond, R. C., Adamo, M., Afzal, U., . . . Chambers, J. C. (2017). Epigenome-wide association study of body mass index, and the adverse outcomes of adiposity. *Nature*, *541*(7635), 81-86. https://doi.org/10.1038/nature20784

Walther, T. C., Chung, J., & Farese, R. V., Jr. (2017). Lipid Droplet Biogenesis. *Annu Rev Cell Dev Biol*, *33*, 491-510. https://doi.org/10.1146/annurev-cellbio-100616-060608

Wilfling, F., Haas, J. T., Walther, T. C., & Farese, R. V., Jr. (2014). Lipid droplet biogenesis. *Curr Opin Cell Biol*, *29*, 39-45. https://doi.org/10.1016/j.ceb.2014.03.008

Wittenbecher, C., Cuadrat, R., Johnston, L., Eichelmann, F., Jager, S., Kuxhaus, O., Prada, M., Del Greco, M. F., Hicks, A. A., Hoffman, P., Krumsiek, J., Hu, F. B., & Schulze, M. B. (2022). Dihydroceramide- and ceramide-profiling provides insights into human cardiometabolic disease etiology. *Nat Commun*, *13*(1), 936. https://doi.org/10.1038/s41467-022-28496-1

Wymann, M. P., & Schneiter, R. (2008). Lipid signalling in disease. *Nat Rev Mol Cell Biol*, *9*(2), 162-176. https://doi.org/10.1038/nrm2335

Xia, J. Y., Holland, W. L., Kusminski, C. M., Sun, K., Sharma, A. X., Pearson, M. J., Sifuentes, A. J., McDonald, J. G., Gordillo, R., & Scherer, P. E. (2015). Targeted Induction of Ceramide Degradation Leads to Improved Systemic Metabolism and Reduced Hepatic Steatosis. *Cell Metab*, *22*(2), 266-278. https://doi.org/10.1016/j.cmet.2015.06.007

Yang, H., Jiang, W., Gentry, M., & Hallberg, R. L. (2000). Loss of a protein phosphatase 2A regulatory subunit (Cdc55p) elicits improper regulation of Swe1p degradation. *Mol Cell Biol*, *20*(21), 8143-8156. https://doi.org/10.1128/MCB.20.21.8143-8156.2000

Yang, R. X., Pan, Q., Liu, X. L., Zhou, D., Xin, F. Z., Zhao, Z. H., Zhang, R. N., Zeng, J., Qiao, L., Hu, C. X., Xu, G. W., & Fan, J. G. (2019). Therapeutic effect and autophagy regulation of myriocin in nonalcoholic steatohepatitis. *Lipids Health Dis*, *18*(1), 179. https://doi.org/10.1186/s12944-019-1118-0

Zhang, C., & Liu, P. (2017). The lipid droplet: A conserved cellular organelle. *Protein Cell*, *8*(11), 796-800. https://doi.org/10.1007/s13238-017-0467-6

Ziegler, D., Strom, A., Strassburger, K., Knebel, B., Bonhof, G. J., Kotzka, J., Szendroedi, J., Roden, M., & German Diabetes Study, g. (2021). Association of cardiac autonomic dysfunction with higher levels of plasma lipid metabolites in recent-onset type 2 diabetes. *Diabetologia*, *64*(2), 458-468. https://doi.org/10.1007/s00125-020-05310-5

Zweytick, D., Athenstaedt, K., & Daum, G. (2000). Intracellular lipid particles of eukaryotic cells. *Biochim Biophys Acta*, *1469*(2), 101-120. https://doi.org/10.1016/s0005-2736(00)00294-7

9. Danksagung

Mein erster Dank geht an Jun-Prof. Mathias Beller, welcher den Mut bewies mich und meine Themenstellung an seinem Institut anzunehmen und die Jahre über zu begleiten. Wohl hat die Ferne beider Institute unsere gemeinsamen Treffen geschmälert, jedoch zeigten einige davon, welch großartiger Erstkorrektor du bist. Danke für jegliches Verständnis und Vertrauen, das du mir schenktest.

Desweitern gilt mein Dank Dr. Markgraf und Christina Preuss. Ihr habt mich während meiner Zeit als studentische Hilfskraft in die liebevolle Gemeinschaft des DDZ integriert und mir die Furcht vor der Komplexität der Lipide, sowie deren pathologischen Auswirkungen genommen. Danke Daniel, dass du mit mir die ersten Schritte meines Doktorwerdens gegangen bist und mir die faszinierende Welt der Lipid Droplets offenbart hast.

Liebe AG Energy, danke für die freundliche Aufnahme in eure Gruppe. Ich konnte mir eine Menge bei so vielen klugen Köpfen abschauen. Kurzum, ich habe mich sehr wohl bei euch gefühlt. Nicht nur der wissenschaftliche Diskurs war wichtig sondern ebenso der gesellige Austausch. Diese Kombination gibt die „Energy“ Doktorarbeiten zu meistern. Ein großer Dank geht an Lucia. Molto bene Lucia! Du hast dich der Herausforderung mein Projekt weiter zu betreuen gestellt und stets geholfen. Unter deinen Fittichen als Mentorin ist man gut aufgehoben.

Ein gewichtiger Dank geht an Univ.-Prof. Dr. Michael Roden. Ich durfte Sie die letzten Jahre dabei beobachten, wie Sie mit Ihrer Expertise die Wissenschaft handhaben und ich bin begeistert von Ihrem universellen Geist. Trotz der ihnen eher fremden Bierhefe konnten Sie mir stets dabei helfen, Fehler zu verbessern und das Niveau meiner Arbeit anzuheben. Ich bin froh, Ihre Lehre genossen zu haben, zudem noch mit Dank für die freundliche Übernahme der Zweitbetreuung und somit die Möglichkeit meine Doktorarbeit fortzuführen und beenden zu können.

Ein weiterer Dank geht an unser Biomedizinisches Labor. Es war mir eine Freude mein experimentelles Wesen mit euch zusammen ausleben zu dürfen. Danke Dr. Trenkamp und Dr. Heilmann für das Ermöglichen der MassSpec-Messungen. Danke Christina, dass du mir eine Mentorin in der Lipidextraktion und anderen Aspekten des Lebens warst.

Danke liebes DDZ. Von Neu bis Alt, von U2 bis auf die Dachterrasse. Vielen lieben Dank für alles!

10. Eidestaatliche Erklärung

Ich erkläre hiermit an Eides Statt, dass ich die vorliegende Arbeit selbstständig und nur unter Zuhilfenahme der ausgewiesenen Hilfsmittel angefertigt habe. Sämtliche Stellen der Arbeit, die im Wortlaut oder dem Sinn nach anderen gedruckten oder im Internet verfügbaren Werken entnommen sind, habe ich durch genaue Quellenangaben kenntlich gemacht. Ferner versichere ich, dass ich bisher keinen Promotionsversuch unternommen habe. Ebenso wurde die Arbeit an keiner anderen Hochschule eingereicht.

Düsseldorf, den

_____

Manuel Hertel